

1-1-2007

Geochemical and transport modeling of selected radionuclides at Yucca Mountain

Yuyu Lin

University of Nevada, Las Vegas

Follow this and additional works at: <https://digitalscholarship.unlv.edu/rtds>

Repository Citation

Lin, Yuyu, "Geochemical and transport modeling of selected radionuclides at Yucca Mountain" (2007).

UNLV Retrospective Theses & Dissertations. 2128.

<http://dx.doi.org/10.25669/lqt4-i7uy>

This Thesis is protected by copyright and/or related rights. It has been brought to you by Digital Scholarship@UNLV with permission from the rights-holder(s). You are free to use this Thesis in any way that is permitted by the copyright and related rights legislation that applies to your use. For other uses you need to obtain permission from the rights-holder(s) directly, unless additional rights are indicated by a Creative Commons license in the record and/or on the work itself.

This Thesis has been accepted for inclusion in UNLV Retrospective Theses & Dissertations by an authorized administrator of Digital Scholarship@UNLV. For more information, please contact digitalscholarship@unlv.edu.

GEOCHEMICAL AND TRANSPORT MODELING OF SELECTED
RADIONUCLIDES AT YUCCA MOUNTAIN

by

Yuyu Lin

Bachelor of Engineering
Hohai University, China
2003

A thesis submitted in partial fulfillment
of the requirements for the

Master of Science Degree in Geoscience
Department of Geoscience
College of Sciences

Graduate College
University of Nevada, Las Vegas
May 2007

UMI Number: 1443776

INFORMATION TO USERS

The quality of this reproduction is dependent upon the quality of the copy submitted. Broken or indistinct print, colored or poor quality illustrations and photographs, print bleed-through, substandard margins, and improper alignment can adversely affect reproduction.

In the unlikely event that the author did not send a complete manuscript and there are missing pages, these will be noted. Also, if unauthorized copyright material had to be removed, a note will indicate the deletion.

UMI[®]

UMI Microform 1443776

Copyright 2007 by ProQuest Information and Learning Company.

All rights reserved. This microform edition is protected against unauthorized copying under Title 17, United States Code.

ProQuest Information and Learning Company
300 North Zeeb Road
P.O. Box 1346
Ann Arbor, MI 48106-1346



Thesis Approval
The Graduate College
University of Nevada, Las Vegas

FEBRUARY 21, _____, 2007

The Thesis prepared by

YUYU LIN

Entitled

GEOCHEMICAL AND TRANSPORT MODELING OF RADIONUCLIDES AT YUCCA MOUNTAIN

is approved in partial fulfillment of the requirements for the degree of

MASTER OF SCIENCE

Zhongbo Yu

Examination Committee Chair

[Signature]

Dean of the Graduate College

[Signature]

Examination Committee Member

Michael Nield

Examination Committee Member

[Signature]

Graduate College Faculty Representative

ABSTRACT

Geochemical and Transport Modeling of Selected Radionuclides at Yucca Mountain

by

Yuyu Lin

Dr. Zhongbo Yu, Examination Committee Chair
Associate Professor of Hydrogeology
University of Nevada, Las Vegas

Yucca Mountain, Nevada has been selected as a potential high-level nuclear waste repository. The groundwater system at Yucca Mountain is a primary medium through which radionuclides might move away from the potential repository. Characterization studies have identified ^{237}Np , ^{235}U and ^{239}Pu as radionuclides of concern. In this study, simulations of solid solubility, solution speciation, and transport of selected radionuclides are conducted with PHREEQC, a geochemical modeling system. Results from solubility and speciation simulations indicate the influence of pH value and CO_2 fugacity on radionuclide dissolution and aqueous species in solution. Kinetic transport simulations produced radionuclide breakthrough curves under various conditions including sorption / no sorption, different flow velocities, and mixing of two types of groundwater. Results from transport modeling indicate that sorption activity makes a significant contribution to the retardation of solute transport whereas flow velocity controls the contact time between solutions and sediments which has different effects on the sorption activity.

TABLE OF CONTENTS

ABSTRACT	iii
LISTS OF TABLES.....	vi
LISTS OF FIGURES	vii
ACKNOWLEDGEMENT	ix
CHAPTER 1 INTRODUCTION	1
1.1 Radionuclides of Concern and Previous Work.....	3
1.2 Objectives	5
CHAPTER 2 BACKGROUND INFORMATION	7
2.1 SNF and Chemical Properties of Selected Radionuclides	7
2.1.1 Information about SNF	7
2.1.2 Uranium	8
2.1.3 Neptunium.....	9
2.1.4 Plutonium.....	10
2.2 Study Site.....	12
2.2.1 Climate at Yucca Mountain	12
2.2.2 Geologic and Hydrogeologic Setting of Saturated Zone	14
2.2.3 Regional Groundwater and Flow Paths	17
2.2.4 Geochemistry of Unsaturated Zone and Saturated Zone	19
CHAPTER 3 METHODOLOGY	22
3.1 Modeling Approach	23
3.2 Description of PHREEQC	24
3.3 Solid Solubility of Uranium, Neptunium, and Plutonium	26
3.4 Speciation of Uranium, Neptunium, and Plutonium.....	30
3.5 Principles of Transport Simulation	32
3.5.1 Numerical Equations for Transport	32
3.5.2 Principle Transport Mechanics of Radionuclides in SZ	33
3.5.2.1 Transport Features of Fractured Volcanic Tuffs.....	34
3.5.2.2 Transport Features of Alluvium.....	34
3.6 Implementation of Conceptual Model	36
3.6.1 Conceptual Hydrological Strata of Saturated Zone	36
3.6.2 Other Features of Solute Transport.....	38
3.7 Description of Simulation Input and Output.....	39

CHAPTER 4 MODEL PROCEDURES AND RESULTS	41
4.1 Dissolution Simulation.....	44
4.1.1 Uranium	44
4.1.2 Neptunium.....	48
4.1.3 Plutonium.....	51
4.2 Speciation Simulation.....	53
4.2.1 Uranium	54
4.2.2 Neptunium.....	54
4.2.3 Plutonium.....	55
4.3 Transport Simulation Results.....	58
4.3.1 Setup of Transport Simulation.....	58
4.3.2 Breakthrough Curve.....	60
4.3.3 Effect of Sorption Activity and Stagnant Zone.....	63
4.3.4 Effect of Mixing with Groundwater from Carbonate Aquifer.....	69
4.3.5 Effect of Groundwater Flow Velocity	71
 CHAPTER 5 CONCLUSIONS	 77
 APPENDIX A EXAMPLES OF SIMULATION INPUT AND OUTPUT	 80
A.1 Input Files for Dissolution and Speciation Simulations of Neptunium	80
A.2 Input File for Transport Simulation of Uranium.....	82
 APPENDIX B EFFECT OF GROUNDWATER VELOCITY ON TRANSPORT PROCESS	 85
B.1 Uranium Profile in Volcanic and Alluvial Aquifers	85
B.2 Neptunium Profile in Volcanic and Alluvial Aquifers.....	87
B.3 Plutonium Profile in Volcanic and Alluvial Aquifers.....	89
 APPENDIX C SCALING EFFECTS	 91
 REFERENCES	 94
 VITA.....	 99

LISTS OF TABLES

Table 2.1	Chemical compositions of solutions used in all simulations	20
Table 3.1	Dissolution equations of principal alteration phases of uranium, neptunium and plutonium at 25 °C.....	29
Table 3.2	Speciation reactions of neptunium and plutonium at 25 °C.....	31
Table 4.1	Solution Master Species, Equilibrium Phases, and sorption coefficient used in the simulation with PHREEQC.	43
Table 4.2	Transport parameters used for volcanic and alluvial aquifers	43
Table 4.3	Calculated dissolution for uranium controlled by secondary minerals (mol/L)	46
Table 4.4	Calculated neptunium dissolution controlled by Np_2O_5 (mol/L).....	49
Table 4.5	Calculated plutonium dissolution controlled by PuO_2 (mol/L).	52
Table 4.6	Concentration alteration before and after mixing with carbonate groundwater.	70
Table B.1	Uranium transport in volcanic aquifer at different flow velocities.	85
Table B.2	Uranium transport in alluvial aquifer at different flow velocities.....	86
Table B.3	Neptunium transport in volcanic aquifer at different flow velocities.	87
Table B.4	Neptunium transport in alluvial aquifer at different flow velocities.....	88
Table B.5	Plutonium transport in volcanic aquifer at different flow velocities.....	89
Table B.6	Plutonium transport in alluvial aquifer at different flow velocities.	90
Table C.1	Transport simulation of uranium and neptunium of 200 and 20 cells in alluvium aquifer.	92
Table C.2	Transport simulation of uranium and neptunium of 200 and 20 cells in alluvium aquifer without stagnant zone.	93

LISTS OF FIGURES

Figure 1.1	Schematic cross-section of Yucca Mountain saturated zone (including volcanic tuffs and alluvium).	2
Figure 2.1	Map of study site at Yucca Mountain.....	13
Figure 2.2	Schematic chart of major hydrogeologic and geologic units.	16
Figure 2.3	Predicted groundwater flow path by particle-tracking method.	18
Figure 2.4	Major geological structures and well locations.	21
Figure 3.1	Schematic flow diagram of modeling stages of radionuclides.	23
Figure 3.2	The paragenetic sequence of alteration phases on the top of sample in the experiment.	27
Figure 3.3	Cross-section of conceptual hydro-stratigraphy of SZ.	37
Figure 4.1	Uranium dissolution simulation as a function of pH and f_{CO_2}	46
Figure 4.2	Uranium dissolution simulation with percolating water (pH = 7.5~8.5) in WP.....	47
Figure 4.3	Analysis of uranium secondary minerals with dissolution simulation within WP.....	47
Figure 4.4	Uranium dissolution changes with increasing temperature.	48
Figure 4.5	Neptunium dissolution simulation as a function of pH and f_{CO_2}	50
Figure 4.6	Neptunium dissolution simulation with percolating water (pH = 7.5~8.5) in WP.	51
Figure 4.7	Plutonium dissolution simulation as a function of pH and f_{CO_2}	52
Figure 4.8	Speciation results of uranyl carbonate species with UZ pore water.....	56
Figure 4.9	Speciation results of uranyl hydroxide species with UZ pore water.	56
Figure 4.10	Speciation results of neptunium aqueous species with UZ pore water.	57
Figure 4.11	Speciation results of plutonium aqueous species with UZ pore water.....	57
Figure 4.12	Breakthrough curves of total uranium species at 20 km south boundary.....	62
Figure 4.13	Breakthrough curves of neptunium species at 20 km south boundary.....	62
Figure 4.14	Breakthrough curves of plutonium in alluvium aquiferspecies at 20 km south boundary	63
Figure 4.15	Uranium sorption activity within transport processes.	64
Figure 4.16	Comparison of uranium breakthrough curves w/o sorption.	65
Figure 4.17	Comparison of uranium breakthrough curves w/o stagnant zone.	65
Figure 4.18	Neptunium sorption activity within transport processes.	66
Figure 4.19	Comparison of neptunium breakthrough curves w/o stagnant zone.	67
Figure 4.20	Plutonium sorption activity within transport processes.....	68
Figure 4.21	Comparison of plutonium breakthrough curves w/o sorption.....	68
Figure 4.22	Comparison of plutonium breakthrough curves w/o stagnant zone.	69
Figure 4.23	Comparison of breakthrough curves of uranium at different flow velocity in volcanic aquifer.	72
Figure 4.24	Comparison of breakthrough curves of uranium at different flow velocity in	

	alluvium aquifer.....	73
Figure 4.25	Comparison of breakthrough curves of neptunium at different flow velocity in volcanic aquifer.....	73
Figure 4.26	Comparison of breakthrough curves of neptunium at different flow velocity in alluvium aquifer.....	74
Figure 4.27	Comparison of breakthrough curves of plutonium at different flow velocity in volcanic aquifer.....	75
Figure 4.28	Comparison of breakthrough curves of plutonium at different flow velocity in alluvium aquifer.....	75
Figure A.1	Input File for Dissolution and Speciation Simulations of Neptunium.	81
Figure A.2	Input File for Transport Simulation of Uranium.	84

ACKNOWLEDGEMENT

I would like to thank the Department of Energy for funding this project through the Harry Reid Center for Environmental Studies at University of Nevada Las Vegas (UNLV). I would also like to thank the numerous individuals who provided the necessary support and guidance to make my study possible.

I sincerely thank and acknowledge my advisor Dr. Zhongbo Yu for his guidance, criticism, and encouragement throughout this course of study. Also, I really appreciate my thesis committee, Dr. Nicholl, Dr. Jiang, and Dr. Li for their support and input on my thesis.

I wish to thank QA supervisors on this project, Amy Smiecinski, Terry Mueller, Julie Berboil, and Dr. James Cizdziel for their patient instructions with the quality assurance review as well as technical review on my scientific notebook and final model report of this project.

Finally, thanks to my parents. They have provided long-distance love and support throughout.

CHAPTER 1

INTRODUCTION

The U.S. Department of Energy (DOE) has selected Yucca Mountain (YM), Nevada, to be the permanent site for a geological repository of spent nuclear fuel (SNF) and high-level radioactive waste (RW). The decision was based on the following factors. The area has an arid climate under which small amount of available water would limit the potential transport of radionuclides in the subsurface, and also extend the life of the canisters used to house the waste. The regional hydrogeologic system is within an enclosed basin without any surface or subsurface discharge to oceans, by which the risk of radioactive leakage can be constrained within a specific region. Also, there is a thick unsaturated zone (UZ) at YM with water table at depth of approximately 500 to 700 m (about 2000 feet) below the surface (BSC, 2004c; Bodvarsson, et al, 1998). This is an ideal condition for the geologic disposal of RW. The long distance and partially filled pores provide numerous resting places for any percolating water slowing its descent to the water table. This would effectively extend the radionuclide transport time before reaching the groundwater table. In addition, the factor of sparse population in the area could minimize any potential impact of radioactive contamination.

RW package or canisters, located in the UZ are thought to be in a reducing environment (BSC, 2004b). However, the oxygen-bearing percolating water from precipitation might penetrate into the package and then dissolve the radionuclides

from the package. The dissolved radionuclides may transport with percolating water through the UZ to reach the groundwater table, and then travel along potential groundwater flow paths to reach the accessible environment. For this reason, the saturated zone (SZ) acts as a natural barrier that provides a transport time delay and contaminant concentration dilution (CRWMS M&O, 2000a). Therefore, the simulations of geochemical reactions and radionuclide transport are of paramount importance in quantifying the risk of contamination to the ecosystem safety. Processes relevant to the performance of the SZ barrier at YM region are described conceptually in Figure 1.1.

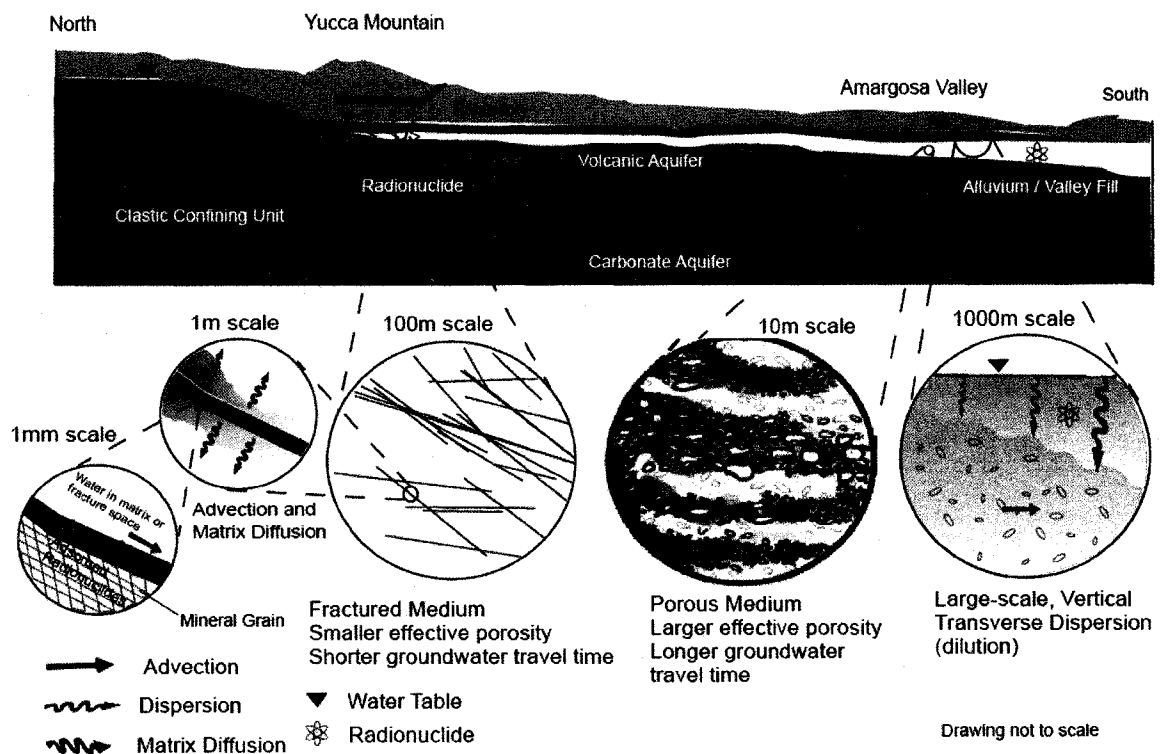


Figure 1.1. Schematic cross-section of Yucca Mountain saturated zone (including volcanic tuffs and alluvium) (modified after BSC, 2004a).

1.1 Radionuclides of Concern and Previous Work

There are a number of fission products of highly active radionuclides such as ^{137}Cs and ^{90}Sr and of long half-life such as ^{99}Tc , (200,000 years); ^{129}I , (1.6×10^7 years) in SNF. Actinides and their daughter products account for most of the radiotoxicity of nuclear wastes after the first 500 years of disposal (Ewing, 1999). Uranium makes up 95.6% of SNF. In SNF, the main sources of radioactivity from the time scale of 1,000 to 10,000 years are americium and plutonium isotopes (Langmuir, 1997). From the time scale of 10,000 to 100,000 years, neptunium-237 contributes the most to radioactivity (Langmuir, 1997). Even with an initial neptunium concentration of less than 0.03%, it will increase with time due to the radioactive decay of ^{241}Am , which has a half-life of 432 years (Kaszuba and Runde, 1999). Also, neptunium has a relatively high solubility and a low sorption rate. Both neptunium and plutonium have a relatively longer half-life compared to other radionuclides, with 2.14×10^6 years and 2.41×10^4 years, respectively. After hundreds of years, radiotoxicity is dominated by neptunium-237 and plutonium-239 in SNF (Ewing, 1999). Thus, a major part of the long-term (about first one million years) risk is directly related to the fate of these two actinides in the geosphere.

Consequently, the radionuclides of interest in the study include uranium, neptunium, and plutonium, because they would influence the long-term system performance of a RW repository. These three radioactive elements are redox-sensitive with two or more oxidation states in the natural environment (CRWMS M&O, 2000c; Kaplan et al., 2001; Murphy and Shock, 1999; Kaszuba and Runde, 1999; Langmuir, 1997). The different valence states of these elements determine their geochemical properties, such as solubility, speciation, and migration behaviors (Waite et al., 1997).

Many studies on the radionuclide solubility within the RW repository and migration in the groundwater system had been conducted in the last two decades (OCRWM, 2003a; BSC, 2003d; Davis and Curtis, 2003; Fjeld et al., 2003; Glynn, 2003; Windt et al., 2003; Runde et al., 2002; Pirlet, 2001; Kaszuba and Runde, 1999; Viswanathan et al., 1998; Efurud et al., 1998). Windt et al. (2003) simulated uranium dioxide (UO_2) dissolution in an underground waste disposal site with three reactive transport models, including CASTEM, CHEMTRAP, and HYTEC, as an inter-comparison study. OCRWM (2003a) calculated the solubility limits of 14 actinide elements within waste package by using the computer program EQ 3/6. Glynn (2003) used a 1-D numerical transport model to demonstrate the effects of speciation and sorption reactions for neptunium and plutonium in the groundwater system. It would be better to have a study consider different aspects including solubility and speciation, as well as transport processes from repository to an accessible environment. In this study, PHREEQC (Parkhurst and Appelo, 1999), a geochemical model, is used to evaluate the mineral solubility within RW packages, aqueous speciation in the UZ, and transport processes in groundwater for three radionuclides: uranium, neptunium, and plutonium. The description of PHREEQC is presented in Section 3.1.

Since YM has been selected for the storage site of radioactive wastes, assurances must be made that the materials escaping from engineered and natural barriers and migrating to the accessible environment from the repository would not exceed the regulatory limits. Thus, the retardation of radionuclide movement and dilution of radionuclide concentrations during migration need to be evaluated. These processes depend on the geological media, hydrologic settings, and aqueous species of

radionuclides after dissolution. To determine the aqueous speciation, initial conditions of solid dissolution are necessary noting that the initial conditions depend on the solubility of radionuclide secondary minerals. Groundwater in the SZ is the primary medium through which most dissolved radioactive species might move away from the potential repository (CRWMS M&O, 2000b).

Solid dissolution, aqueous speciation, and solute transport in groundwater are a sequence of migration steps starting from waste package, through the UZ, thereafter enter the SZ, and finally reach the accessible environment. The major role of the SZ, a mechanic barrier as well as a chemical buffer, is to delay the transport of radionuclides to the breakthrough boundary and reduce the concentration of radionuclides at the accessible environment. Therefore, the radionuclide transport along with dissolution and speciation are the focal point of this study.

1.2 Objectives

The specific objectives of this study are: (1) to further understand chemical properties of three radioactive elements (^{239}Pu , ^{237}Np , and ^{238}U); (2) to evaluate the dissolution control for different radionuclide minerals within the RWP and calculate their dissolution concentration with zero saturation index (SI); (3) to select major chemical reactions with reasonable thermodynamic data and calculate aqueous speciation of dissolved species; (4) to simulate radionuclide transport along the potential groundwater flow path; and (5) to conduct analysis on how chemical mixing, sorption, flow velocity, and flow condition could affect the radionuclide transport in the SZ.

The thesis is organized in the following format. Chapter 2 introduces related background information, including background information of nuclear waste and study site. Chapter 3 describes the research methodology on how to design various components of the model for geochemical and transport simulation of three radionuclides. Chapter 4 presents the simulation outputs, and discusses the simulated results, whereas Chapter 5 summarizes the major findings in this study.

CHAPTER 2

BACKGROUND INFORMATION

In early 1960s, the Nuclear Waste Policy Act made the DOE responsible for finding a suitable site for building and operating an underground disposal facility or repository site. In 1983, the DOE selected nine locations in six states as potential repository sites (OCRWM, 2004). In 1987, Congress amended the Nuclear Waste Policy Act and directed DOE to study YM only. The characterization study of YM had already started in the early 1980s with a combination of approaches, including surface exploration, drilling of deep boreholes, laboratory experiments, and computer modeling activities. Most studies showed satisfactory results considering two principal factors, which are retardation of radionuclide movement and dilution of radionuclide concentrations during migration. The facility may accept wastes as early as in 2010 (OCRWM, 2004).

2.1 SNF and Chemical Properties of Selected Radionuclides

2.1.1 Information about SNF

Spent Nuclear Fuel (SNF) is the radioactive by-product of electric power generation at commercial nuclear power plants. RW is the waste material containing radioactive chemical elements, which do not have a practical purpose (ORCWM, 2004). Most of RW is the product of nuclear process, such as nuclear fission. The high-level RW arises from

the use of uranium fuel in a nuclear reactor. It contains the fission products and transuranic elements generated in the reactor core. SNF from nuclear power plants to be disposed on the potential repository is largely in the form of UO_2 (CRWMS M&O, 2000c).

The high-level RW at YM will include two types of SNF. One contains commercial SNF (CSNF), which contains more than 90% of the planned waste inventory, and the other, called co-disposal packages, contains defense SNF and high-level waste glass that makes up the remainder. The waste glass is composed of crystalline ceramics, cement, and vitrified glass created from the mixture of glass frit, radioactive liquid, and radioactive salt wastes (Wronkiewicz and Buck, 1999). Both CSNF and high-level waste glass are characterized by a high concentration of radionuclides, especially the radioactive actinide elements. About three thousand tons of commercial SNF were in storage at power reactors in 1995 and this amount will be more than double by 2010 (Wronkiewicz and Buck, 1999). For this purpose, YM was designed to hold 70,000 tons of waste.

2.1.2 Uranium

Uranium-235, No. 92 element in the periodic table of chemical elements, is one of the naturally occurring radioactive elements. Natural uranium contains three isotopes ^{238}U (99.3%), ^{235}U (0.72%), and ^{234}U (negligible amount). Some other relatively short-lived isotopes can be obtained artificially by various nuclear reactions. Isotope ^{235}U is capable of fission, which makes it valuable as a fuel in nuclear reactors used to generate electricity and for use in national defense. The half-life of ^{235}U is 7×10^8 years.

Murphy and Shock (1999) concluded that the tetravalent form of uranium has a relatively low solubility because the concentration is limited by mineral phases such as uraninite and coffinite; the hexavalent form is soluble as the uranyl ion (UO_2^{2+}) and its complex. This means that the solubility of uranium may increase many orders of magnitude from reducing conditions to the oxidizing conditions. The transport of uranium is greatly enhanced if it is present in solution as UO_2^{2+} .

The distribution of aqueous species of uranium can be highly dependent on chemical conditions, especially pH value and concentrations of complexing ligands, such as carbonate ions and calcium. In natural water, important complexing ligands for U(VI) include hydroxide, carbonate and dissolved organic carbon. These ligands may compete with adsorption sites for the complexation of UO_2^{2+} , and decrease adsorption capability through the formation of nonadsorbing aqueous complexes (Davis and Curtis, 2003). Under YM conditions, the most important ligands for uranium are OH^- and CO_3^{2-} . In the more oxidizing regions of uraninite (UO_2) stability, the solution species in equilibrium with the U(IV) solid can be a U(VI) solution species, either a uranyl hydroxide species or a carbonate species (Langmuir, 1997). Important uranyl solution species under YM groundwater (UE-25, J-13) include, with increasing importance with pH value, UO_2^{2+} , UO_2OH^+ , UO_2CO_3 , $(\text{UO}_2)_2(\text{CO}_3)(\text{OH})_3^-$, $\text{UO}_2(\text{CO}_3)_2^{2-}$, and $\text{UO}_2(\text{CO}_3)_3^{4-}$ (CRWMS M&O, 2000c).

2.1.3 Neptunium

Neptunium-237, No. 93 element in the periodic table of chemical elements, is the first artificially synthesized transuranium element. It is considered to be the largest contributor to the radioactivity of a radioactive waste repository at times between 10,000 to 100,000

years (CRWMS M&O, 2000c). Also neptunium is environmentally mobile due to the high solubility and low sorption affinity (Runde et al., 2002; Kumata et al., 1998).

In natural water, Np(IV) is expected to be the dominant oxidation state under reducing conditions, while Np(V) is the dominant oxidation state in oxidizing waters (Katz et al., 1986). The oxidizing conditions are generally expected to prevail in the UZ as well as SZ at YM. Np(V) tends to be stable as NpO_2^+ under a wide range of environmental conditions because of its high solubility and low sorption affinity. Therefore, Np(V) is considered to be the most mobile actinide species (Runde et al., 2002). As shown in Viswanathan's work (1998), in contrast to the strong influence of pH on sorption and solubility, simulations performed over a range of bicarbonate concentrations measured in the pore fluids indicated that bicarbonate concentration does not significantly affect neptunium migration.

Actually, there are many factors that could affect the sorption and solubility behavior of neptunium. When contacting with solids, the mobile concentrations of radionuclides are usually several orders of magnitude lower than those only with natural groundwater because of the very high sorption capacity on the environmental materials such as different kinds of rocks or clays. The geochemical processes that strongly affect ^{237}Np migration include: (1) the solubility-limitation that influences the release of ^{237}Np , (2) the aqueous speciation of neptunium into non-sorbing carbonate or hydroxyl complexes (Viswanathan et al., 1998), (3) the sorption of NpO_2^+ , and (4) radioactive decay.

2.1.4 Plutonium

Plutonium-239 is the No. 94 element in the periodic table of chemical elements. At present, 15 isotopes of plutonium are known. The most important and easily accessible

isotope is ^{239}Pu with a half-life of 24,110 years, decaying to ^{235}U . Plutonium is a priority radionuclide in the waste package, because a large quantity exists in the radioactive waste inventory. Also in the oxidized form, it can be quite mobile.

Unlike most metal cations, plutonium can exist in multiple oxidation states simultaneously. The III, IV, V, and VI states of plutonium are readily attainable under environmentally relevant conditions (CRWMS M&O, 2000c). The main speciation reactions involved with plutonium in the groundwater system are hydrolysis, and those that involve carbonate minerals. Specific reactions are highly dependent on the plutonium valence state and aqueous pH value (Skipperub et al., 2000). Actual plutonium concentrations in solution are further complicated due to the redistribution of oxidation states through disproportionation.

In the solution phase, dilute plutonium solution expected in the environment is likely to have a distribution of oxidation states dominated by +4 oxidation state (CRWMS M&O, 2000c). The tendency of Pu (IV) to hydrolyze is extremely strong, which leads to the formation of radio-colloids at neutral pH values and also a high concentration of plutonium that is approximately greater than 10^{-7} M (Nitsche et al., 1993). Additionally, all oxidation states of plutonium form strong carbonate complexes even at a relatively low total carbonate concentration (10^{-2} M) (CRWMS M&O, 2000c) and when pH value is greater than 5.

Some conclusions were drawn in the Westinghouse Savannah River Site by Kaplan (2001): (1) the presence of two plutonium (IV and V) species with distinctly different mobilities, (2) a decrease in mobility with increasing pH for both species, and (3) a decrease in fractional recovery with increasing pH for the more mobile species.

2.2 Study Site

YM is located at the southwest side of Nevada Test Site (NTS) in southern Nevada (Figure 2.1). The NTS is a DOE reservation located in Nye County, Nevada, about 65 miles (105 km) northwest of the City of Las Vegas (latitude: 37°07' N, longitude: 116°03' W) (OCRWM, 2004). It was established on January 11, 1951 for the testing of nuclear weapons and composed of approximately 1,350 square miles (3,500 km²) of desert and mountainous terrain.

2.2.1 Climate at Yucca Mountain

The central region around the NTS and Yucca Mountain has been viewed as a transition desert, and represents a combination of two kinds of climates. The northern part of this region is characterized with warm, dry summers and cold, dry winters while the southern part of the region has hot, dry summers and warm, dry winters (CRWMS M&O, 2000c).

Annually, YM receives an average of 7.5 inches (0.19 m) of rainfall. About 95% of the precipitation evaporates, runs off of the mountain, or is absorbed by vegetation. Average annual lake-evaporation values range from about 1.1 m (43 inches) in the north to more than 2 m (79 inches) in Death Valley (CRWMS M&O, 2000c). Only about 5% of average rainfall actually penetrates the ground (BSC, 2004c).

The precipitation in this region determines the quantity of infiltration, which is the very source of percolation flux in the UZ and provides the water flow as mechanic source for transport (BSC, 2004b). Based on the research of Flint et al. (1996), during an average precipitation year, the net infiltration ranges from zero, where alluvial thickness is 6 m (20 ft) or more, to more than 80 mm/yr (3.1 in/yr) where thin alluvium overlies

highly permeable bedrocks on north facing slopes at high elevation (CRWMS M&O, 2000a). The averaged net infiltration is 4.5 mm/yr over the study area. This is the force that may move radionuclides from the repository through the UZ to the water table. However, the net infiltration is spatially and temporally variable based on the nature of the storm event.



Figure 2.1. Map of study site at Yucca Mountain.

2.2.2 Geologic and Hydrogeologic Setting of Saturated Zone

Groundwater flow in the SZ is largely controlled by the distribution of rock types and their respective permeabilities and storativities. CRWMS M&O (2000a) classified the rocks and deposits of the Death Valley region into 10 hydrogeologic units (from the surface downward), including Quaternary Playa Deposits, Quaternary-Tertiary Valley Fill, Quaternary-Tertiary Volcanic Rocks, Tertiary Volcanic Rocks, Tertiary Volcanic and Volcaniclastic Rocks, Tertiary-Late Jurassic Granitic Rocks, Mesozoic Sedimentary and Meta-volcanic Rocks, Paleozoic Carbonate Rocks, Paleozoic-Precambrian Clastic Rocks, Precambrian Igneous and Metamorphic, listed in Figure 2.2 by the name of formations in accordance with aquifers and confining units. Each of these hydrogeologic units has considerable lateral extent and reasonably distinctive properties (CRWMS M&O, 2000a). Some of the regional units are not included because they are not present in the study area, and some of the regional units are subdivided into additional units by the United States Geological Survey (USGS).

The following descriptions are the eight principal aquifers and confining units based on the classification by CRWMS M&O (2000a):

Basin Fill Aquifer - This aquifer underlies most of the Amargosa Desert area to the east and south of YM. It is composed of alluvial fan, lakebed, and mudflow deposits, and has a thickness of hundreds of meters. This aquifer is the main water source for domestic and irrigation uses in the Amargosa Valley.

Upper Volcanic Aquifer - The Topopah Spring unit of the Paintbrush Tuff is the uppermost water-bearing unit of the SZ and is the upper volcanic aquifer in the YM area. It consists of variably welded ash-flow tuffs and rhyolite lavas (nonwelded tuffs).

Upper Volcanic Confining Unit - This confining unit consists of rhyolitic lavas, volcanic breccias and nonwelded to welded tuffs, and usually is argillaceous or zeolitic.

Lower Volcanic Aquifer - This aquifer consists of variably welded ash-flow tuffs and rhyolite lava. This aquifer underlies YM, but tends to produce less water than the upper volcanic aquifer.

Lower Volcanic Confining Unit - This confining unit consists of nonwelded and commonly zeolitized units of the Lithic Ridge Tuff.

Older Confining Unit - In areas where the upper carbonate aquifer is not present, such as in the YM area, the older confining unit consists of the lowermost part of the volcanic sequence and the uppermost part of the pre-Cenozoic sequence.

Carbonate Aquifer – The upper and lower carbonate aquifers have been identified regionally and the upper carbonate aquifer (a limestone aquifer) may not be present at YM. The unit of upper carbonate aquifer consists of low permeability siliceous siltstone, sandstone, quartzite, conglomerate, and limestone. The unit of lower carbonate aquifer consists of Paleozoic dolomite and limestone.

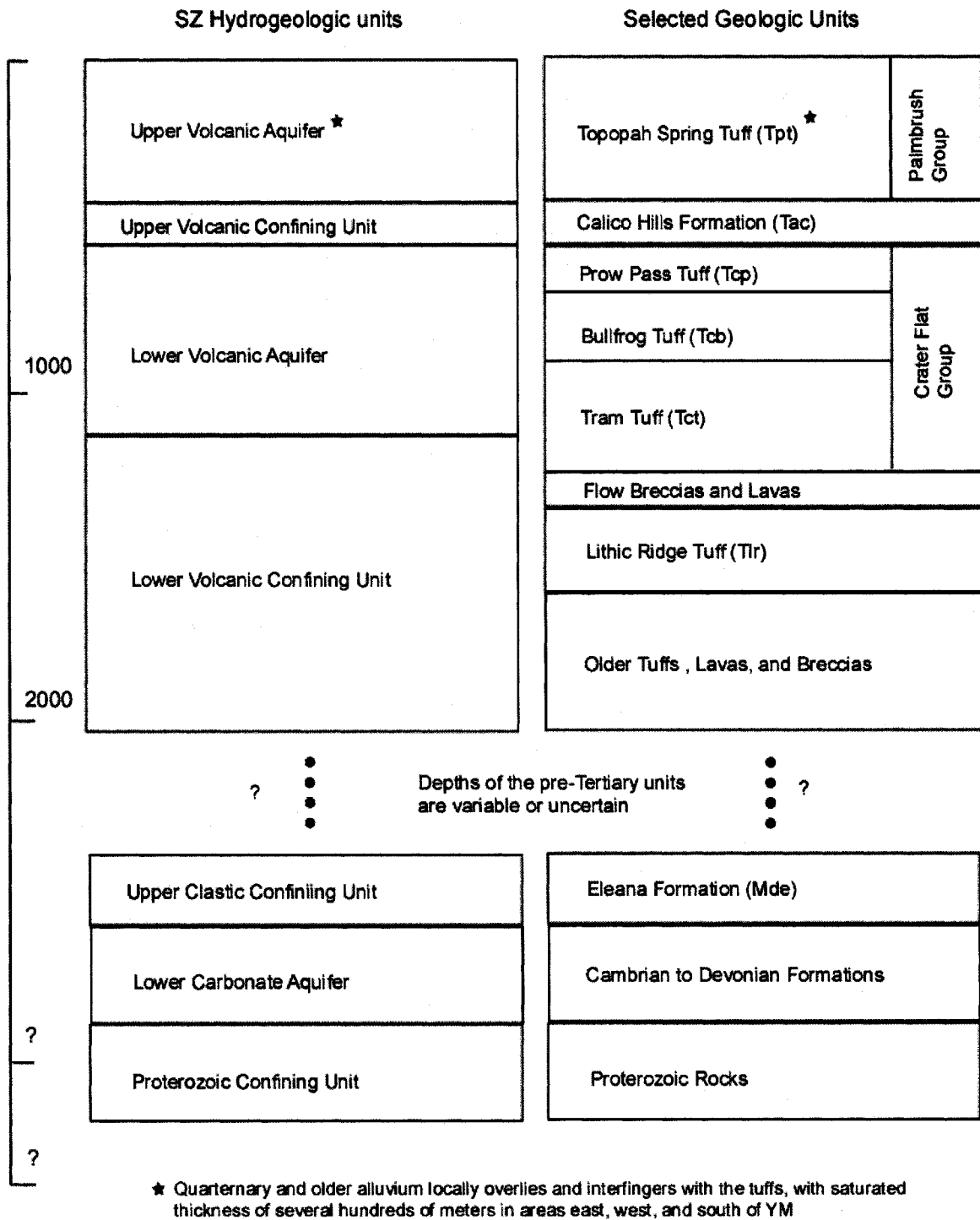


Figure 2.2. Schematic chart of major hydrogeologic and geologic units (edited from Eddebarha et al., 2003).

To better understand radionuclide transport along the groundwater flow path, a batch of information is needed to accomplish the work, including the geochemical properties of groundwater, information about aquifers, and potential groundwater flow paths. For the radionuclide part, the chemical properties of important radionuclides, their dissolution and aqueous speciation in percolating water, and their transport properties within different aquifers are necessary. This information will be elaborated in related sections later.

2.2.3 Regional Groundwater and Flow Paths

The groundwater table at YM is located 300 to 400 m beneath the RW repository. The SZ in YM belongs to the Death Valley regional groundwater flow system. Recharge within the flow system occurs at high elevations where relatively larger amounts of snow and rainfall occur, including Timber Mountain, Pahute Mesa, Rainier Mesa, Shoshone Mountain, and YM, while the discharge occurs at the Death Valley flow system including Ash Meadows, Oasis Valley, and Death Valley (Figure 2.1) (BSC, 2004b; CRWMS M&O, 2000a). In addition to natural discharge, groundwater has been withdrawn from the aquifers in the Death Valley regional groundwater basin for various domestic, agricultural, industrial, and government purposes over the last several decades (BSC, 2003a).

Determined by the potentiometric surface map, groundwater flow direction in the aquifer underlying YM is generally from the north to the south. A proper method to determine the likely flow path is by identifying areas that had similar concentrations of conservative chemical species (e.g., chloride or sulfate) and tracing paths through these chemically similar areas in a down-gradient direction (CRWMS M&O, 2000a). The

calibrated site-scale flow model and the particle-tracking capability of Finite Element Heat and Mass Transfer Code (Zyvoloski et al., 1997) showed that one hundred particles were distributed uniformly over the area of the repository and they were allowed to migrate until reaching the model boundary (BSC, 2003a). The pathways leave the repository toward the south-southeastern direction to approximate 20 km compliance boundary shown in Figure 2.3.



Figure 2.3. Predicted groundwater flow path by particle-tracking method (BSC, 2003a).

Groundwater flow in the SZ is controlled largely by the distribution of rock types and their respective permeabilities and porosities (Eddebbarha et al., 2003). Faults, shears, and joints in welded tuffs form a network of fractures that provide pathways for water movement through the rock mass both above and below the water table (Paces et al., 2002). The properties of partly welded tuffs that affect groundwater flow vary between those of fractured, welded tuffs and those of altered, nonwelded tuffs. Where interconnected, fractures can easily transmit water, and highly fractured units function as aquifers (CRWMS M&O, 2000a). The groundwater flow path from water table beneath the repository to the accessible environment is conceptualized from volcanic tuffs to alluvium, which will be described in detail in Section 3.2. The flow path transition affects the contaminant transport properties in both volcanic tuffs and alluvium (see detail in Section 4.4).

2.2.4 Geochemistry of Unsaturated Zone and Saturated Zone

The composition of infiltrating water at the top of the model domain is assumed to be the same as the initial fracture and matrix pore-water composition above the WP, with the exception of minor changes of pH value (7.5~8.5). The water reflects a higher CO₂ partial pressure and a lower temperature at the top. In this study, the pore water samples, which were derived from Exploratory Studies Facility (ESF), ESF-HD-PERM-2 and 3 (serial number for boreholes in ESF) are used as representative for percolating water above RWP and implemented as initial solution for solubility simulations.

After a long travel time in the UZ, the water composition is determined by rock-water interactions. The water samples from UZ #16 (OCRWM, 2001) (Figure 2.4) are selected to be representative for UZ pore water below RWP. Ten samples of UZ #16 from the

depth of 290 to 414 m are selected and averaged to implement in the speciation simulations. The compositions of these solutions are listed in Table 2.1.

The hydrochemistry of the SZ at YM controls the dissolution and speciation of radionuclides in the groundwater and, hence, their transport characteristics. Based on the regional-scale groundwater chemistry, there are two basic types of water: a relatively dilute sodium-bicarbonate water of high silica content associated with volcanic rocks and derivative sediments, and a more concentrated calcium-magnesium-bicarbonate water of low silica content associated with carbonate rocks. A water of calcium-magnesium-sodium-bicarbonate composition commonly results when these two basic rock types are mixed (CRWMS M&O, 2000b). The conceptual model as well as evidence of different types of water mixing in alluvial valley fills will be illustrated in Section 3.5.

Table 2.1. Chemical compositions of solutions used in all simulations (BSC, 2005; BSC, 2004a; BSC, 2003a; OCRWM, 2001).

	Solution I	Solution II	Solution III	Solution IV	Solution V
Description	UZ pore water above repository	UZ pore water below repository	Groundwater in volcanic aquifer	Groundwater in alluvium	Groundwater in carbonate aquifer
Na ⁺ (mg/L)	61.5	72.5	45	91.5	150
Ca ²⁺ (mg/L)	101	22	13	3.7	100
Mg ²⁺ (mg/L)	17	8.4	2	0.31	39
K ⁺ (mg/L)	8.0	N/A	5.3	3.7	12
Cl ⁻ (mg/L)	117	44.2	7.1	6.1	28
SiO ₂ (mg/L)	70.5	62.1	61	22	64.2
HCO ₃ ⁻ (mg/L)	200	171	130	189	694
SO ₄ ²⁻ (mg/L)	116	23.6	18.4	22	160
NO ₃ ⁻ (mg/L)	6.5	21.7	N/A	N/A	N/A
F ⁻ (mg/L)	1.0	N/A	2.2	2.0	N/A

Samples from UE-25 J-13 is selected to be representative groundwater within volcanic aquifer and used in SZ transport simulations. Sample from NC-EWDP-19D is selected to be representative groundwater within alluvial aquifer. Sample from UE-25 p#1 is selected to be representative of carbonate water that flows up into the alluvial aquifer. The locations of wells are shown in Figure 2.4.

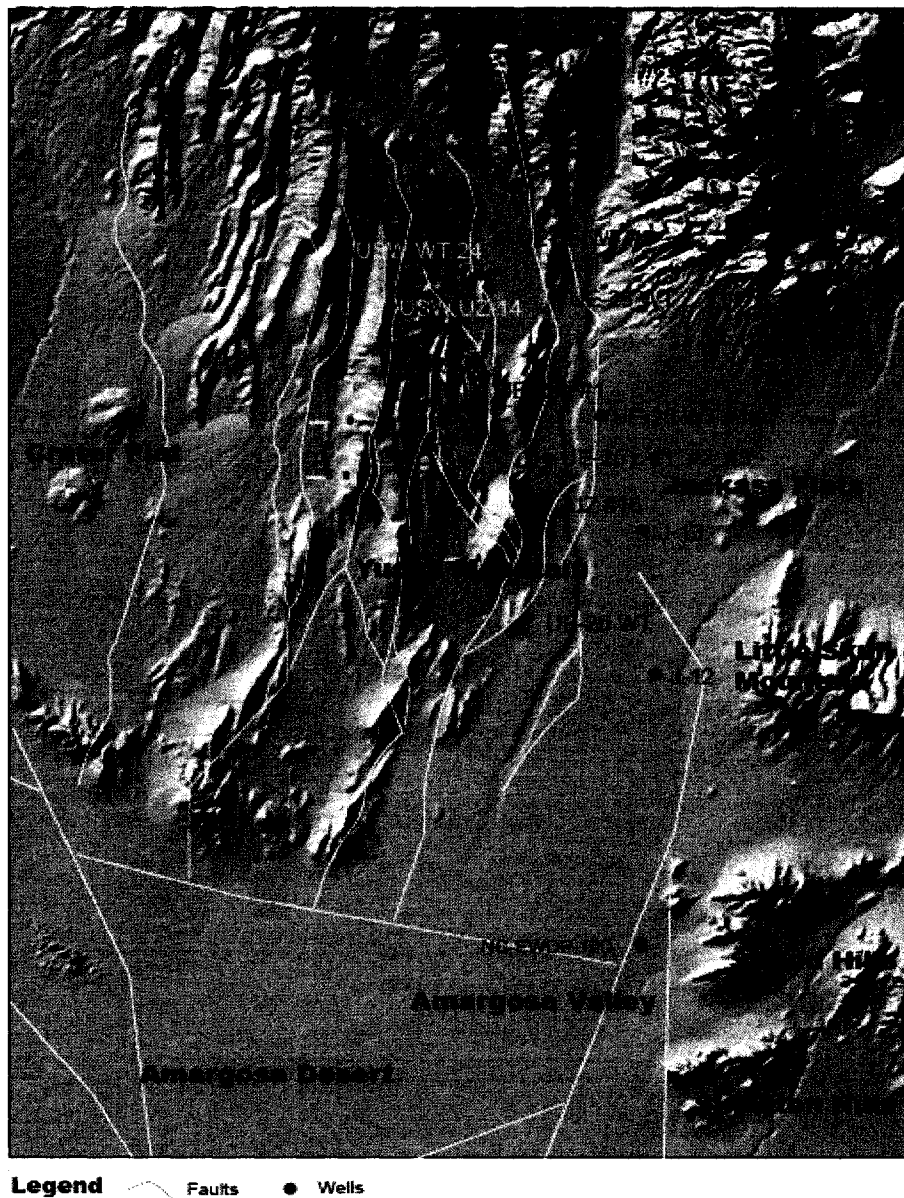


Figure 2.4. Major geological structures and well locations (background map is edited from BSC, 2003a).

CHAPTER 3

METHODOLOGY

After percolating water penetrates into the RWP, the dissolved radionuclides are expected to form a series of complex alteration phases or secondary minerals, and then undergo re-precipitation and re-dissolution throughout the canisters. Some of the dissolved phases may leave the waste packages and enter the UZ. Traveling through the UZ, the dissolved radionuclide species lead to a series of chemical reactions, such as hydrolysis, reactions with carbonate ligands over a range of pH values and so forth. Transported by percolating water, radionuclides might migrate into the SZ below the repository site through fractured volcanic tuffs toward the south/southeast. Leaving volcanic tuffs while enters porous media of alluvial aquifer, the groundwater flow couples with kinetic reaction of sorption and stagnant zone to undergo the retardation and reduction of contaminant concentration. The vertical flow occurs between alluvial aquifer and carbonate aquifer underlie the alluvium fills. Finally, the radionuclides reach the southern boundary of the study area. The schematic flow chart of simulation procedures is shown in Figure 3.1.

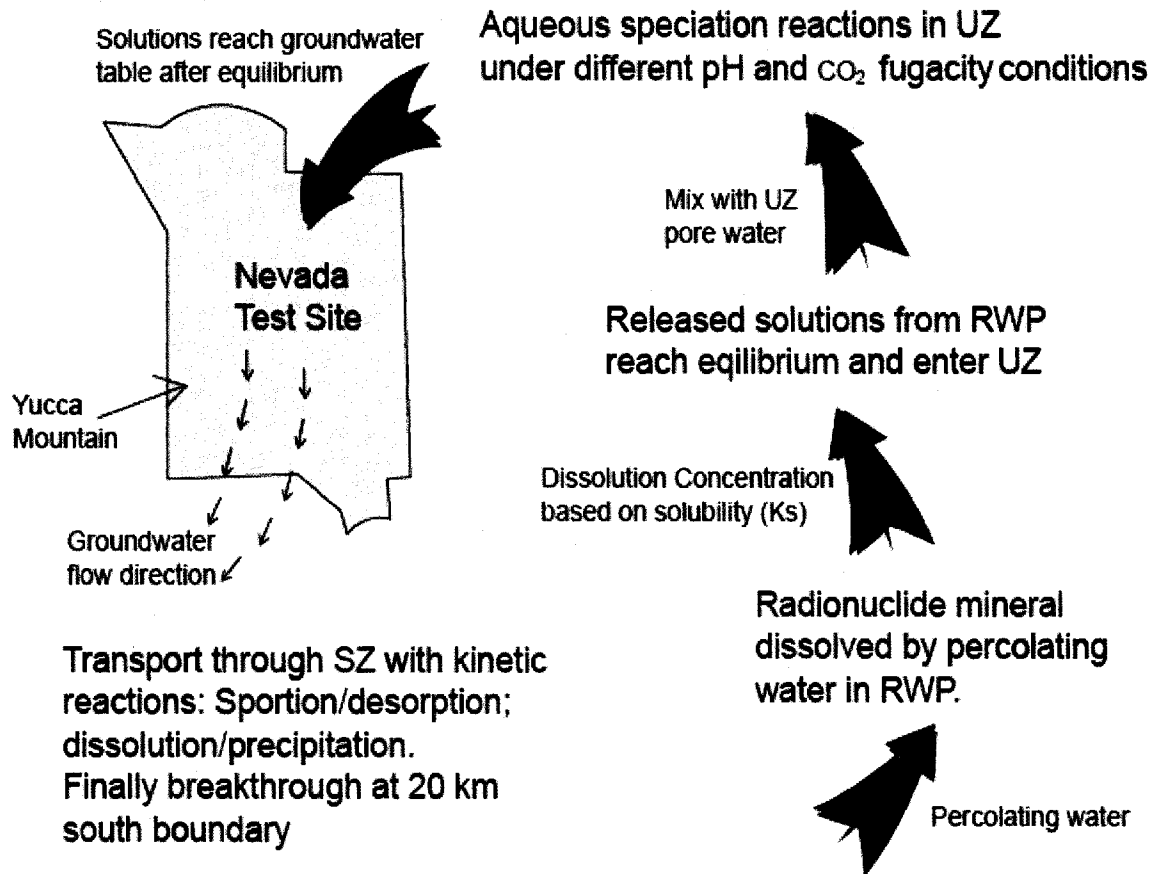


Figure 3.1. Schematic flow diagram of modeling stages of radionuclides.

3.1 Modeling Approach

To complete various modeling stages described above, a geochemical model introduced in next section is used to conduct three major simulations, which are described as follows.

Solid dissolution – when contacting with percolating water, radionuclides in the disposal repository will gradually degrade to less complex minerals. Even small quantity and sparse spatial distribution, the oxygen-bearing water reacts with the minerals and causes dissolution. When the dissolution reactions reach equilibrium, a certain amount of

radionuclides will be dissolved into solution with various aqueous species according to solubility constants (K_s).

Solution and speciation - solutions of dissolved radionuclide species migrate from the RWP and mix with pore water in the UZ, which provokes new speciation reactions. This step of simulation calculates the aqueous speciation of these dissolved species when equilibrium by mixing Solution I with Solution II. The results include each predominant species and understanding of chemical properties based on the pore water composition in the UZ.

Solute transport - the transport processes of radionuclides within the volcanic and alluvial aquifers (BSC, 2003b) are simulated along with the calculation of kinetic reactions at each time step. The simulation includes: (1) one dimensional advection of groundwater; (2) advection, diffusion, and dispersion of radionuclides in groundwater; (3) sorption/desorption of radionuclide species onto porous alluvium; and (4) precipitation/dissolution of secondary phase minerals during migration.

As showed in Figure 3.1, the simulation of solid dissolution is the second red arrow from the bottom. As a consequence, the third arrow at right-up corner represents solution and speciation simulation; the last arrow indicates solute transport simulation.

3.2 Description of PHREEQC

The acronym PHREEQC (Parkhurst and Appelo, 2000) stands for PH (pH value), RE (redox), EQ (equilibrium), and C (program written in C language). It is a family of software products originated in the late 1970's and was developed by the USGS. PHREEQC (V2.3 and V2.11) contains capabilities such as speciation-solubility and

kinetically controlled reaction pathway features, which are found in many geochemical software packages, but also includes surface complexation, ion exchange, absorption and solid solutions, and a very versatile treatment of rate laws (BSC, 2004d). In addition, PHREEQC has features for transport simulation which can handle dispersion and diffusion in a double-porosity medium. It also has inverse modeling capabilities.

PHREEQC models the consequences of reactions in an aqueous solution with a set of reactants in accordance with equilibrium thermodynamics. It can also include kinetics laws through a BASIC interpreter coupled to the program. PHREEQC handles advective transport by moving aqueous solutions from one cell to the next, allowing the contents of each cell to reach equilibrium (or not) with the solids and surface features present in the cell. PHREEQC needs an input file in which the problem is specified via KEYWORDS and associated data blocks.

In this study, PHREEQC is used to perform a variety of low-temperature (around 25 °C) geochemical calculations. To specify, there are three major tasks of PHREEQC in this study. Firstly, calculate the dissolution concentration under a range of pH values and the CO₂ fugacity of uranium, neptunium, and plutonium minerals to understand their solubility and sensitivity of solubility; secondly, to calculate the aqueous speciation of hydroxides, carbonates, oxidants of three radioactive elements with mixed solution; and thirdly, to conduct the modeling of 1-D transport processes of radionuclides toward the accessible environment along the potential groundwater flow path with kinetic reactions calculated at each time step.

3.3 Solid Solubility of Uranium, Neptunium, and Plutonium

From the viewpoint of laboratory chemistry, solubility is defined as the concentration of a substance when the solution is saturated with that substance (Atkins, 1994). In other words, solubility is the concentration of a substance when the substance is at equilibrium (either stable or metastable) with the solution. For this case, the substance is a radionuclide-bearing solid. In practice, radionuclide-bearing minerals are always used to evaluate solubility (OCRWM, 2003a). Among several available radionuclide-bearing minerals in WP, one has a relative large composition as well as least solubility is defined as solubility-controlling solid.

Except for colloidal and kinetically transient phenomena such as over-saturation, solubility is “the maximum quantity of one phase dissolved by another under specified conditions. In the case of solutions of solids or liquids in liquids, the solubility is usually expressed as the weight (or mass) dissolved in a given weight (mass) or volume of the solvent at a specified temperate.” (Sharp, 1990) and a solubility-controlling mineral phase will set the limits.

An important criterion to evaluate the solution equilibrium is saturation index (SI), which is defined as the logarithm of the quotient of the ion activity product (IAP) and solubility product constant (K_{sp}). The IAP is derived from the activities that are calculated from analytically determined concentrations by considering the ionic strength, temperature, and complex formation. The solubility product is derived in the similar way as the IAP just using equilibrium solubility data corrected to the appropriate water temperature (Merkel and Planer-Friedrich, 2005). The equation of SI is defined as:

$$SI = \log \frac{IAP}{K_{sp}}$$

where IAP is ion activity product, and K_{sp} is solubility product constant.

The relevant thermodynamics controlling uranium solubility have been evaluated by many scientists. The dissolution reactions of uranium were examined in many tests conducted by Argonne National Laboratory (Wronkiewicz and Buck, 1999). An experiment which lasted eight years on UO_2 samples indicates that about 95% of the uranium species that released from a waste package during corrosion of the sample had subsequently precipitated back onto the sample surface, tested container, or in the corroded intergrain boundary regions. Most commonly uranium occurred in the form of dehydrated schoepite, which only consists of uranium from the sample, oxygen, and water (Wronkiewicz et al., 1992). The sequence of alteration phases on the sample surface within 3.5 years of reaction is shown in Figure 3.2.

The dissolution equations of uranium secondary minerals, including Na-boltwoodite, Soddyite, Schoepite, and Uranophane, are listed in Table 3.1, which are considered as solubility-controlling minerals of uranium and verified by many researchers (Wronkiewicz and Buck, 1999; Davis and Curtis, 2003; Windt, et al., 2003).

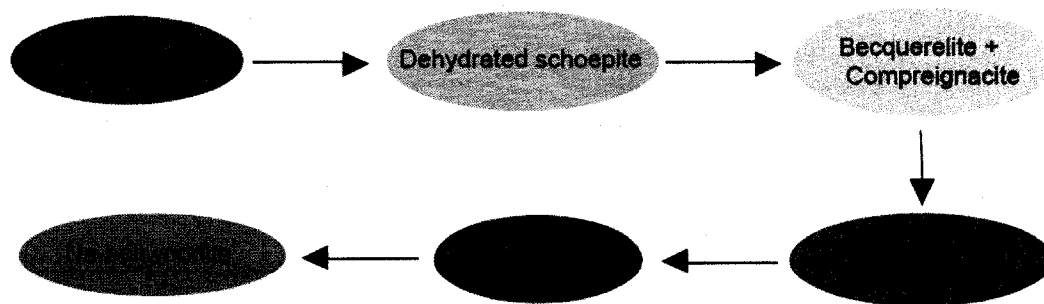


Figure 3.2. The paragenetic sequence of alteration phases on the top of sample in the experiment.

The solubility of neptunium is more complex than uranium. Several pure neptunium phases have been identified in neptunium solubility experiments, including Np_2O_5 , $\text{NaNpO}_2\text{CO}_3 \cdot x\text{H}_2\text{O}$, and NpO_2 . At the conditions relevant to the repository (oxidizing conditions and temperature from 25 to 90°C), the precipitates in solubility experiments are $\text{Np}_2\text{O}_5 \cdot x\text{H}_2\text{O}$ and $\text{NaNpO}_2\text{CO}_3 \cdot x\text{H}_2\text{O}$ (Efurd et al., 1998; Nitsche et al., 1993).

Theoretical calculations using different thermodynamic databases predict that the solubility controlling solid phase would be either a Np (IV) or Np (V) compound, depending on the redox state of the water. Based on the x-ray diffraction data and through further analyzing the stability field for Np(V) solid phases (Np_2O_5 , $\text{NpO}_2(\text{OH})$, and $\text{NaNpO}_2\text{CO}_3 \cdot 5\text{H}_2\text{O}$), Np_2O_5 is concluded as the solubility controlling phase in J-13 (Figure 2.4) well water under oxidizing conditions (CRWMS M&O, 2001). Also the EQ3NR geochemical model selected Np_2O_5 to be solubility-controlling solid (OCRWM, 2003a).

Evaluation of solubility data for the dissolution of plutonium dioxide (PuO_2) and tetrahydroxide ($\text{Pu}(\text{OH})_4$) in laboratory and natural waters shows that the selection of $\text{Pu}(\text{OH})_4$ as the solubility-controlling solid results in predicted steady-state plutonium concentrations that are not conservative and oxidation-state distributions are inconsistent with modeling calculations by Haschke and Bassett (2002). The observed co-existence of both crystalline and amorphous materials in experiments by OCRWM (2003a) can be explained with the aging of precipitates, which actually means more crystalline, less surface area per unit volume. Therefore, it appears that the solubility-controlling solids in those laboratory experiments are $\text{Pu}(\text{OH})_4$, which “age towards $\text{PuO}_2 \cdot x\text{H}_2\text{O}$ ” (CRWMS

M&O, 2001). The value of X could vary from 2 to 0. For X = 2, it is Pu(OH)₄, the amorphous end member. For X = 0, it is PuO₂, the crystal end member.

The crystalline phase has been formed within laboratory time scale (less than one year), so it is reasonable to expect that over geological time, plutonium hydroxides will convert to PuO₂ (crystalline) (OCRWM, 2003a). Therefore, PuO₂ would be used as the solubility-controlling mineral for plutonium in the solubility simulation.

In general, plutonium is approximately 3 orders of magnitude less soluble than neptunium and the pH value does not affect the solubility of plutonium as much as neptunium (Efurd et al., 1998). Another point is that Pu(OH)₄ has a high sorption rate onto the surfaces that limits the solubility of plutonium in natural water. The dissolution equations of plutonium and neptunium solubility-controlling minerals are also listed in Table 3.1. They are implemented into dissolution simulation to calculate concentration. The calculation results are used for the second step of modeling.

Table 3.1. Dissolution equations of principal alteration phases of uranium, neptunium and plutonium at 25 °C.

<i>Phase Name</i>	<i>Dissolution Equations</i>	<i>Log k</i>
Uranophane	$\text{Ca}(\text{UO}_2)_2(\text{SiO}_3\text{OH})_2 \cdot 5\text{H}_2\text{O} + 6\text{H}^+ = \text{Ca}^{2+} + 2\text{UO}_2^{2+} + 2\text{H}_4\text{SiO}_4 + 5\text{H}_2\text{O}$	11.69
Schoepite	$\text{UO}_3\text{H}_2\text{O} + 2\text{H}^+ = \text{UO}_2^{2+} + 2\text{H}_2\text{O}$	4.84
Na-boltwoodite	$\text{NaUO}_2\text{SiO}_3\text{OH} \cdot 1.5\text{H}_2\text{O} + 3\text{H}^+ = \text{Na}^+ + \text{UO}_2^{2+} + \text{H}_4\text{SiO}_4 + 1.5\text{H}_2\text{O}$	5.96
Soddyite	$(\text{UO}_2)_2\text{SiO}_4 \cdot 2\text{H}_2\text{O} + 4\text{H}^+ = 2\text{UO}_2^{2+} + \text{H}_4\text{SiO}_4 + 2\text{H}_2\text{O}$	6.03
PuO ₂	$\text{PuO}_2 + 4\text{H}^+ = \text{Pu}^{4+} + 2\text{H}_2\text{O}$	-1.02
Np ₂ O ₅	$\text{Np}_2\text{O}_5 + 2\text{H}^+ = 2\text{NpO}_2^+ + \text{H}_2\text{O}$	5.2

3.4 Speciation of Uranium, Neptunium, and Plutonium

The speciation refers to the form that one element is in the solution including aqueous complexes, redox species, free ions, colloidal, etc. When percolating water continues flowing through the waste container, the alteration phases of radionuclides, especially those on the bottom of a rod or package, would further be dissolved by water. The dissolved aqueous species would be carried by the percolating water toward rock matrices and fractures beneath the disposal repository. After leaking out of RWP and mixing with pore water in the UZ, the radionuclides undergo chemical reactions that allow some of the species become dominant in the solution while others are consumed.

In order to make the simulations most close to geochemical conditions in the UZ, the chemical compositions of ten pore water samples from UZ#16 (Figure 2.4) were selected. This pore water chemical component is used in all speciation simulations under equilibrium status.

When chemical species are transported in fracture waters at rates greater than the rate of equilibration with the rock matrix, disequilibrium will exist between waters in fractures and matrix. However, when the travel rates, no matter the waters in fractures or matrix, are much lesser than the rate of chemical reaction such as sorption and mineral precipitation, equilibrium will be achieved. In this model, the travel rate of groundwater as well as pore water in the UZ is much smaller than the rate of sorption or mineral precipitation/dissolution; therefore, we assume that the whole domain has reached equilibrium.

Wateq4f.dat in PHREEQC is the database file for running uranium speciation simulation. One valence state of uranium (VI) is applied and master species is defined as

UO₂²⁺ in the simulation. New species of uranium are generated based on the solution after solubility equilibrium and the solution of UZ pore water.

Since there is no built-in database for neptunium and plutonium in PHREEQC, their speciation reactions were entered manually through an input file. According to the chemical components of UZ pore water, close attention is paid to the reactions with hydrolysis and carbonate ligands of neptunium and plutonium in the speciation simulation. There are two valence states of neptunium studied: IV and V. The master species is defined as NpO₂⁺ (V) based on the neptunium solid dissolution reaction. Four valence states of plutonium studied (III, IV, V, and VI) are used in the simulation while the master species is defined as Pu⁴⁺ (IV). Table 3.2 shows selected speciation reactions of neptunium and plutonium.

The understanding of aqueous speciation of the dissolved species of those three radionuclides helps further the understanding of their transport properties. In the flow and contaminant transport section, the aqueous speciation reactions are also calculated at each time step.

Table 3.2. Speciation reactions of neptunium and plutonium at 25 °C.

Speciation Reaction Equations	Log k
$\text{NpO}_2^+ + \text{OH}^- = \text{NpO}_2\text{OH}$	2.7
$\text{NpO}_2^+ + 3\text{CO}_3^{2-} = \text{NpO}_2(\text{CO}_3)_3^{5-}$	5.37
$\text{Np}^{4+} + 4\text{H}_2\text{O} = \text{Np}(\text{OH})_4 + 4\text{H}^+$	-8.28
$\text{Pu}^{4+} + \text{H}_2\text{O} = \text{Pu}(\text{OH})^{3+} + \text{H}^+$	-0.68
$\text{Pu}^{4+} + 4\text{CO}_3^{2-} = \text{Pu}(\text{CO}_3)_4^{4-}$	34.1
$\text{PuO}_2^+ + \text{H}_2\text{O} = \text{PuO}_2\text{OH} + \text{H}^+$	-9.73

3.5 Principles of Transport Simulation

After escaping from the potential repository at YM, radionuclides can migrate through the UZ and then reach the groundwater table as dissolved molecular species. These radionuclide-bearing solutes undergo several transport processes, including advection, hydrodynamic dispersion, matrix diffusion, and sorption at different scales within the SZ. Factors which affect radionuclides transport in the SZ include (1) velocity of the groundwater flow (depending on the distribution of the matrix and fractured rocks); (2) chemistry of the groundwater (i.e., chemical constituents, oxidation and reduction potential), and (3) physical and chemical properties of rocks (i.e., capability of sorption/desorption) along the flow path.

To understand the interaction between the chemistry of groundwater and rock properties, chemical behavior of the solutions during the transport processes is typically modeled by simulating sorption/desorption, complexation and dissolution/precipitation of them along a flow path (Domenico and Schwartz, 1998; Bauer et al., 2001).

3.5.1 Numerical Equations for Transport

The most common approach is to employ Darcy's law as the controlling equation for groundwater flow and a linear adsorption isotherm or distribution coefficient, K_d , to account for the sorption of reactive solutes to aquifer surfaces (Domenico, 1987; Bethke and Bradey, 2000). In this case, the 1-D governing equation has the form (Parkhurst and Appelo, 2000; Zhu and Anderson, 2002; Merkel and Planer-Friedrich, 2005):

$$D_{ix} \frac{\partial^2 C_i}{\partial x^2} - v_x \frac{\partial C_i}{\partial x} \pm \sum_{k=1}^n R_k = R_f \frac{\partial C_i}{\partial t} \quad (1)$$

where C_i is the concentration of solute i in the groundwater; x is the distance traveled in the x direction along a groundwater flow path; t is time, D_{ix} (m^2/s) is the coefficient of

hydrodynamic dispersion in the x direction; R_i denotes the rate of addition or removal of solute i to or from groundwater due to reaction k , and n represents the total number of reactions affecting i ; v_x stands for the average linear velocity of groundwater; and D_{ix} accounts for both mechanical mixing and molecular/chemical diffusion, having the form of $D_{ix} = D_e + \alpha_L v$ (D_e is the effective diffusion coefficient and α_L is the dispersivity), $-v_x \frac{\partial C_i}{\partial x}$ represents advective transport, $D_{ix} \frac{\partial^2 C_i}{\partial x^2}$ represents dispersive transport, and $\sum_{k=1}^n R_i$ is the change of concentration due to chemical reactions.

The transport part of equation (1) is solved with an explicit finite difference scheme that is forward in time, central in space for dispersion, and upwind for advective transport.

The chemical interaction term $\sum_{k=1}^n R_i$ for each element is calculated separately from the transport part for each time step and is the sum of all equilibrium and non-equilibrium reaction rates. At each time step, advective transport and all equilibrium and kinetically controlled chemical reactions are calculated, and then dispersive transport is simulated, followed again by the calculation of all equilibrium and kinetically controlled chemical reactions (Parkhurst and Appelo, 2000).

3.5.2 Principle Transport Mechanics of Radionuclides in SZ

The transport simulations are conducted for both volcanic and alluvial aquifers since the transport mechanics are quite different from each other. Appropriate transport parameters are respectively prepared for two sets of simulations in this study. The following section discusses the transport properties for the tuffaceous and alluvial aquifer separately.

3.5.2.1 Transport Features of Fractured Volcanic Tuffs

Factors influencing the radionuclide transport through non-welded fracture tuffs beneath RWP include the fracture spacing (advection), the effective fracture porosity, hydrodynamic dispersion, and matrix diffusion, which have been inferred from hydraulic testing in boreholes that penetrate the SZ.

Advection is the dominant transport mechanism and conceptualized to occur primarily within the fracture network of the volcanic tuff because of high permeability, limited fracture pore volumes, limited contact area, and relative short contact times between the radionuclide-bearing water and the matrix (only at the fracture walls). Hydrodynamic dispersion can occur at a range of scales and at directions longitudinal or transverse to the major groundwater flow direction (BSC, 2003a).

Matrix diffusion is a process in which diffusing particles move, via Brownian motion, through both mobile and immobile fluids (OCRWM, 2003b). Diffusion can play an important role in radionuclide exchange between the fractures and the rock matrix. During the diffusion process, species move from high concentration to low concentration.

Sorption reactions can potentially occur on the surfaces of fractures as well as within the rock matrix of fractured tuff. However, because of the lack of data and to be conservative, sorption on fracture surfaces is neglected in the fractured volcanic tuffs.

3.5.2.2 Transport Features of Alluvium

Fluid flow in the alluvium is well represented using a porous continuum conceptual model based on the nature of alluvial material that is porous. As a result, besides those specified for volcanic tuffs, the principal transport characteristic of the alluvium relevant to radionuclide migration is the effective porosity (BSC, 2003a).

The total porosity of the alluvium was determined to be about 33% from analysis of grain size distributions by DOE (BSC, 2003a). An estimation of total porosity using the storage coefficient from the cross-hole hydraulic test, the thickness of the tested interval, and the barometric efficiency of the formation was determined to be 40% (BSC, 2003a). These values represent upper bounds of total porosity that are needed to evaluate the effective porosity through which water and dissolved radionuclides are likely to be transported. In this study, a 30% of effective porosity is used for sorption reaction in alluvial transport.

A single-porosity flow and transport system was verified by the evidence that the tracer concentrations had no increase after flow interruptions during the tailing portions of the tracer test (BSC, 2003a). The lack of increase in tracer concentrations indicates a lack of diffusive mass transfer between flowing and stagnant water in the system. As a result, the alluvium diffusion was not considered in the alluvial transport. Instead, stagnant zones, which are used to represent preferential flow within alluvial materials, are defined in PHREEQC input files by stagnant (immobile) cells associated with each mobile cell in which advection occurs. The immobile cells are usually defined to be a 1D column that is connected to the mobile cell; however, the connections among the immobile cells are defined arbitrarily with mix function of PHREEQC.

Because of the strong dependence on scale, dispersivity in the alluvium has not been measured in the field by any of institutes. Several column tracer experiments were conducted instead using alluvial material from situ borehole and a sorbing tracer (lithium bromide). The results from these experiments render a range of dispersivity value of 1.8 to 5.4 cm (BSC, 2003a).

The conceptual model of radionuclide sorption in the SZ has the assumption of local equilibrium between the dissolved aqueous species and the aquifer sediments. This distribution is defined by the linear sorption coefficient relationship. Distribution coefficient of the three radionuclides to alluvial materials under conditions relevant to the field had been determined by site and laboratory experiments (Table 4.2).

3.6 Implementation of Conceptual Model

3.6.1 Conceptual Hydrological Strata of Saturated Zone

Regional understanding of hydraulic potential of recharge/discharge and geochemistry are summarized in the previous sections. Groundwater flow models (BSC, 2003a; BSC, 2003c; OCRWM, 2003b) indicate that the groundwater flows through volcanic tuff towards south beneath the alluvium fill. Within the alluvial aquifer underlying the Amargosa Valley, groundwater mixes with other type of water, and then naturally discharges into Death Valley region.

In this study, the groundwater flow system at YM is visualized as a multi-layer system and simplified to consist of three aquifers and one aquitard. There are three major hydrogeologic units taken into consideration, which are a volcanic tuffaceous aquifer, an alluvial aquifer, and a carbonate aquifer. The volcanic aquifer lies above the carbonate aquifer and there is a layer of aquitard between these two. This aquitard has been characterized as the upper clastic aquitard (CRWMS M&O, 2000a). Figure 3.3 is the visualization of the cross-sectional hydrogeologic strata for this study.

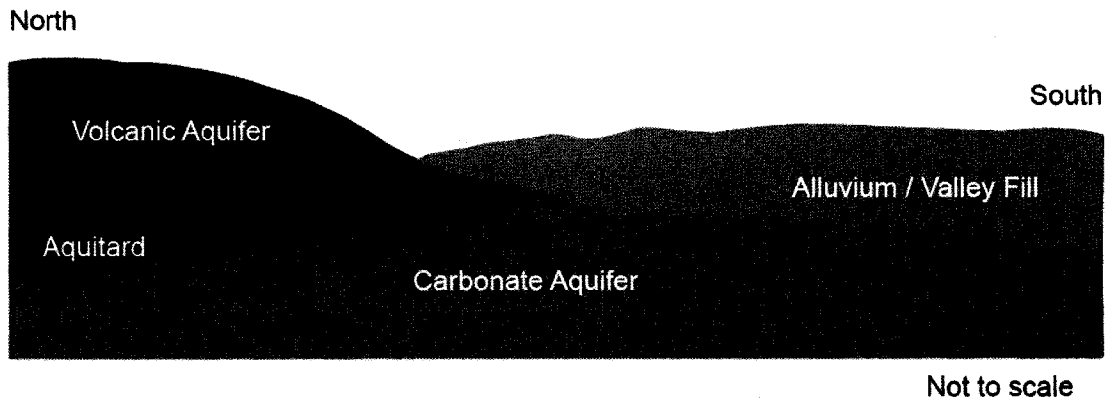


Figure 3.3. Cross-section of conceptual hydro-stratigraphy of SZ.

Based on this conceptual geological model, we consider that groundwater flows pass volcanic aquifer where the volcanic rocks pinch out beneath the alluvium fill, whereas, the water table changes gradually from volcanic aquifer to alluvium fill; also some deep water from carbonate aquifer would flow upward mixing with water in alluvium. Groundwater level measurement in boreholes penetrating Paleozoic carbonate aquifer at YM indicated upward flow from deeper to shallower aquifer because of pressure head difference (CRWMS M&O, 2000a). This phenomenon will dilute the contaminant concentration as well as slightly change the chemical composition of the groundwater.

To be compatible with the conceptual model of SZ, the total length of flow path from repository to the compliance boundary for the transport simulation are determined to be around 20 km, depending on the location of contaminant source and the horizontal anisotropy in permeability both in volcanic and alluvial units (BSC, 2003a). Based on the geochemical analyses as well as groundwater flow model results, if the total water flows to approximate 20 km compliance boundary, 18 km of flow path through tuffaceous aquifer (BSC, 2003c) while 2 km flow path through alluvial fills.

The conceptual model validity is established by comparing model-generated parameters with the related data from field and laboratory tests; by comparing fluid path obtained from the SZ flow models (BSC, 2003a; BSC, 2003c) with those inferred from hydrochemical data; and by comparing the upward gradient generated with the models with these observed in the field (BSC, 2001).

3.6.2 Other Features of Solute Transport

There are two kinetics reactions within this simulation. One is the element sorption; another is mineral dissolution/precipitation. Each kinetic reaction needs a corresponding rate definition. The rate expression for mineral dissolution/precipitation is derived from the time-dependent calcite dissolution in Merkel and Planer-Friedrich (2005) and Barnett et al. (2000). The rate expression for element sorption is derived from PHREEQC manual. Expression in the keyword RATES in PHREEQC used the mathematics term in the form of BASIC language.

Several methods are applied to evaluate the sensitivity and effect of transport simulation including the mixing of groundwater from volcanic aquifer and carbonate aquifer beneath, sorption/no sorption, stagnant zone/no stagnant zone, and large cell/small cell. The effect of carbonate water is examined with one simulation of normal flow velocity is included in Solution V (carbonate water) to Solution III in a 1:1 ratio (Table 2.1). On the evaluation of the effect of groundwater flow velocity on the transport results, the velocity is doubled and halved to be 92 and 23 m/yr for volcanic aquifer, while 20 and 5 m/yr for alluvial aquifer. To evaluate the effect of sorption and stagnant zone, one simulation is without the sorption; one without the stagnant cells; and one

without both two. All cell numbers are divided by 10 (by 2 for plutonium because of program convergence) for evaluating the scaling effect.

3.7 Description of Simulation Input and Output

The inputs for the solubility simulation include chemical components of percolating water that seeping into the failed waste package, secondary minerals or alternative phases of uranium, neptunium, and plutonium as equilibrium phases, and related chemical reactions with thermodynamic data from the YM Database. The outputs from the dissolution simulation include concentrations of dissolved radionuclides changing with pH value as well as partial CO₂ pressure. Also, the outputs include saturation indices for each secondary minerals or alternative phases before and after dissolution. Appendix A lists the examples of neptunium solubility/speciation input and output files.

The setup of speciation simulation is based on solubility. Besides the solution from the result of dissolution simulation, the inputs include chemical components of pore water in the UZ, and mixing of these two by the ratio of 1:1. The outputs include the concentration of various aqueous species of dissolved abundance.

The setup of transport simulations are based on both dissolution and speciation results, as well as chemical components of groundwater in the volcanic aquifer, geological properties of SZ, sorption affinity of radioactive elements, and precipitation/dissolution kinetic reactions. The outputs produce contaminant breakthrough curve from alluvium aquifer, sorption activity, and mineral precipitation. Appendix A lists the example of uranium transport input file. Moreover, some other results are designed to analyze the sensitivity of transport cells, effect of retardation, and

effect of groundwater flow velocity on the radionuclide breakthrough time and breakthrough concentration.

CHAPTER 4

MODEL PROCEDURES AND RESULTS

In this study, four sets of simulations with PHREEQC were designed for each radionuclide, one for solid dissolution, one for speciation, and two for solute transport (one in the volcanic aquifer and one in the alluvial aquifer). The results from the simulation of solid dissolution evaluate the limitation of selected solubility for controlling minerals, which are defined as Equilibrium Phases in the program. The speciation simulation provides the concentration of related aqueous species, whereas the breakthrough curves will be constructed in the transport simulation. Also, simulations have been conducted to evaluate how groundwater mixing of different aquifers, changing groundwater flow velocity, different numbers of grid cells, and with/without sorption reaction and stagnant zones would affect radionuclide transport in the groundwater.

The simulation of solid dissolution is initiated with the UZ pore water, Solution I (see Table 2.1), above RWP. Solution Master Species and Equilibrium Phases for each element are listed in Table 4.1. The saturation indices for each mineral are set to be zero to indicate an equilibrium status. The most important outputs from these simulations are the radionuclide dissolution concentration to show how much radionuclide is dissolved in the solution by the time of equilibrium in Solution I.

Based on these outputs from the simulation of solid dissolution, speciation simulation starts with the UZ pore water below the RWP (Solution II). It is calculated by mixing Solution I and Solution II in a 1:1 ratio (approximately). The product of porosity and flow velocity should match the preserved continuity (Equation 4.2). The equation could be balanced manually by adjusting the mixing ratio of solutions.

$$V_v \times n_v = V_a \times n_a \quad (4.2)$$

where V is the flow velocity, n is the porosity; v denotes the volcanic tuff; a denotes the alluvium. The porosity and flow velocity for volcanic is 0.06 and 46 m/yr; for alluvial aquifer is 0.3 and 10 m/yr. Thus, the mixing ratio of 1:1 here can satisfy Equation 4.2 according to the accuracy of PHREEQC. The simulation provides the concentration of different aqueous species of uranium, neptunium, and plutonium.

Using the generated solution from the speciation simulation as inflow, the transport simulation starts with SZ groundwater as background solution. The inflow solution enters continuously and moves forward with an assigned velocity. Parameters describing transport properties for both volcanic and alluvial aquifers are summarized in Table 4.2. The transport simulations within volcanic and alluvial aquifers are programmed separately. Precipitation/dissolution reaction is built into the transport simulation for the volcanic aquifer, whereas both precipitation/dissolution and sorption kinetic reactions as well as stagnant cells are included into the transport simulation for the alluvial aquifer. For sorption process, the selection of a distribution coefficient for three elements is based on the published literatures (BSC, 2004a; Barnett et al., 2000; Kessler and Doering, 2000; OCRWM, 2003b); coefficient values are listed in Table 4.2.

Table 4.1. Solution Master Species, Equilibrium Phases, and sorption coefficient used in the simulation with PHREEQC.

	Uranium	Neptunium	Plutonium
Solution Master Species	UO ₂ ²⁺	NpO ₂ ⁺	Pu ⁴⁺
Equilibrium Phases	Schoepite, Uranophane, Na-boltwoodite, Soddyite	Np ₂ O ₅	PuO ₂
K _d (l/g)	0.005	0.006	0.1

Table 4.2. Transport parameters used for volcanic and alluvial aquifers (BSC, 2003a; BSC, 2003c; CRWMS M&O, 2000a; OCRWM, 2003b).

	Volcanic tuffaceous aquifer	Alluvial aquifer
Length	18 km	2 km
Number of cells	400	200
Number of stagnant cells	None	200
Flow velocity	46m/yr	7.5-15 m/yr
Dispersivity coefficient	2	5
Diffusive coefficient (cm ² /s)	5e-11	N/A
Porosity	0.01 (Average fracture porosity) 0.21 (average matrix porosity)	0.3
Bulk density (mg/l)	1900	1270
k ₁ (temperature coefficient)	0.05	0.05
k ₂ (temperature coefficient)	3.4e-5	3.4e-5
k ₃ (temperature coefficient)	1.2e-7	1.2e-7

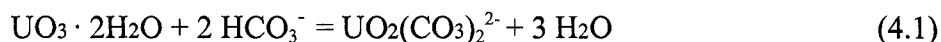
4.1 Dissolution Simulation

The dissolution simulation establishes an upper limit for the dissolved components in the source term of radionuclides. Because chemical conditions controlling dissolution concentrations may vary widely from place to place and at different periods of repository evolution, the solubility calculations were conducted over a range of conditions. Both pH value and CO₂ fugacity are considered to be uncertain variables. In the simulation, the pH range is set to be 4.0 ~ 10.0 (BSC, 2003a; BSC, 2003c) and CO₂ fugacity range is set to be 10^{-2.0} ~ 10^{-3.6} (OCRWM, 2003a).

4.1.1 Uranium

Uranium solubility altered by CO₂ fugacity (partial pressure) and pH value is displayed in Figure 4.1. The increment for pH value is set as 0.5 pH units whereas log fCO₂ has an increment of 0.4 log units, which are same for the dissolution simulations of neptunium and plutonium. Among 65 calculations, 4 calculations are beyond the valid ionic strength range, which are marked as “ionic strength > 1”. Of those converged calculations that are listed in Table 4.3, the maximum concentration is 1.3 × 10⁻¹ mol/L, which appears at pH = 9.5 / log fCO₂ = -2.4. The minimum concentration is 1.58 × 10⁻⁷ mol/L, which appears at pH = 4 / log fCO₂ = -3.6. As observed on the reversed “L” shape curves in Figure 4.1, the dissolution concentration is essentially constant for pH < 6, whereas the dissolution concentration increases rapidly under alkaline conditions. With the same pH value, the higher the fCO₂ value, the higher the dissolution concentration, because the concentration of uranyl carbonate species increases with [HCO₃⁻] increases, which results in the increase of total dissolved concentration of uranium according to the

Henry's Law based on Equation 4.1. Also, five curves representing different f_{CO_2} values are almost parallel to each other.



The dissolution concentration of uranium increases with almost two orders of magnitude due to the pH increase in a more realistic range of 7.5 to 8.5 (Figure 4.2). Saturation Index (SI) is used here to indicate uranium secondary mineral dissolution/precipitation processes. No matter how much pH increases, uranophane will not dissolve; whereas Na-boltwoodite remains an almost constant concentration of around 4.0×10^{-3} mol/L in the solution. When pH is higher than 8.2, soddyite begins to dissolve. At point of pH = 8, schoepite has its lowest concentration of 1.48×10^{-3} mol/L and then increases to 3.14×10^{-3} by pH = 8.5. Dissolution of Na-boltwoodite and schoepite contributes to the entire dissolution increase of uranium. When partial pressure of CO_2 increases with fixed pH = 8, soddyite precipitates much less, whereas schoepite dissolves more. The general tendency of dissolved uranium concentration increases with pH value.

A range of surrounding environmental temperatures (15~50 °C) was used in the simulation to evaluate how the temperature could affect the dissolution simulation of uranium. The predicted highest temperature within the RWP is up to 146 °C. There is no thermodynamic data at such ultimate temperature for uranium, neptunium, or plutonium available in YM databases. Thus, the range of simulated temperature is set to be 15~50 °C based on data availability. The results indicate that the concentration of uranium in solution increases as temperature increases (Figure 4.4). When temperature is greater than 40 °C, the solubility of uranium undergoes a significant increase.

Table 4.3. Calculated dissolution for uranium controlled by secondary minerals (mol/L).

pH/pCO ₂	-2	-2.4	-2.8	-3.2	-3.6
4	1.93E-06	5.30E-07	2.47E-07	1.78E-07	1.58E-07
4.5	1.97E-06	5.35E-07	2.47E-07	1.78E-07	1.58E-07
5	2.08E-06	5.55E-07	2.51E-07	1.79E-07	1.58E-07
5.5	2.45E-06	6.26E-07	2.67E-07	1.83E-07	1.59E-07
6	3.85E-06	8.82E-07	3.20E-07	1.97E-07	1.63E-07
6.5	1.05E-05	2.04E-06	5.46E-07	2.49E-07	1.78E-07
7	5.32E-05	9.18E-06	1.81E-06	5.02E-07	2.39E-07
7.5	4.05E-04	6.72E-05	1.14E-05	2.19E-06	5.72E-07
8	3.38E-03	6.06E-04	1.00E-04	1.68E-05	3.09E-06
8.5	2.23E-02	5.33E-03	9.96E-04	1.67E-04	2.75E-05
9	9.38E-02	3.20E-02	8.84E-03	1.85E-03	3.23E-04
9.5 ionic strength >1		1.30E-01	4.74E-02	1.55E-02	4.02E-03
10 ionic strength >1	ionic strength >1	ionic strength >1	ionic strength >1	9.29E-02	3.22E-02

Minimum = marked red; maximum = marked blue

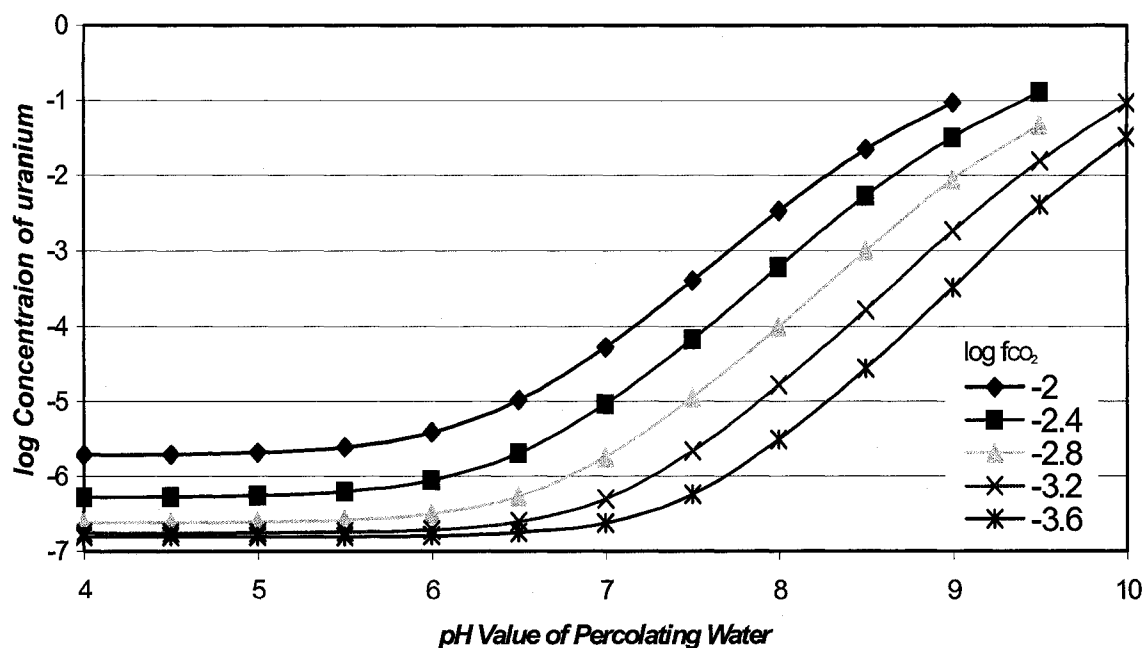


Figure 4.1. Uranium dissolution simulation as a function of pH and fCO₂.

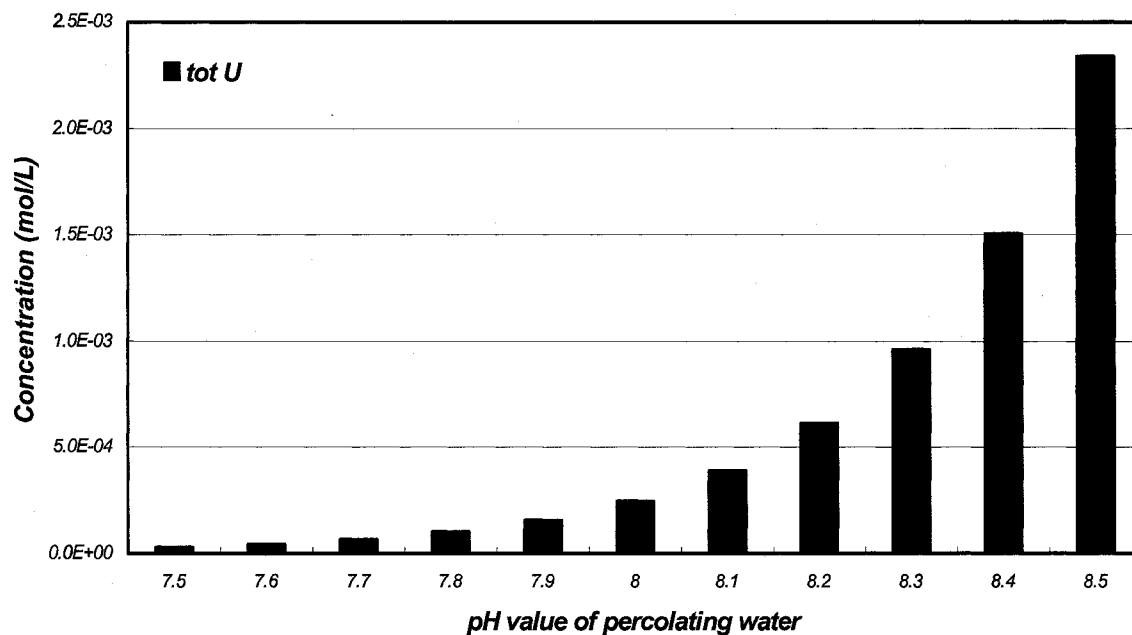


Figure 4.2. Uranium dissolution simulation with percolating water (pH = 7.5~8.5) in WP.

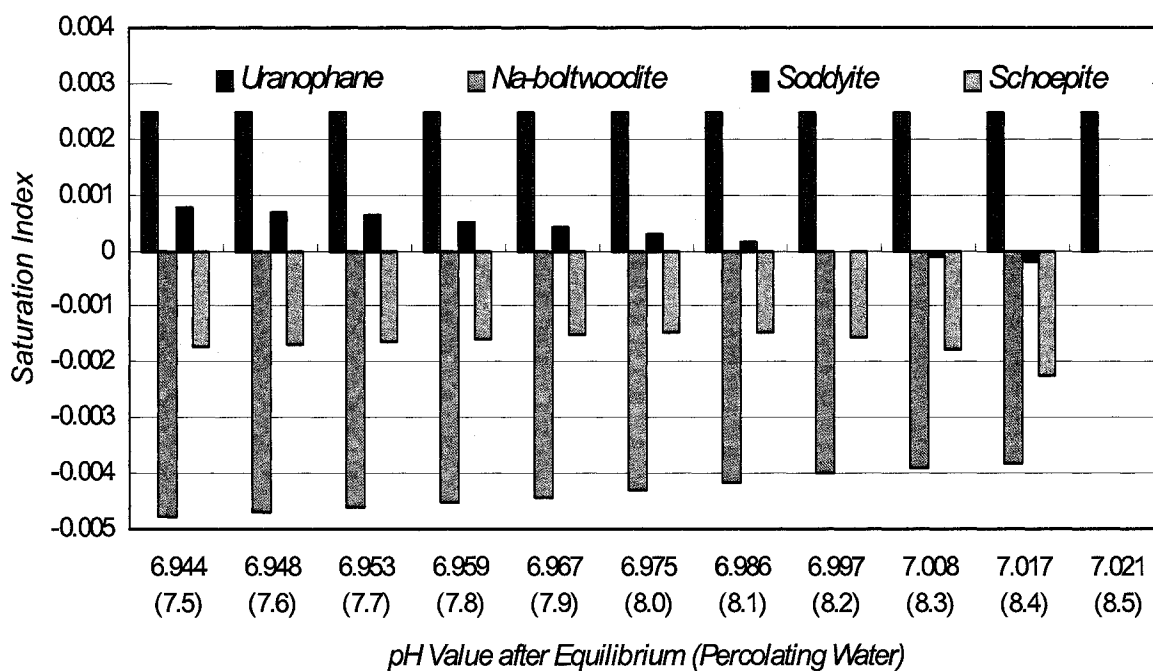


Figure 4.3. Analysis of uranium secondary minerals with dissolution simulation within WP.

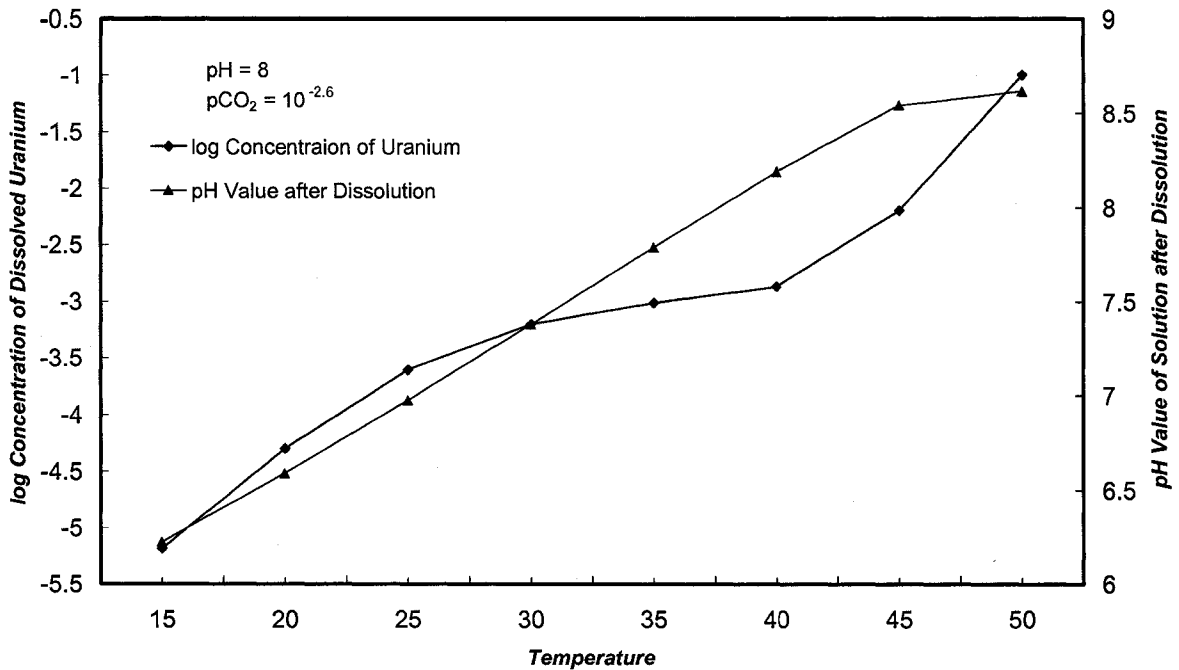


Figure 4.4. Uranium dissolution changes with increasing temperature.

4.1.2 Neptunium

Four calculations beyond valid ionic strength ranges were observed in the dissolution simulation for neptunium. The remained 59 calculations are listed in Table 4.4, with a maximum of 6.29×10^{-3} mol/L at pH = 9.5 / $\log f_{\text{CO}_2} = -2.4$ and a minimum of 4.07×10^{-6} mol/L at pH = 8.5 / $\log f_{\text{CO}_2} = -3.6$. For the $\log f_{\text{CO}_2}$ from -2, -2.4, -2.8, -3.2, to -3.6, the low points of dissolution concentration in solution vary from 7.5, 7.8, 8.0, 8.1, to 8.4 respectively. The concentration decreases slightly from pH 4 to 8 whereas it increases dramatically for pH above 8.0.

The tendency of neptunium dissolution altered by f_{CO_2} and pH appears in a “V” shape curves (Figure 4.5). Calculated concentration curves with different f_{CO_2} values do not cross each other. The concentration changes from high to low as pH changes from 4 towards 8, and then goes back to high again as pH changes from 8 towards 10. This is in

line with neptunium solubility experiments and extrapolations presented by Efurd et al. (1998). Moreover, Efurd et al. (1998) concluded that the solubility of neptunium would increase at high pH due to the formation of higher complexed anionic neptunium species in solution.

The dissolution equation of Np_2O_5 in Table 3.1 explains the tendency of solubility decrease between $\text{pH} = 4$ to 8 based on Henry's Law: $[\text{NpO}_2^+]$ decreases in response of $[\text{H}^+]$ decrease to keep the fixed K_{sp} ($10^{5.2}$ in this case). Under alkaline conditions ($\text{pH} > 8$) where $[\text{OH}^-]$ dominates instead of $[\text{H}^+]$, there is a series of reactions going on that result in a quick increase of solution concentration of neptunium (OCRWM, 2003a). For a given pH value, the higher the f_{CO_2} value, the higher the solubility concentration, which is identical to those changes of uranium.

Table 4.4. Calculated neptunium dissolution controlled by Np_2O_5 (mol/L).

pH/lg f_{CO_2}	-2	-2.4	-2.8	-3.2	-3.6
4	2.75E-04	1.95E-04	1.55E-04	1.36E-04	1.28E-04
4.5	2.12E-04	1.26E-04	7.96E-05	5.74E-05	4.78E-05
5	1.90E-04	1.04E-04	5.65E-05	3.36E-05	2.38E-05
5.5	1.73E-04	9.40E-05	4.86E-05	2.62E-05	1.70E-05
6	1.43E-04	8.29E-05	4.39E-05	2.34E-05	1.49E-05
6.5	9.07E-05	6.18E-05	3.69E-05	2.10E-05	1.38E-05
7	4.22E-05	3.41E-05	2.49E-05	1.67E-05	1.20E-05
7.5	2.44E-05	1.72E-05	1.33E-05	1.05E-05	8.62E-06
8	3.94E-05	1.80E-05	9.67E-06	6.29E-06	4.84E-06
8.5	1.26E-04	4.64E-05	1.87E-05	8.18E-06	4.07E-06
9	1.09E-03	2.07E-04	6.23E-05	2.28E-05	9.07E-06
9.5	Ionic strength>1	6.29E-03	6.85E-04	1.13E-04	3.20E-05
10	ionic strength>1	ionic strength>1	ionic strength>1	5.48E-03	5.38E-04

Minimum = marked red; maximum = marked blue

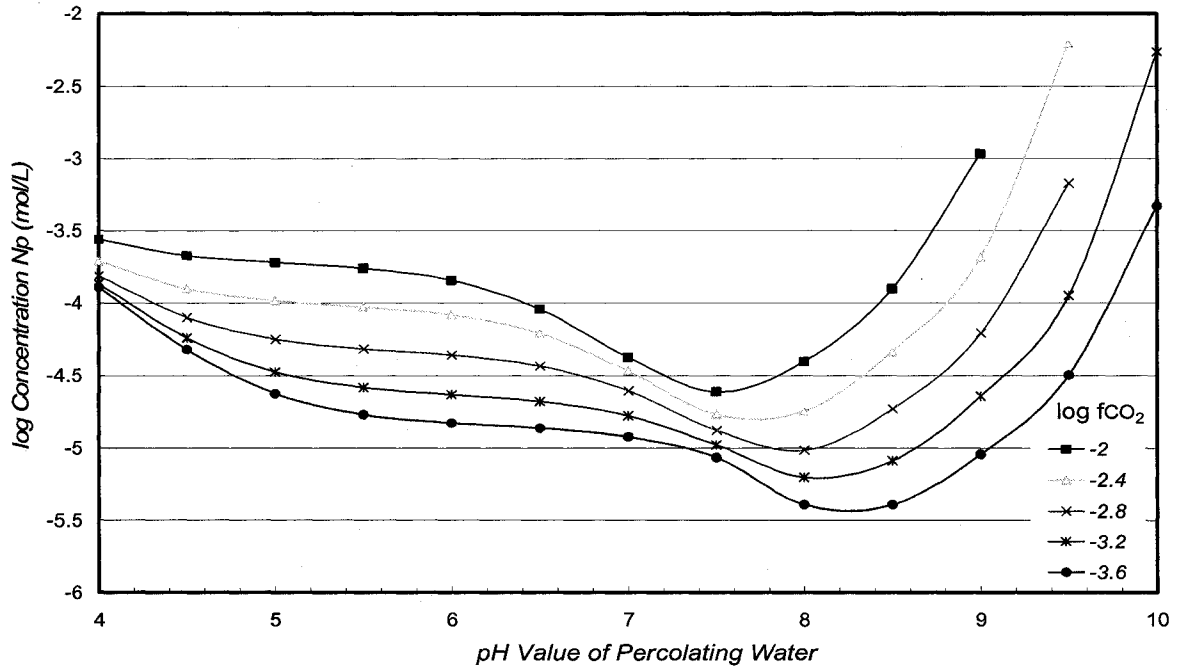


Figure 4.5. Neptunium dissolution simulation as a function of pH and f_{CO_2} .

From the enlarged solubility curve of Np_2O_5 under a pH range of 7.5 to 8.5 ($f_{CO_2} = 2.6$), which represents pH value of percolating water at YM area (Figure 4.6), the solubility curve has the lowest point of 1.21×10^{-5} mol/L for pH = 7.8 / log $f_{CO_2} = 2.6$.

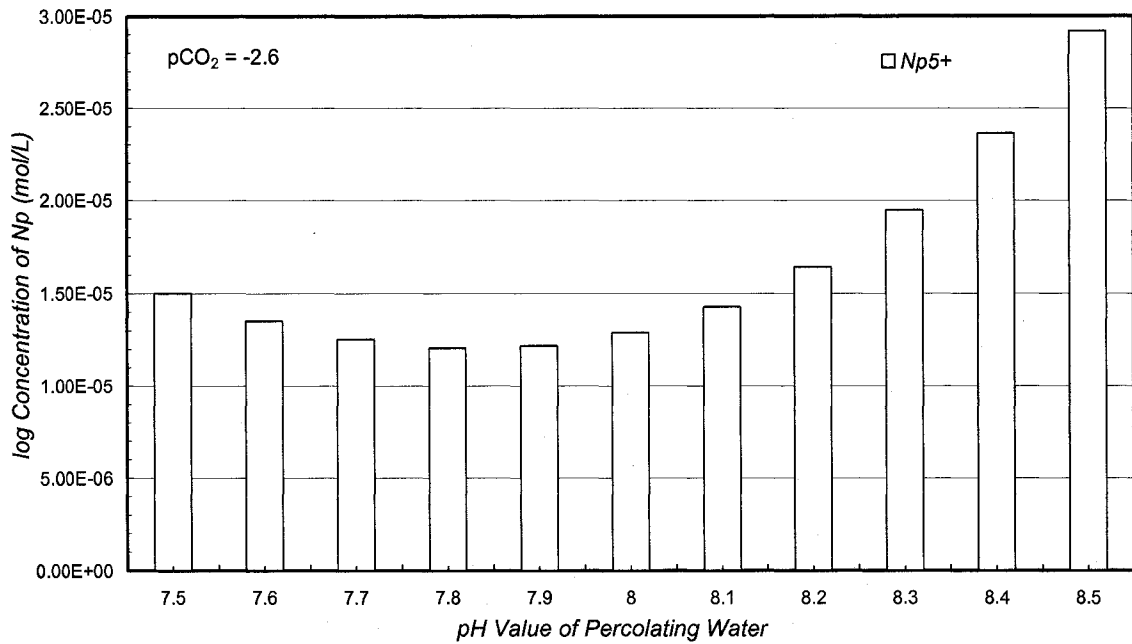


Figure 4.6. Neptunium dissolution simulation with percolating water (pH = 7.5~8.5) in WP.

4.1.3 Plutonium

The dissolution simulations for plutonium have six calculations beyond valid ionic strength range (Table 4.5). Alteration of the plutonium dissolution by different CO₂ fugacity and pH value is displayed in Figure 4.7 with a maximum of 1.21×10^{-9} mol/L at pH = 4.0 over the whole range of CO₂ fugacity and a minimum of 5.8×10^{-10} mol/L at pH = 10 / log fCO₂ = -3.6. Five curves in Figure 4.7 overlap each other, which is quite different from those of uranium and neptunium. Overall, the dissolution of plutonium does not change much over both pH and CO₂ fugacity ranges. Also, plutonium is 6-7 orders of magnitude less soluble than uranium and 4-5 orders less than neptunium (Rard, 2000; Kaplan et al., 2001; CRWMS M&O, 2001; OCRWM, 2003a; Efurud et al., 1998).

Table 4.5. Calculated plutonium dissolution controlled by PuO₂ (mol/L).

pH/pCO ₂	-2	-2.4	-2.8	-3.2	-3.6
4	1.21E-09	1.21E-09	1.21E-09	1.21E-09	1.21E-09
4.5	6.73E-10	6.73E-10	6.73E-10	6.73E-10	6.73E-10
5	6.12E-10	6.12E-10	6.12E-10	6.12E-10	6.12E-10
5.5	6.03E-10	6.03E-10	6.03E-10	6.03E-10	6.03E-10
6	6.01E-10	6.01E-10	6.01E-10	6.01E-10	6.01E-10
6.5	6.01E-10	6.01E-10	6.01E-10	6.01E-10	6.01E-10
7	6.01E-10	6.01E-10	6.01E-10	6.01E-10	6.01E-10
7.5	6.00E-10	6.01E-10	6.01E-10	6.01E-10	6.01E-10
8	5.99E-10	6.00E-10	6.01E-10	6.01E-10	6.01E-10
8.5	5.96E-10	6.00E-10	6.01E-10	6.01E-10	6.01E-10
9 ionic strength>1		5.95E-10	5.98E-10	6.00E-10	6.00E-10
9.5 ionic strength>1	ionic strength>1		5.97E-10	5.96E-10	5.99E-10
10 ionic strength>1	ionic strength>1	ionic strength>1	6.74E-10	5.83E-10	

Minimum = marked red; maximum = marked blue

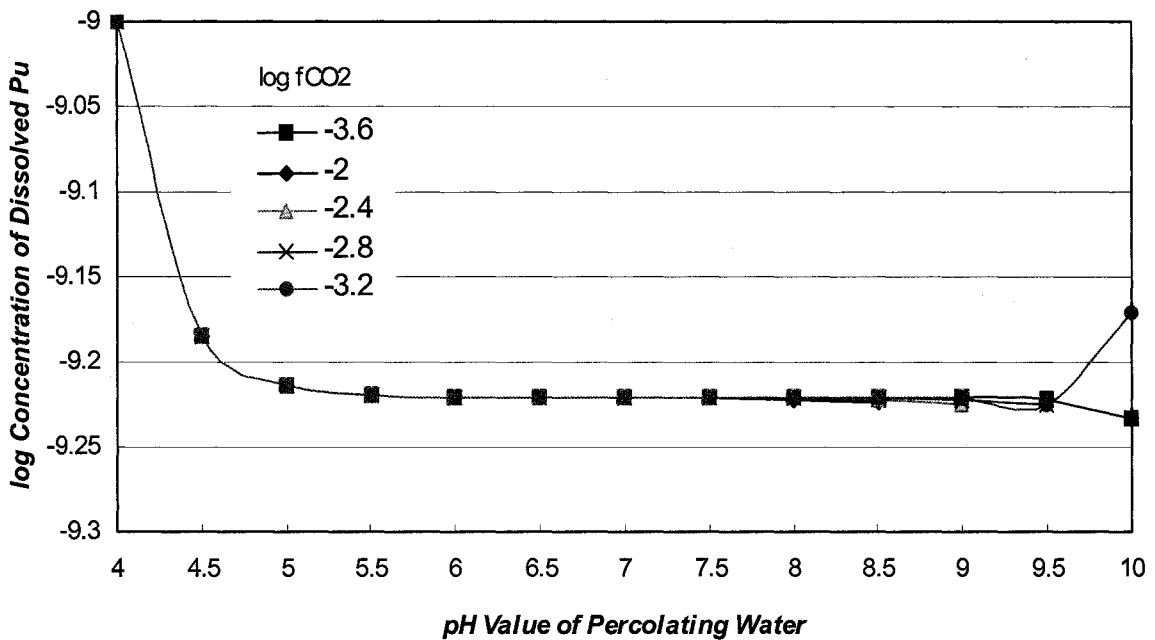


Figure 4.7. Plutonium dissolution simulation as a function of pH and fCO₂.

Compared with plutonium, the dissolution concentration of uranium and neptunium are several orders of magnitude higher. Thus, these elements should be given more concern in terms of the larger amount of mobile fraction available for being carried by

percolating water. The overall dissolution concentration of neptunium ranges from 10^{-4} to 10^{-5} , whereas uranium has a wide range from 10^{-1} to 10^{-7} . In the speciation simulation, a 7.5~8.5 pH range (OCRWM, 2001) with a fixed $f_{\text{CO}_2} = -2.6$ is assumed to represent in situ conditions. Over this pH range and f_{CO_2} value, the dissolution concentration of uranium is expected to be higher than that of neptunium.

Radionuclide dissolution depends not only on the properties of its controlling solids, but also on the properties of its aqueous species that contribute to the total solution concentration (OCRWM, 2003a). There are uncertainties lie in selection of the solubility-controlling phase, $\log K_s$ of dissolution of controlling phase, as well as the temperature and pH variations. The dissolution simulations offer information regarding the available amount of radionuclide for the initial speciation calculation. Accordingly, the speciation simulation provides the dominant aqueous species which is necessary for the evaluation of dissolution uncertainty. Also, the dissolution simulation results are essential for transport simulation as one of the important initial condition inputs.

4.2 Speciation Simulation

The equilibrium solution with a certain amount of dissolved radionuclide species would escape from the WP and migrate downward to the UZ. The aqueous speciation is calculated by mixing the UZ pore water with the solution coming from the WP. The major ion concentrations are averaged from ten pore water samples in the UZ at different depths from 290 ~ 414 m (950 ~ 1400 feet), which is just below RWP. The pH value is over a range of 7.5~8.5 and $\log f_{\text{CO}_2}$ is fixed at -2.6 (OCRWM, 2001). The thermodynamic values of $\log K$ derived from YM database are employed as speciation

reaction constants for uranium, neptunium, and plutonium. Uncertainties that come from here are acceptable and produce a conservative effect on simulated results based on conclusion from YM Review Plan (CRWMS M&O, 2001).

4.2.1 Uranium

The simulation results of uranium speciation are plotted in Figure 4.8 for uranyl carbonate species and Figure 4.9 for uranyl hydroxide species. The concentration of dominating species does not change too much over one unit of pH, so the diagram is expressed in column instead of straight line.

The concentration of uranyl carbonate species is several orders of magnitude higher than these of uranyl hydroxide species. In Figure 4.9, $\text{UO}_2\text{CO}_3^{2-}$ is the predominant species over other uranyl carbonate species, and its concentration decreases, whereas the concentration of $\text{UO}_2(\text{CO}_3)_3^{4-}$ slightly increases as pH increases. This is consistent with these of Waite et al. (1997) and OCRWM (2003a). In Figure 4.9, $\text{UO}_2(\text{OH})_3^-$ is the predominant species over other uranyl hydroxide species and its concentration remains constant over the pH range. The concentration of UO_2OH^+ is secondary in uranyl hydroxide species and decreases when pH increases. These results are in line with the speciation diagram of Davis and Curtis (2003), which indicated the predominant species between pH 6-8 is $\text{UO}_2(\text{CO}_3)_2^{2-}$, followed by $\text{UO}_2(\text{CO}_3)_3^{4-}$.

4.2.2 Neptunium

The simulation results of neptunium speciation is shown in Figure 4.10 using semi-log axis over a pH range of 7.5 ~ 8.5, which is identical with uranium speciation simulation. The thermodynamic data (logK) inputs to PHREEQC are mostly derived from Kaszuba and Runde (1999). The predominant species over this pH range is $\text{NpO}_2\text{CO}_3^-$

and its concentration slightly increases as pH increases. This is caused by more available CO_3^{2-} ion in the mixing solution when pH value increases. NpO_2^+ is the secondary dominant species whose concentration decreases when pH value increases, since Np (V) is consumed to form $\text{NpO}_2\text{CO}_3^-$. NpO_2OH (aq) is the minor species, several orders of magnitude lower in concentration than other neptunium aqueous species.

The results are consistent with Viswanathana et al. (1998) and Efurud et al. (1998), whose experimental results show NpO_2^+ and $\text{NpO}_2\text{CO}_3^-$ (at pH 7-10) as the predominant species in solution. Not like uranium, the direct product from the neptunium dissolution equation (NpO_2^+) is one of the two predominant species in solution, whereas the direct product from the dissolution equation of uranium (UO_2^{2+}) can hardly be found in solution. The reason is that most UO_2^{2+} was consumed by the speciation reaction with HCO_3^- (Table 3.1; Equation 4.1).

4.2.3 Plutonium

Figure 4.11 shows the plutonium aqueous speciation diagram. The obviously predominant species over 7.5 ~ 8.5 is $\text{Pu}(\text{OH})_4$ (aq). $\text{Pu}(\text{OH})_3^+$ is the secondary dominant species and its concentration decreases slightly when pH increases. The concentration of $\text{Pu}(\text{CO}_3)_2^-$ and PuCO_3^+ produces a small peak for pH around 7.6 with the maximum value of 2.44×10^{-16} and 3.01×10^{-16} mol/L respectively. When pH equals to 8.5, the minimum concentration of $\text{Pu}(\text{CO}_3)_2^-$ and PuCO_3^+ is 4.64×10^{-17} and 2.47×10^{-17} mol/L respectively. The concentration of $\text{PuO}_2\text{CO}_3^-$ has a low point of 9.9×10^{-18} for pH = 8.2, whereas a high point of 2×10^{-17} for pH = 7.5. The concentration of PuO_2^+ decreases one-third from pH = 7.5 to 7.6 and then remains 5.1×10^{-18} mol/L for the rest of calculation. The results of plutonium speciation are in accordance with Rard (1997) and Kaplan et al. (2001).

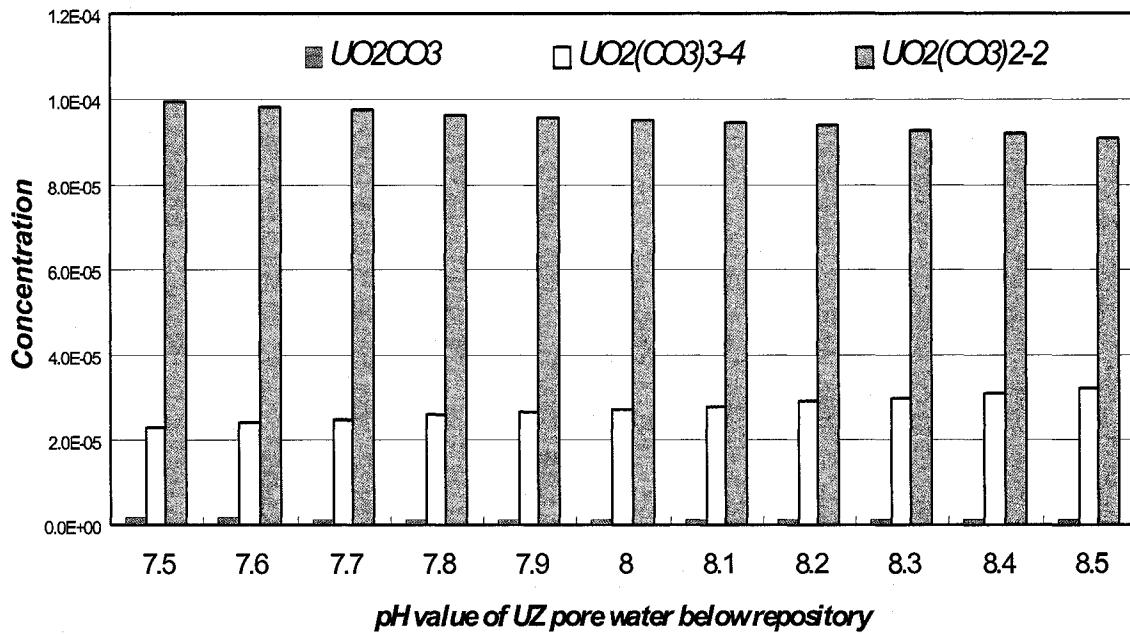


Figure 4.8. Speciation results of uranyl carbonate species with UZ pore water.

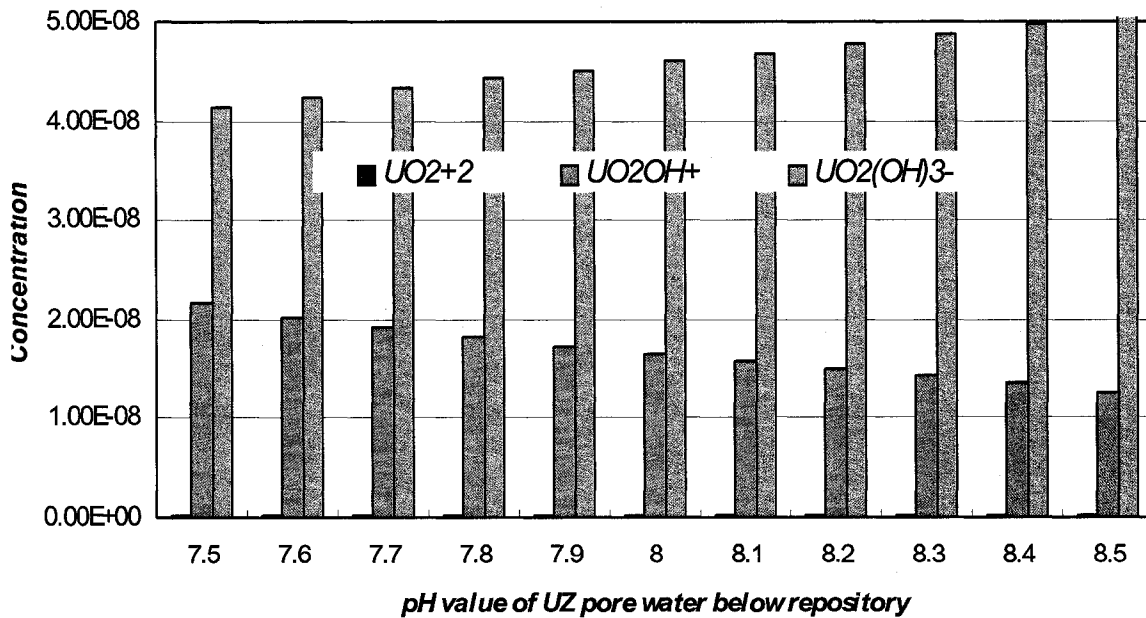


Figure 4.9. Speciation results of uranyl hydroxide species with UZ pore water.

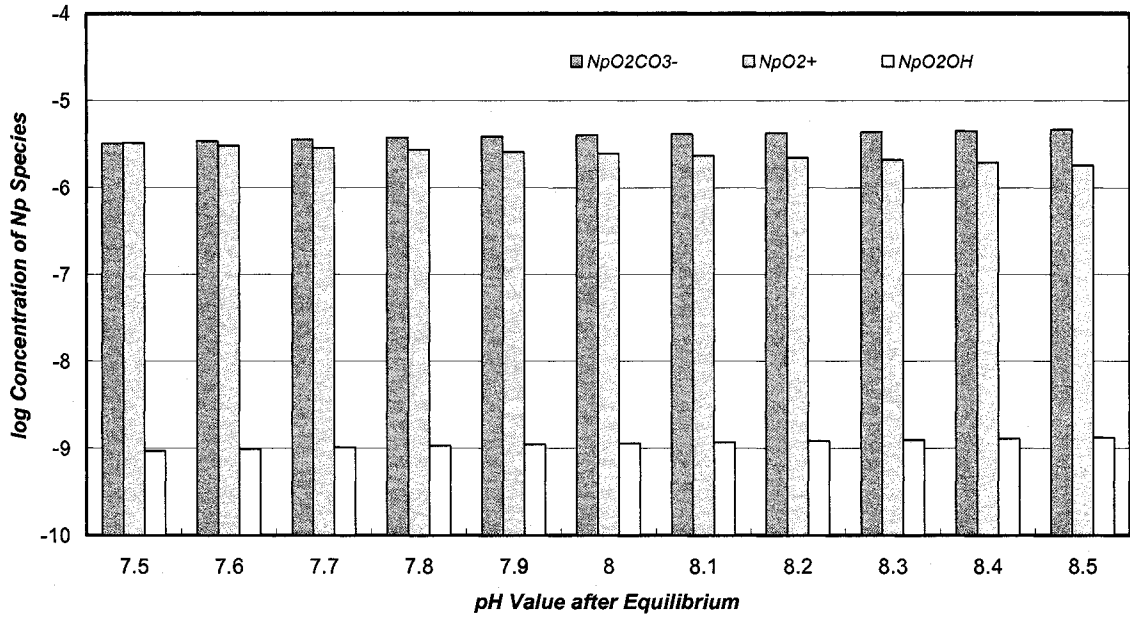


Figure 4.10. Speciation results of neptunium aqueous species with UZ pore water.

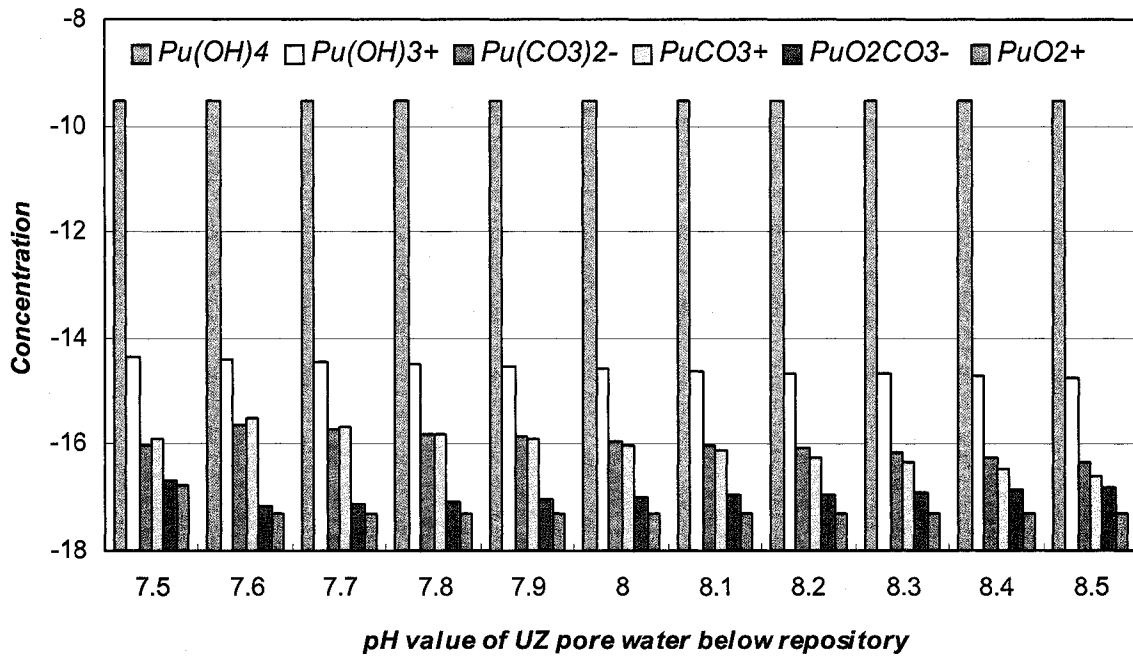


Figure 4.11. Speciation results of plutonium aqueous species with UZ pore water.

The study of speciation provides knowledge of the oxidation state for the soluble aqueous species, as well as their distribution at equilibrium. Also, it provides guidance in choosing the starting concentrations for radionuclide sorption simulation and the essential information for the transport simulations.

4.3 Transport Simulation Results

The groundwater flow path from the repository to the accessible environment is conceptualized from volcanic tuffs to alluvium as mentioned in Sections 3.4 and 3.5. To represent different geological properties, the transport simulations are conducted in both volcanic and alluvial aquifers separately. Appropriate transport parameters are respectively assigned in two sets of simulation (Table 4.2).

In the volcanic aquifer, fractures are expected to dominate transport behavior because liquid water mainly flows through fracture networks in the geological units. Consequently, the sorption process is not included in volcanic aquifer transport. In the alluvial aquifer, kinetic reaction of sorption as well as stagnant zones is assumed to delay contaminant release and reduce solute breakthrough concentration. Calibration of groundwater flow field uses measured (BSC, 2001) and model-generated water levels data, specific discharge data, and flux comparisons along several simulation paths.

4.3.1 Setup of Transport Simulation

The 1-D transport simulation defines 18 km migration distance of radionuclide in volcanic tuff and 2 km distance in alluvium. 400 cells with length of 46 m each (a total of 18.4 km) are used for the volcanic tuff section. Because groundwater velocity in volcanic tuff is around 46 m/yr (BSC, 2003a), the 46 m is the distance groundwater travel within 1

year, subsequently defined as time step in the simulation. A porosity of 0.065 was selected for fractured network in the volcanic tuff. The hydrodynamic dispersivity of 2 and diffusion coefficient of $5 \times 10^{-11} \text{ m}^2/\text{s}$ (BSC, 2003c) were selected in the simulation. The boundary condition for this section is defined to be constant hydraulic gradient at the entrance whereas flux at the end (contact point with alluvium).

200 cells with a length of 10 m each (a total of 2 km) are set up for the simulation in the alluvium. The groundwater velocity in the alluvium is approximate 7.5~15 m/yr (BSC, 2003a); the 10 m is the distance that groundwater travels within one year based on the average velocity. So the time step is defined to be 1 year for the simulation as well. An effective porosity of 0.3 was used for kinetic reaction of sorption. A hydrodynamic dispersivity of 5 (BSC, 2003c) was selected in the simulation where the diffusion coefficient is zero (BSC, 2003a). The boundary condition for this section is defined to be flux at the entrance (contact point with volcanic tuffs) whereas constant hydraulic gradient at the end. Moreover, stagnant (immobile) cells were set up with a porosity of 0.1 based on several situ sampling results (BSC, 2004a), and an exchange factor of 6.8×10^{-6} (Parkhurst and Appelo, 2000). The transport parameters, such as diffusion coefficient, dispersivity coefficient, porosity, and exchange factor of stagnant cells are subject to uncertainty of the model.

For plutonium, the numerical simulations failed on all combinations of convergence parameters. After tests for all *acceptable* parameters, the maximum cell numbers could not exceed 100 for transport simulations. Therefore, the cell number of plutonium transport simulation is reduced to make simulation results convergent. In fact, the total cell number for plutonium is one fifth of these of uranium and neptunium, which are 80

with a length of 230 m each for volcanic aquifer and 40 with a length of 50 m each for alluvial aquifer. To keep the same flow velocity, the time step is set to be 5 years.

Observations are made at the last cell of both volcanic and alluvial aquifers. The total shift is 1.5 times of cell number for volcanic aquifer and 2 times for alluvial aquifer. The output frequency is every 10, 20, and 40 years for volcanic aquifer and every 5, 10, and 20 years for the alluvial aquifer depending on the cell numbers in order to make sure that every simulation has 30 or 40 outputs for volcanic or alluvial aquifer respectively.

4.3.2 Breakthrough Curve

The breakthrough curve of total uranium, as well as major aqueous species in the absence of radioactive decay is shown in Figure 4.12 where normalized cumulative mass is plotted on the y -axis and the time in the unit of years is plotted on the x -axis. Based on the information provided by the graphic breakthrough curve, uranium will appear at the 20 km south boundary of waste package after 620 years (after radionuclide entering the SZ). Most of the uranium will be in the form of UO_2CO_3 and $\text{UO}_2(\text{CO}_3)_2^{2-}$, which is consistent with speciation results provided in Section 4.2.1. This breakthrough curve corresponds to a breakthrough time of total uranium at 50% concentration of 680 years.

The breakthrough curve of total neptunium at the simulation boundary with its major aqueous species is shown in Figure 4.13. From the plotted breakthrough curve, we can observe that the neptunium species will appear at the 20 km south boundary of waste package after 610 years. Most of neptunium will be in the form of NpO_2^+ and $\text{NpO}_2\text{CO}_3^-$, which is comparable to the speciation results provided in Section 4.2.2. This breakthrough curve in Figure 4.13 corresponds to a breakthrough time at 50% concentration of 660 years.

Figure 4.14 plots the plutonium breakthrough curve at the end of alluvium with two dominant aqueous species. The plutonium species will appear after 580 years. Most of plutonium will be in the form of $\text{Pu}(\text{OH})_4$, which is in agreement with speciation results of Section 4.2.3. This breakthrough curve corresponds to a breakthrough time at 50% concentration of 620 years.

The sequence of radionuclides appears at 20 km simulation boundary, from first to last, would be plutonium, neptunium, and uranium. The various breakthrough times indicates the different impacts of sorption reactions between individual elements and the surrounding geological material. Even though plutonium has a relative larger sorption coefficient than that of neptunium and uranium, the total sorption quantity is less than these for neptunium and uranium because of much lower solution concentration of plutonium. The assigned sorption coefficients of neptunium and uranium are quite close to each other, however, the total sorption quantity of uranium is more than that of neptunium, because its overall higher solution concentration. These results are consistent with the breakthrough curves of Base Case, conservative, and sorbing radionuclides in the absence of radioactive decay from BSC (2004a).

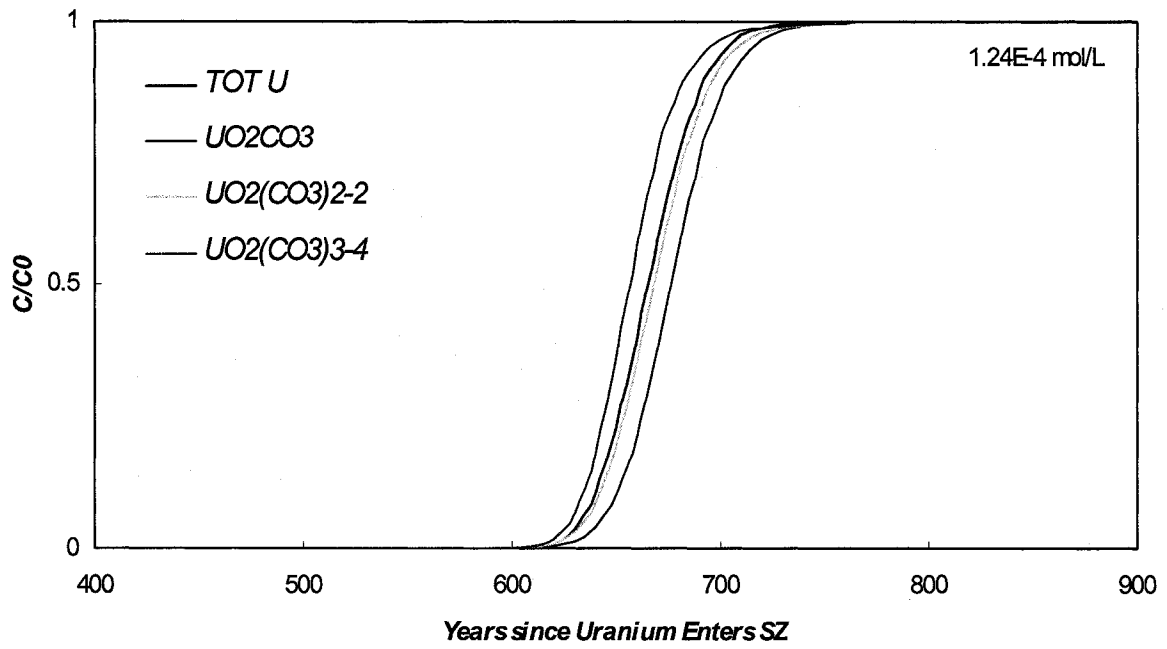


Figure 4.12. Breakthrough curves of total uranium species at 20 km south boundary.

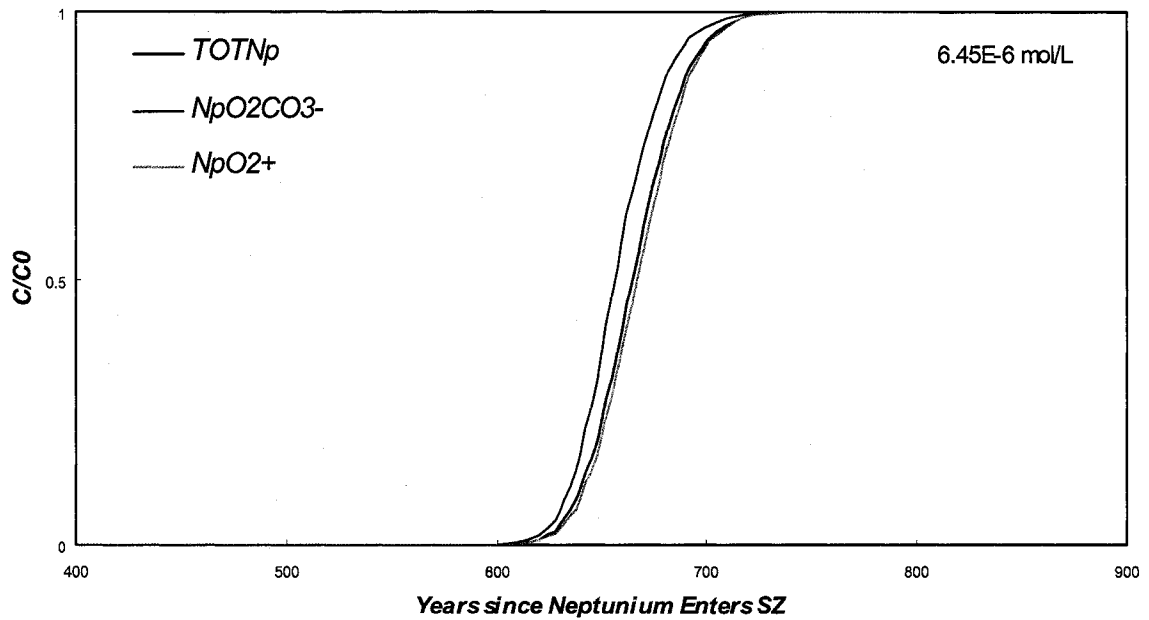


Figure 4.13. Breakthrough curves of neptunium species at 20 km south boundary.

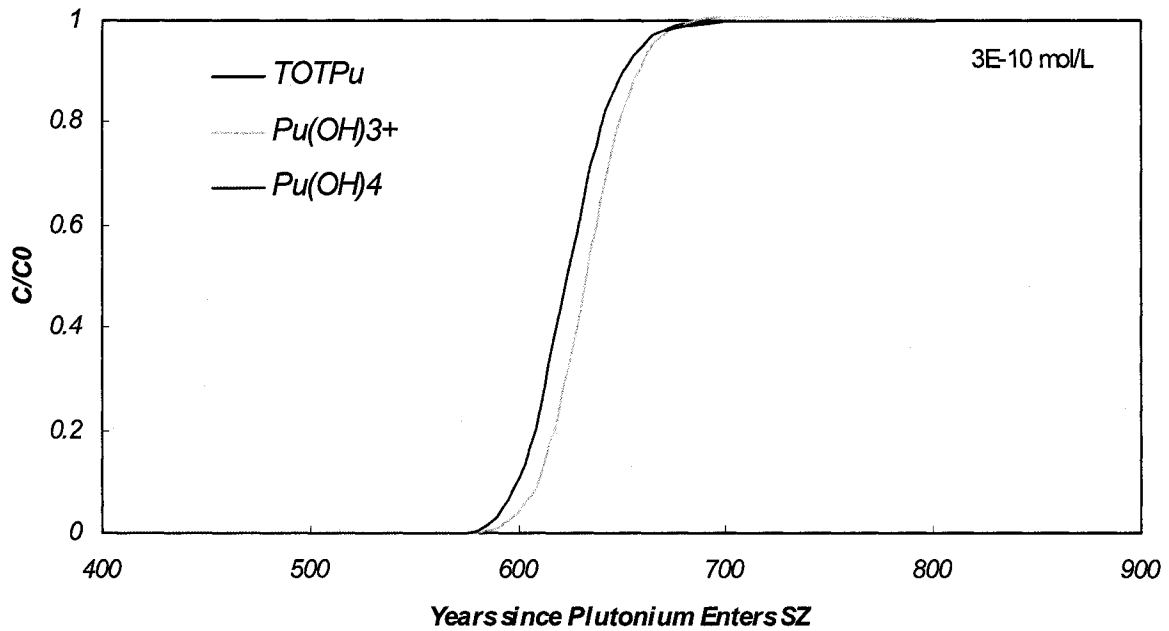


Figure 4.14. Breakthrough curves of plutonium species at 20 km south boundary.

4.3.3 Effect of Sorption Activity and Stagnant Zone

In the alluvium, the solution will mix with water in the porous media, where a certain amount of solution will stay in the stagnant zone. The stagnant zone is represented with the stagnant cell, which is attached to each normal cell of transport processes. The sorption quantity is defined as molar of radionuclide sorbing onto one gram of surrounding rocks. Parameters related to this process include the bulk density of alluvial material, alluvial porosity, sorption coefficient (Table 4.1), and time step (1 year), which are programmed in the RATES data block used for kinetics reactions. This program is calibrated in PHREEQC Manual Example 15 (1D Transport: kinetic biodegradation, cell growth and sorption) with acceptable effectiveness.

The molar of uranium sorption quantity per gram of surrounding rocks versus time is shown in Figure 4.15. From the sorption curve, the sorption quantity of uranium increases

from 640 to 730 years as transported solution passes through alluvial aquifer. Sorption from 750 years falls when the capacity is used up.

The breakthrough curves with/without sorption of uranium element are plotted in Figure 4.16. The total concentration of uranium changes slightly due to sorption activity. Only at the tail or breakthrough curve, we can observe the retardation effect of sorption. The retardation effect is not as strong and obvious as predicted by BSC (2004a), because the concentration of radionuclide input to this simulation is derived from dissolution and speciation simulations, which is much less than the concentration used in other experiments or simulations and much closer to the real situation. The breakthrough curves with/without stagnant cells are shown in Figure 4.17. This yields a breakthrough curve similar to the former curve, but with significantly shortened lengths of transport time. The contaminant without stagnant zones will reach the biosphere almost 50 years earlier than these of the simulation with stagnant cells.

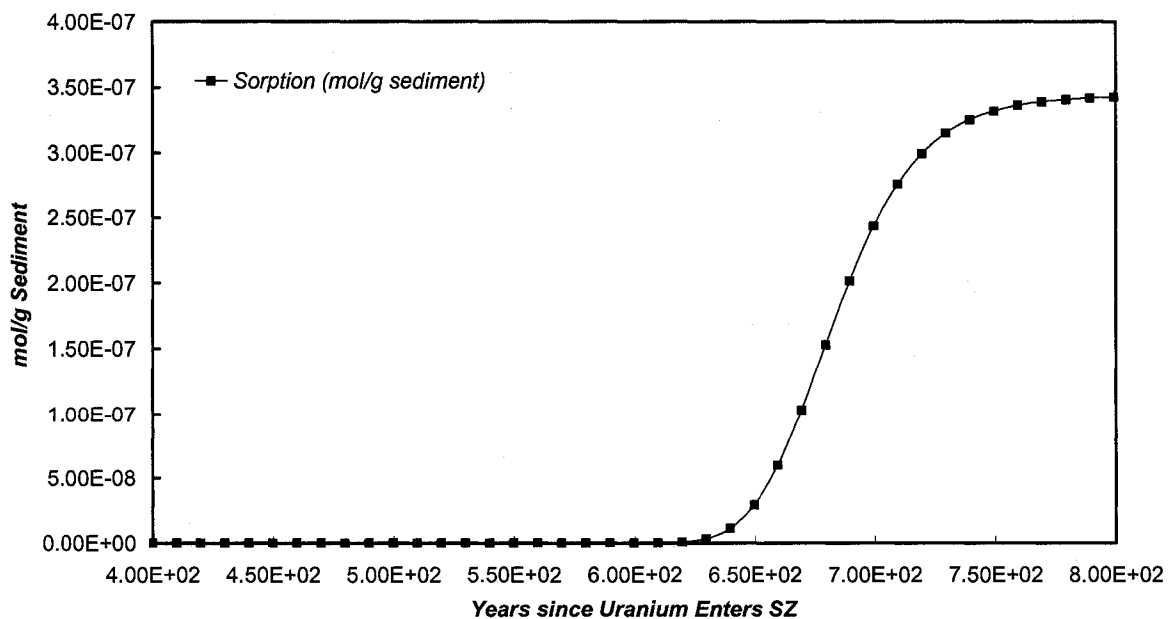


Figure 4.15. Uranium sorption activity within transport processes.

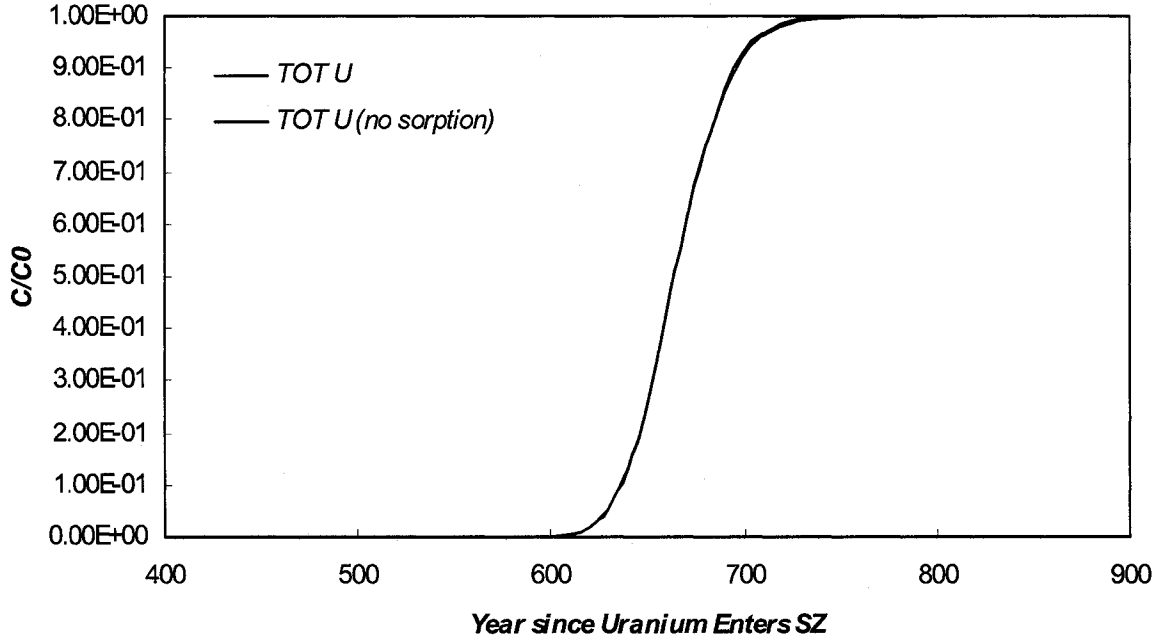


Figure 4.16. Comparison of uranium breakthrough curves w/o sorption.

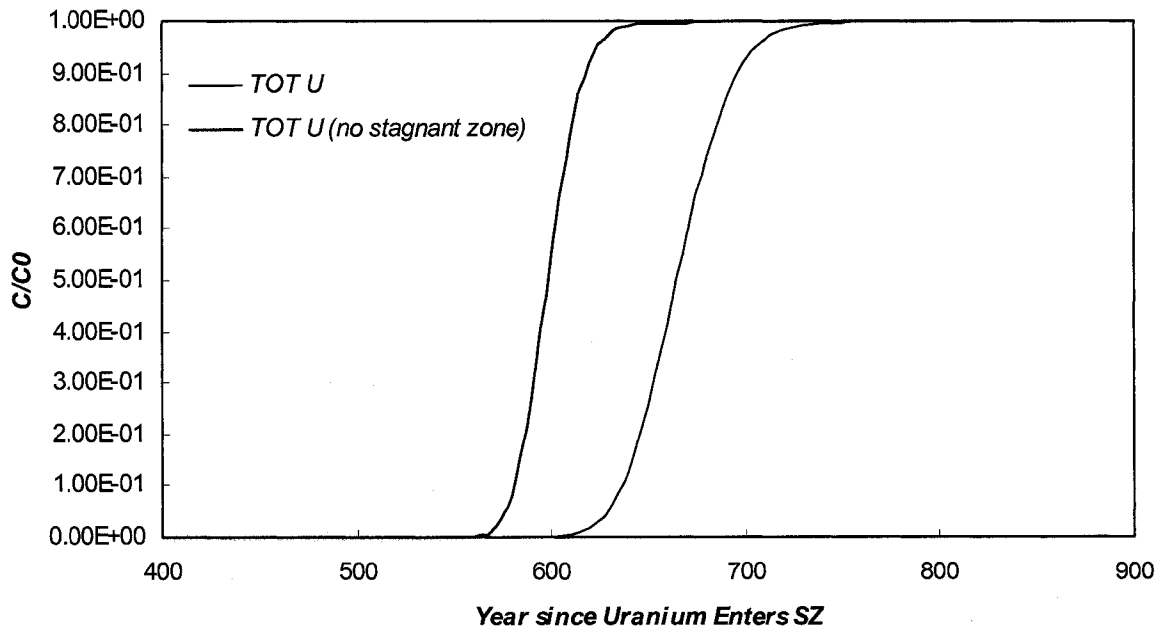


Figure 4.17. Comparison of uranium breakthrough curves w/o stagnant zone.

The molar of neptunium sorption quantity per gram of surrounding rocks through time is plotted in Figure 4.18. The sorption quantity of neptunium increases rapidly between 650 to 720 years and then turns stable after 750 years. Compared to the uranium sorption curve and different solution concentrations of these two elements, neptunium has a weaker affinity to the surrounding rocks than uranium.

Comparing the neptunium breakthrough curves with/without sorption, we hardly found any difference between these two curves that indicate retardation effect, so the diagram of the comparison will not be shown here. The breakthrough curves with/without stagnant cells are shown in Figure 4.19. The contaminant in the simulation without stagnant zones will reach the biosphere ~44 years earlier than these of the simulation with stagnant cells.

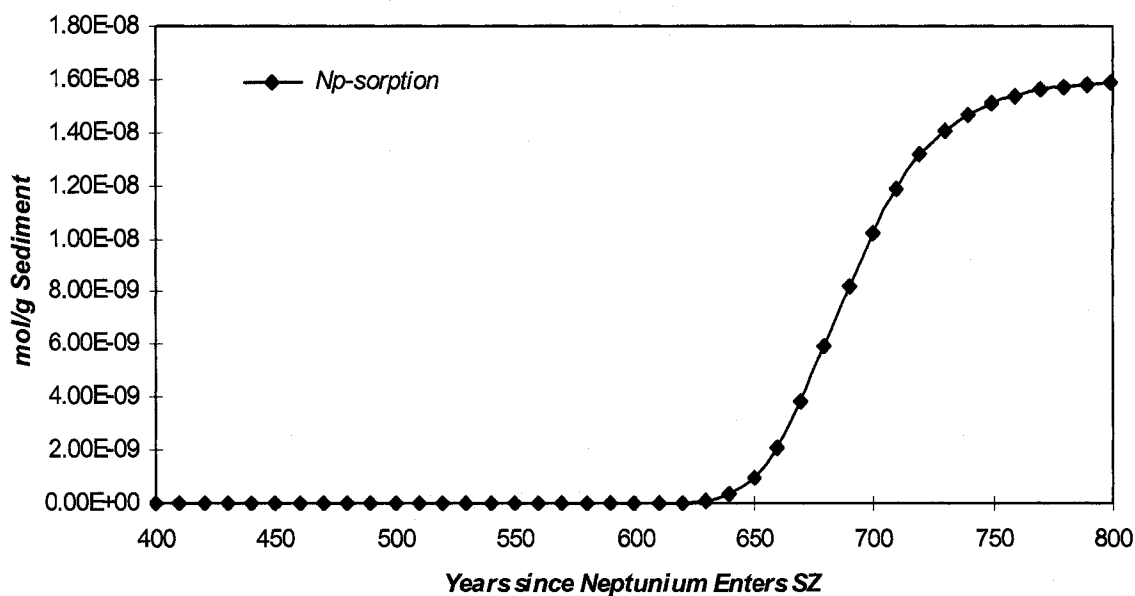


Figure 4.18. Neptunium sorption activity within transport processes.

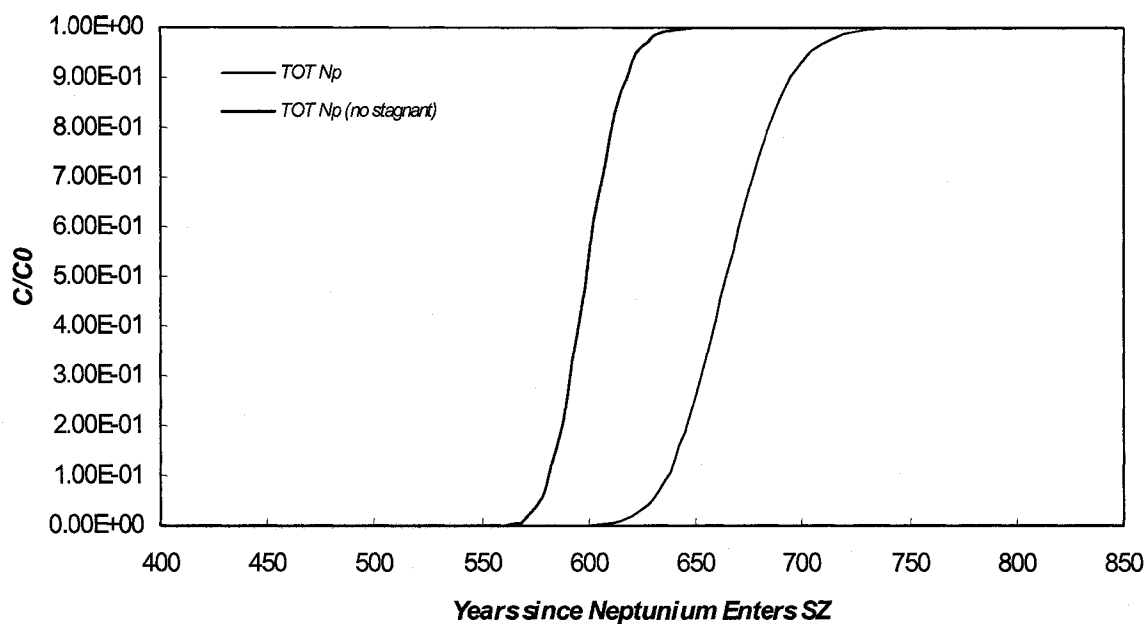


Figure 4.19. Comparison of neptunium breakthrough curves w/o stagnant zone.

Figure 4.20 shows the molar of plutonium sorption quantity per gram of surrounding rocks versus time. Even the distribution coefficient of plutonium is about 20 times larger than those of uranium and neptunium; the sorption curve doesn't show a higher sorption quantity, yet much lesser, than uranium and neptunium. This is mainly due to the low solution concentration of plutonium solution, which is only 3×10^{-10} mol/L. Also, the sorption curve of plutonium has the different pattern as those of uranium and neptunium, where the sorption quantity has kept increasing since 600 years after it enters SZ. This is caused by low solution concentration of plutonium available for sorption reaction, thus still leaving sufficient area of surrounding rock available for sorption.

Comparing plutonium breakthrough curves with/without sorption in Figure 4.21, the sorption activity does not affect too much at the beginning of breakthrough. However, with the transport continuing, the sorption does delay the release of contaminants by 6~9 years. Similarly, Figure 4.22 shows the comparison of the breakthrough curves w/o

stagnant cells. The contaminant in simulation without stagnant zone will release to the biosphere approximate 20 years earlier than those simulations defined with stagnant cells.

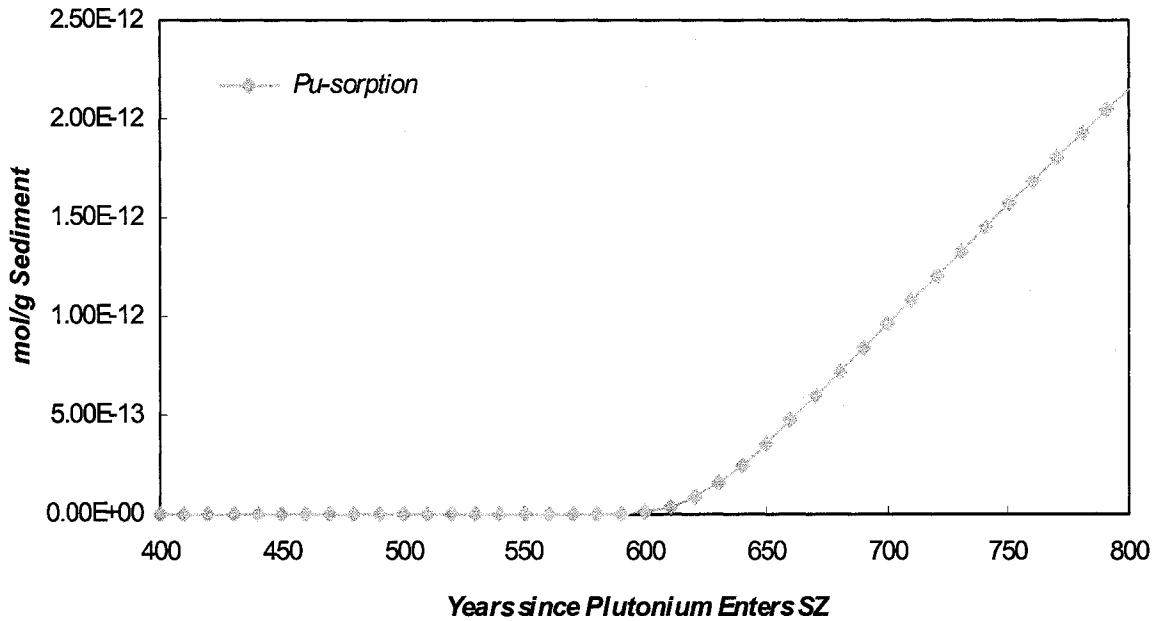


Figure 4.20. Plutonium sorption activity within transport processes.

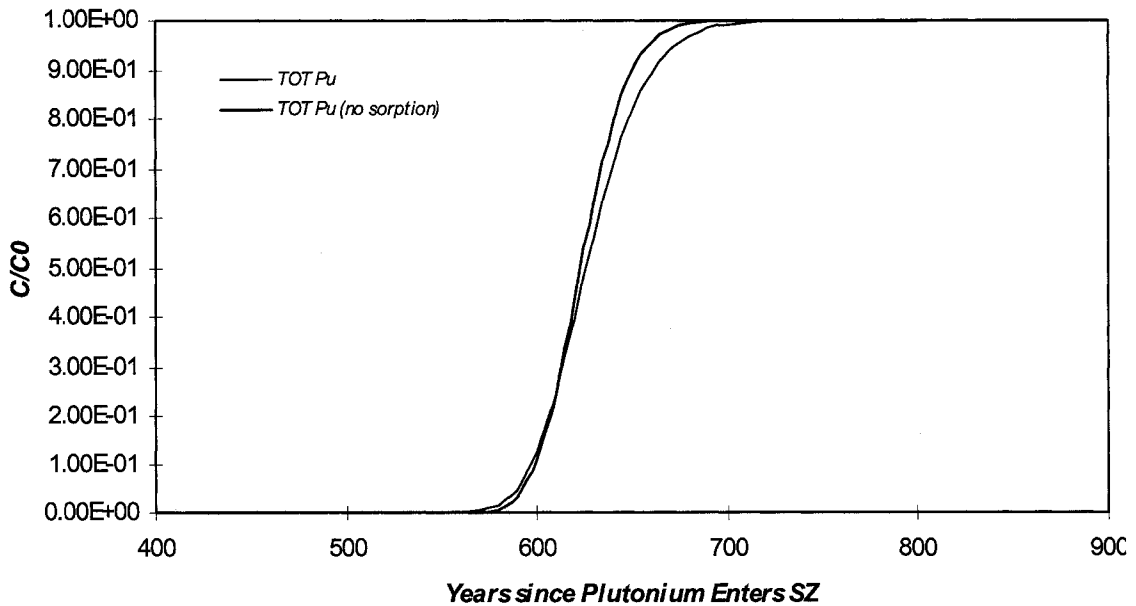


Figure 4.21. Comparison of plutonium breakthrough curves w/o sorption.

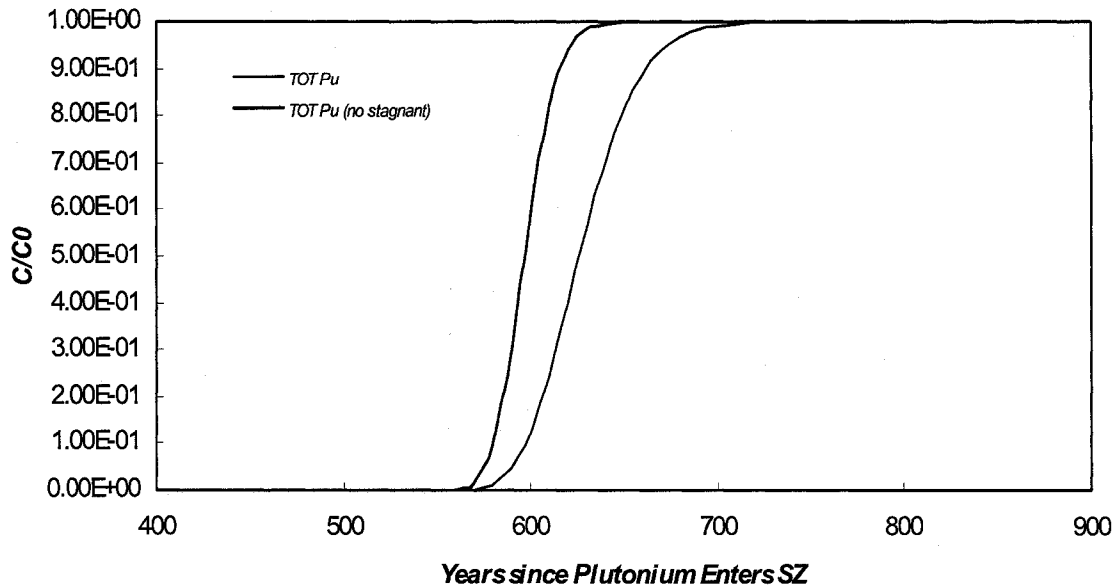


Figure 4.22. Comparison of plutonium breakthrough curves w/o stagnant zone.

4.3.4 Effect of Mixing with Groundwater from Carbonate Aquifer

The conceptual model was setup in Section 3.5.1. Groundwater flow velocity and flow path are also major uncertainty sources according to the time contact with geological materials. Some deep groundwater from carbonate aquifer might flow upwards into the alluvium (CRWMS M&O, 2000a and CRWMS M&O, 2000b); however, the exact contact location of tuff-alluvium is uncertain due to permeability anisotropy of volcanic tuffs and other complex factors (BSC, 2003a).

From the study of thirty monitor wells in the Nye County on the south of RW repository by DOE, uncertainty in the flow path length in the alluvium varies from about 1 to 10 km, which depends on the source location beneath the repository, the horizontal anisotropy in permeability in the volcanic units, and the location of the western boundary of the alluvium uncertainty zone (BSC, 2004a). This phenomenon will dilute the contaminant concentration in solution in the alluvial aquifer as well as change the

chemical composition of the solutions. Table 4.6 lists the concentrations alteration of major species before and after the mixing with carbonate groundwater.

Table 4.6. Concentration alteration before and after mixing with carbonate groundwater.

	Before	After
UO ₂ CO ₃	4.07E-07	4.81E-07
UO ₂ (CO ₃) ₂ ²⁻	4.62E-05	2.48E-05
UO ₂ (CO ₃) ₃ ⁴⁻	9.05E-06	2.61E-06
TOT U	5.58E-05	2.79E-05
NpO ₂ CO ₃ ⁻	7.44E-07	1.80E-07
NpO ₂ ⁺	2.04E-06	1.21E-06
Np(OH) ₄ (aq)	1.13E-07	5.49E-08
NpO ₂ OH	4.28E-10	6.82E-11
TOT Np	2.79E-05	1.45E-06
Pu(OH) ₄	2.66E-10	1.32E-10
Pu(OH) ₃ ⁺	1.36E-14	2.45E-14
Pu(CO ₃) ₂ ⁻	1.67E-16	5.63E-19
PuO ₂ CO ₃ ⁻	1.67E-16	5.63E-19
TOT Pu	2.66E-10	1.32E-10

Observations made from the table indicate that the overall concentration of three elements is halved after mixing with carbonate groundwater with a 1:1 mixing ratio used in the simulation. However, if we examine the concentration of individual species, they do not change always to a half concentration. The concentration of uranium major species UO₂CO₃, for example, even increases. This is due to four times of HCO₃⁻ concentration (see Table 2.1) in carbonate groundwater as these in volcanic groundwater. The similar situation does not apply to carbonate species of neptunium and plutonium.

4.3.5 Effect of Groundwater Flow Velocity

Assuming that groundwater flow velocity changes because of climate change or human activities, we also evaluated how the transport processes respond under the effect of groundwater flow velocity. As mentioned in the beginning of this section, we manually change the length and number of transport cells to accommodate flow velocity to be 23, 46, 92 m/yr in volcanic aquifer; and 5, 10, 20 m/yr in alluvial aquifer. Simulation results are summarized for three radionuclide elements in volcanic aquifer / alluvial aquifer and listed in Appendix B from Table B.1 to B.6.

From Figures 4.23 to 4.28, each figure displays three breakthrough curves of uranium, neptunium, and plutonium at the boundary of volcanic and alluvial aquifers, respectively. The different colors represent different flow velocities, which are implemented with different numbers of cells. Three breakthrough curves from the volcanic aquifer (Figures 4.23, 4.25, 5.27) have the same pattern and the total breakthrough concentrations are almost the same at varied velocities. It indicates that the flow velocity has little effect on transport processes in volcanic aquifer. Thus, the contact time between radionuclide and surrounding geological material would not be significant because the lack of interaction.

The three curves in Figures 4.24, 4.26, and 4.28 have quite different patterns. The lower the flow velocity, the flatter the breakthrough curves that show less breakthrough concentration of the element. As the velocity decreases, so does the total dissolution concentration of radionuclide, which in turn causes the sorption quantity to decrease. The results indicate that low water flow velocity allows plenty of time for radionuclide contact and react with surrounding geological materials. In other words, with longer contacting time, there are more sorption activities going on between transported solution

and rock surface. The sorption quantity does not show higher for the low velocity than these of the high velocity, because the output data indicate only the quantity within one time step (one year), not a cumulative value.

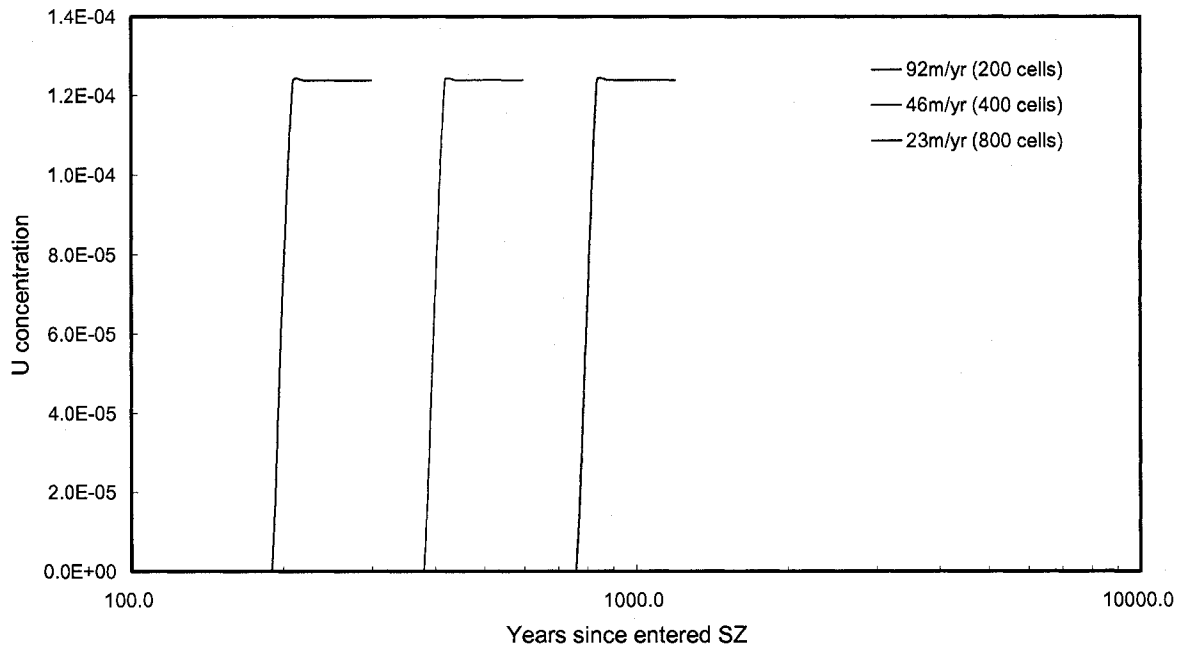


Figure 4.23. Comparison of breakthrough curves of uranium at different flow velocity in volcanic aquifer.

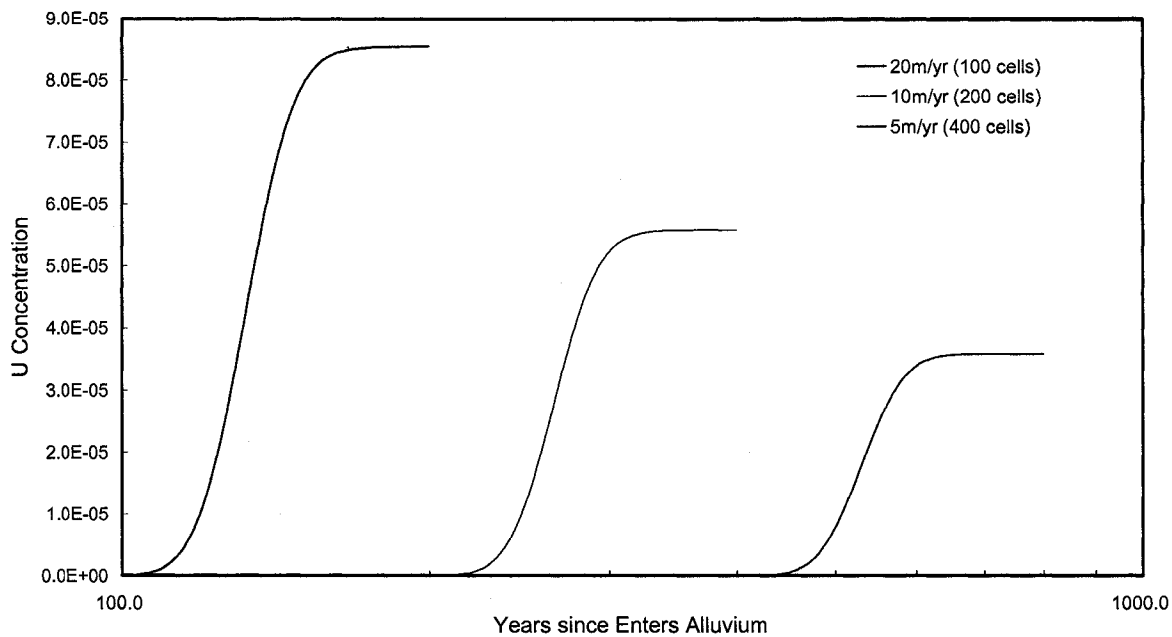


Figure 4.24. Comparison of breakthrough curves of uranium at different flow velocity in alluvium aquifer.

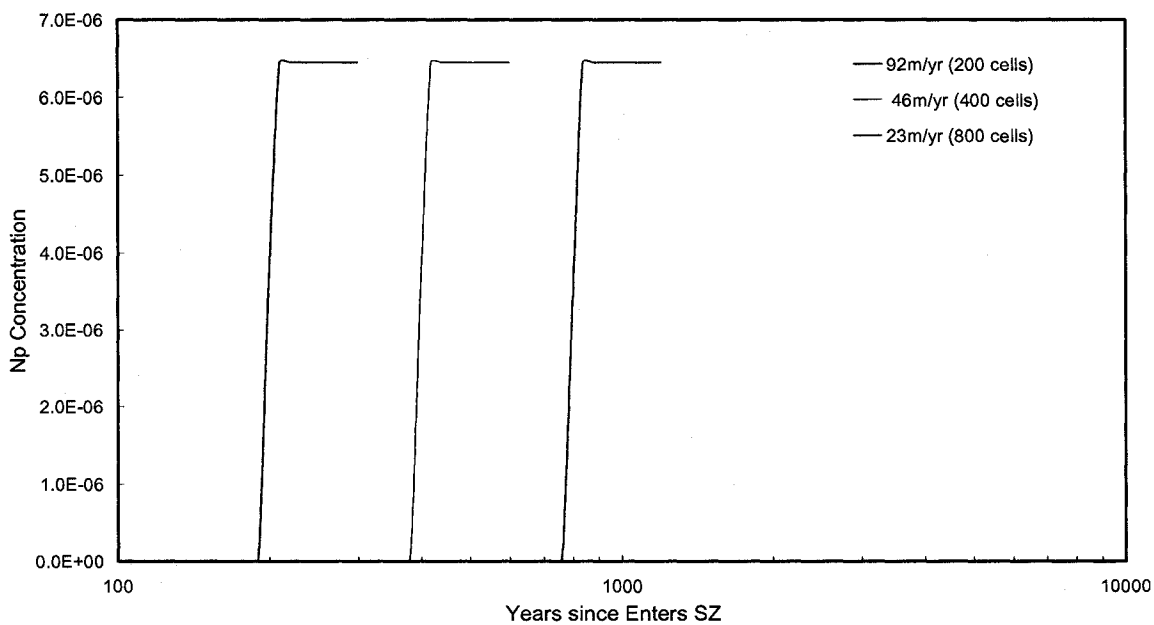


Figure 4.25. Comparison of breakthrough curves of neptunium at different flow velocity in volcanic aquifer.

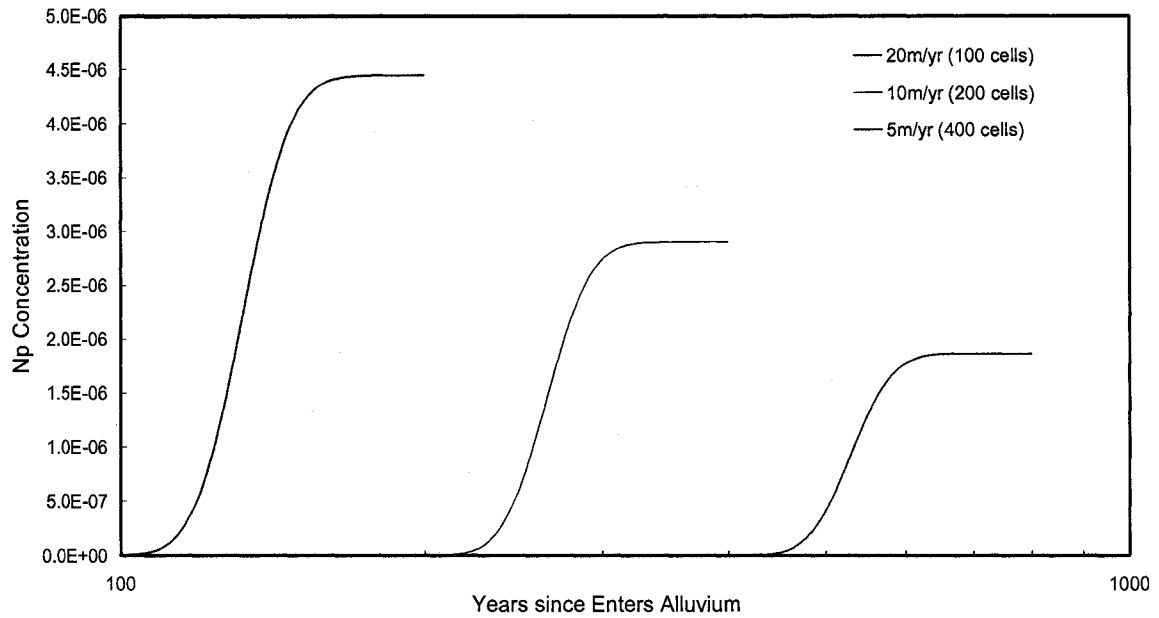


Figure 4.26. Comparison of breakthrough curves of neptunium at different flow velocities in alluvium aquifer.

Between Figures 4.23 and 4.24, the percentage of concentration decrease of uranium in alluvium aquifer is 31% at 20 m/yr, 55% at 10 m/yr, and 71% at 5 m/yr. From Figures 4.25 and 4.26, by same mean, the percentage of neptunium concentration decrease is exactly the same as uranium. Also, there is an obvious contrast on retardation effect among different flow velocities caused by the varied sorption activity as well as stagnant zone. There is 20 years of retardation between velocities of 20 m/yr and 10 m/yr, and more than 30 years between velocities of 10 m/yr and 5 m/yr.

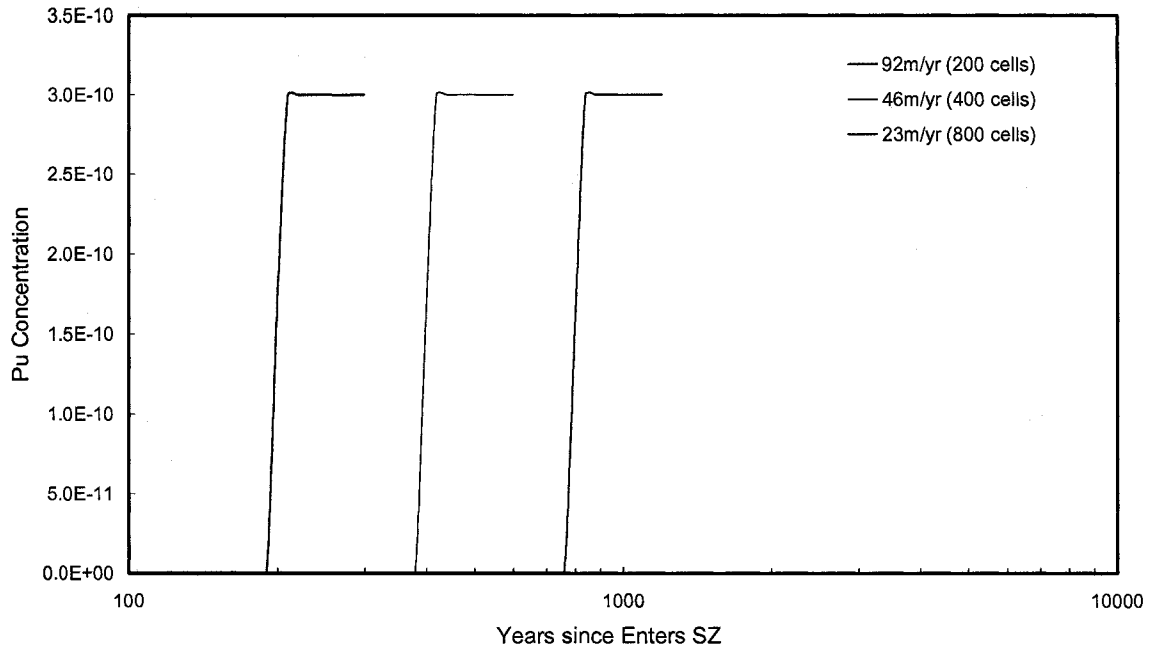


Figure 4.27. Comparison of breakthrough curves of plutonium at different flow velocities in volcanic aquifer.

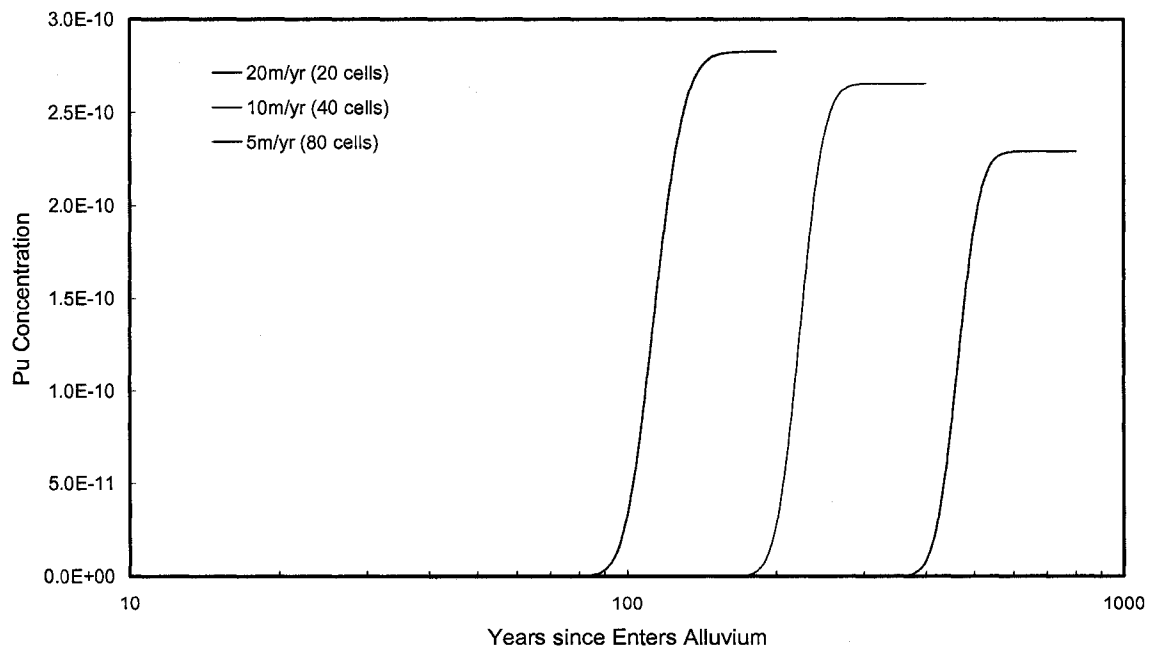


Figure 4.28. Comparison of breakthrough curves of plutonium at different flow velocities in alluvium aquifer.

From Figure 4.28, however, the decrease on plutonium concentration due to varied transport time is different from these of neptunium and uranium, which is 5.7% at 20 m/yr, 11.3% at 10m/yr, and 23.7% at 5 m/yr respectively. This is caused by much larger size of grid cell assigned to transport simulation for plutonium due to system convergence. Also, there is less obvious retardation effect on plutonium transport due to the low concentration in solution.

CHAPTER 5

CONCLUSIONS

In this study, three sets of geochemical simulations, including solid dissolution, solution speciation, and solute transport, are used to model solid dissolution, aqueous speciation, and transport processes of uranium, neptunium, and plutonium at YM. The simulation tool adopted in this study is PHREEQC 2.11 (for Windows). The thermodynamic, kinetic, and geological data used in the PHREEQC input files are derived from YM databases. There are several assumptions as well as uncertainties involved. The results derived from these geochemical simulations are conservative since the radionuclides must then travel through the near-field engineered barrier, the whole thick unsaturated zone, and subsequently through the saturated zone groundwater flow system. Between the repository and the water table, there is significant quantity of sorptive minerals such as zeolites exist in UZ, which results in sorptive retardation of many radionuclides as well.

The simulation of solid dissolution indicates that uranium dissolution increases with both pH value and CO₂ fugacity. Neptunium dissolution increases with CO₂ fugacity; and its values form a curve with a lowest point around pH = 8. Plutonium dissolution does not change with CO₂ fugacity, it declines substantial over the pH range of 4 to 5 and then keeps constant with increase pH. The overall dissolution of uranium is similar to these of

neptunium with one order of magnitude up or down. The dissolution of plutonium is much less, which is five orders of magnitude less than these of uranium and neptunium.

Solution speciation simulation verifies the hypotheses that uranium aqueous species is predominated by uranyl carbonate species; neptunium aqueous species is predominated by $\text{NpO}_2\text{CO}_3^-$ and NpO_2^+ ; plutonium aqueous species is predominated by hydroxide species ($\text{Pu}(\text{OH})_4$), which is different from other two. The speciation of neptunium and plutonium does not alter that much over a pH range of 7.5 to 8.5, which is most close to real environmental conditions. The speciation of uranium alters about 10 % of concentration over the same pH range.

Transport simulations confirm that the lower the groundwater flow velocity, the less dissolved concentration of radionuclide appears at the boundary of the model domain. This is due to surface complexation (sorption) between radionuclides and geological materials; mixing with carbonate groundwater underneath the alluvium does dilute the solution concentration and slightly alter the radionuclide aqueous speciation that does not affect transport processes that much; the stagnant zone of alluvium significantly contributes to the retardation of radionuclide breakthrough. To conclude, the hypotheses are verified that 1) the SZ functions as both mechanical barrier and chemical buffer to delay the release of radionuclides to the accessible environment; and 2) the solution concentration of radionuclides may be diluted during the transport in the SZ. These two factors are of primary significance to the performance of potential RW repository.

For the future works, a comprehensive flow model, such as MODFLOW, is needed to be coupled for simulating more specific and accurate cases of groundwater flow at YM in

order to avoid the scaling effect as well as some other disadvantages lie in the 1-D transport function of PHREEQC.

APPENDIX A

EXAMPLES OF SIMULATION INPUT AND OUTPUT

A.1 In put Files for Dissolution and Speciation Simulations of Neptunium

```

TITLE -- SPECIATION REACTIONS OF RADIONUCLIDES U IN THE
        GROUNDWATERFLOW AT YM
# UZ pore water around and below the Waste Package
# from Drift scale THC seepage model p.366/82 unit Tptpmn [6]
# Equilibrium with out coming radionuclide contained percolating water from WP

SOLUTION 1
      units  mg/L
      temp   25.0
      pH     8.
      C  200 as HCO3  CO2(g) -2.6
      Ca  101
      Na  61.5
      Mg  17
      K   8
      Si  70.5 as SiO2
      Cl  117
      F   1
      S  116 as SO4
      N   6.5 as NO3

EQUILIBRIUM_PHASES 1
      Np2O5  0.0

SOLUTION_MASTER_SPECIES
      Np      NpO2+  0.0  237.048      237.048
      Np(4)   Np+4   0.0  237.048
      Np(5)   NpO2+  0.0  237.048

SOLUTION_SPECIES
      NpO2+ = NpO2+
          log_k      0.0
      NpO2+ + OH- = NpO2OH
          log_k      2.7
      NpO2+ + 2OH- = NpO2(OH)2-
          log_k      4.35
      NpO2+ + CO3-2 = NpO2CO3-
  
```

```

log_k      5.03
NpO2+ + 2CO3-2 = NpO2(CO3)2-3
log_k      6.47
NpO2+ + 3CO3-2 = NpO2(CO3)3-5
log_k      5.37
NpO2+ + 3H+ = Np+4 + 1.5H2O + 0.25O2
log_k     -10.55
Np+4 + H2O = Np(OH)+3 + H+
log_k     -0.5
Np+4 + 2H2O = Np(OH)2+2 + 2H+
log_k     -0.3
Np+4 + 3H2O = Np(OH)3+ + 3H+
log_k     -2.78
Np+4 + 4H2O = Np(OH)4 + 4H+
log_k     -8.28
SAVE SOLUTION 1

PHASES
Np2O5
Np2O5 + 2H+ = 2NpO2+ + H2O
log_k      5.2

SELECTED_OUTPUT
-file C:\yuyu\document\Np\New Version of Np\Neptunium Speciation
results\8.5.out
-reset false
-ph
-molalities  NpO2+  NpO2OH  NpO2CO3-
-totals      Np
-equilibrium_phases  Np2O5
END

SOLUTION 2 #average of 10 samples from UZ#16 from 290-414m p174/282 [8]
units  mg/L
pH     8.5  # 7.5-8.5
temp   25.0
C      171  as HCO3
Ca     22
K      5.04
Na     72.5
Mg     8.4
Si     62.1  as SiO2
Cl     44.2
S      23.6  as SO4
N      21.7  as NO3

MIX 1
1 1
2 1
SAVE solution 3
USE solution 3
END

```

Figure A.1. Input File for Dissolution and Speciation Simulation of Neptunium.

A.2 Input File for Transport Simulation of Uranium

```

TITLE: ADVECTIVE AND DIFFUSIVE TRANSPORT SIMULATION

SOLUTION 0 #Groundwater sample from UE25 J-13
          #Site-scale SZ transport (BSC 2004a Appendix I)
units    mg/L
pH       7.2
temp     25.0
U        1.24e-4 mol/L
C        130 as HCO3
Ca       13
Na       45
Mg       2
K        5.3
Si       61 as SiO2
Cl       7.1
F        2.2
S        18.4 as SO4

SOLUTION_MASTER_SPECIES
U        UO2+2      0.0 254.029 238.029
U(6)    UO2+2      0.0 238.029 UO2+2

SOLUTION_SPECIES
UO2+2 = UO2+2
log_k   0.0

SAVE SOLUTION 101
END

SOLUTION 1-41 # GROUNDWATER FROM WELL NC-EWDP-19D (water in the
              # alluvium) # from site scale SZ transport (BSC 2004a Appendix G)
units    mg/l
pH       7.7
TEMP     32.0
C        189 as HCO3
Ca       3.7
Na       91.5
Mg       0.31
K        3.7
Si       22 as SiO2
Cl       6.1
S        22 as SO4
F        2.0

RATES # RATE EXPRESSIONS FOR FOUR KINETIC REACTIONS OF U
      Schoepite
      -START
      10 si_schoepite = SI ("Schoepite")
      20 if (si_schoepite <= 0) then goto 100
      30 area = 0.0025

```

```

40 k1= 0.05
50 k2= 3.4e-5
60 k3= 1.2e-7
70 rf = k1*act("UO2^2")+k2*act("H+")+k3*act("H2O")
80 rate = rf*area*1e-3*(1-10^si_schoepite)
90 moles = rate * time
100 SAVE moles
-end

```

```

U-sorption
-START

```

```

10 poro = 0.3 # SZ F and T Abstraction (BSC 2003c); Kessler, J. and Doering, T.,
2000
20 bulk = 1270 # g/l Kessler, J. and Doering, T., 2000; BSC 2003c
30 km = 3.17e-9 # time^-1
50 kd = 0.005 # l/g U 0.005 Np 0.015 Pu 0.025 form Kessler, J. and Doering, T.,
2000
60 U = TOT("U")
70 rate = -km*(U -(M*poro/bulk)/kd)
80 moles = rate * time
90 if (M - moles) < 0 then moles = M
100 SAVE moles
-end

```

KINETICS 1-41 # two kinetic reactions for all cells

Schoepite

```

-formula UO3H2O
-tol 1e-11

```

U-sorption

```

-formula UO2CO3 3.109e-06 UO2(CO3)2Cl2 1.087e-04 UO2(CO3)3Cl4
1.165e-05
-m 0.0
-m0 0.0
-tol 1e-11

```

TRANSPORT # 18km flow path of Uranium

```

-cells 20 # in alluvium
-lengths 100 # 20*100=2km
-shifts 40
-time_step 3.15e8 # =10yr groundwater velocity: 7.5-15 m/yr (10)
-flow_direction forward
-boundary_conditions flux constant
-stagnant 1 6.8e-6 0.3 0.1
-dispersivities 5 # Ref BSC 2003c p.89
-diffusion_coefficient 0.0
-punch_cells 20
-punch_frequency 1

```

PRINT

```

-reset false

```

SELECTED_OUTPUT

```
-file C:\yuyu\document\Transport\Uranium Transport\ U in alluvium 20 cells.sel
-reset false
USER_PUNCH

-headings  Years totU UO2CO3 UO2(CO3)2-2 UO2(CO3)3-4 U-sorption SI_Schoepite
-START
10 punch total_time/31536000
20 punch tot("U"), mol("UO2CO3"), mol("UO2(CO3)2-2"), mol("UO2(CO3)3-4")
30 punch kin("U-sorption")/4233, SI("Schoepite")
-END

END
```

Figure A.2. Input File for Transport Simulation of Uranium.

APPENDIX B

EFFECT OF GROUNDWATER VELOCITY ON TRANSPORT PROCESS

B.1 Uranium Profile in Volcanic and Alluvial Aquifers

The years listed in tables indicate the time since radionuclides enter SZ. The simulations started at time equals to zero; yet not all listed in the table since concentration at the last cell remains zero for many years.

Table B.1. Uranium transport in volcanic aquifer at different flow velocities.

200 cells	92m/yr	400 cells	46m/yr	800 cells	23m/yr
Years (300)	TOTU	Years (600)	TOT U	Years (1200)	TOT U
1.10E+02	0.00E+00	2.20E+02	0.00E+00	4.40E+02	0.00E+00
1.20E+02	0.00E+00	2.40E+02	0.00E+00	4.79E+02	0.00E+00
1.30E+02	0.00E+00	2.60E+02	0.00E+00	5.19E+02	0.00E+00
1.40E+02	0.00E+00	2.80E+02	0.00E+00	5.59E+02	0.00E+00
1.50E+02	0.00E+00	3.00E+02	0.00E+00	5.99E+02	0.00E+00
1.60E+02	0.00E+00	3.20E+02	0.00E+00	6.39E+02	0.00E+00
1.70E+02	2.57E-23	3.40E+02	0.00E+00	6.79E+02	0.00E+00
1.80E+02	3.00E-14	3.60E+02	8.03E-16	7.19E+02	1.38E-16
1.90E+02	8.28E-08	3.80E+02	4.90E-08	7.59E+02	3.90E-08
2.00E+02	7.10E-05	4.00E+02	6.67E-05	7.99E+02	6.46E-05
2.10E+02	1.24E-04	4.20E+02	1.24E-04	8.39E+02	1.24E-04
2.20E+02	1.24E-04	4.40E+02	1.24E-04	8.79E+02	1.24E-04
2.30E+02	1.24E-04	4.59E+02	1.24E-04	9.19E+02	1.24E-04
2.40E+02	1.24E-04	4.79E+02	1.24E-04	9.59E+02	1.24E-04
2.50E+02	1.24E-04	4.99E+02	1.24E-04	9.99E+02	1.24E-04
2.60E+02	1.24E-04	5.19E+02	1.24E-04	1.04E+03	1.24E-04
2.70E+02	1.24E-04	5.39E+02	1.24E-04	1.08E+03	1.24E-04
2.80E+02	1.24E-04	5.59E+02	1.24E-04	1.12E+03	1.24E-04
2.90E+02	1.24E-04	5.79E+02	1.24E-04	1.16E+03	1.24E-04
3.00E+02	1.24E-04	5.99E+02	1.24E-04	1.20E+03	1.24E-04

Table B.2. Uranium transport in alluvial aquifer at different flow velocities.

100 cells			200 cells			400 cells		
20m/yr			10m/yr			5m/yr		
Years (200)	TOT U	Sorption	Years (400)	TOT U	Sorption	Years (800)	TOT U	Sorption
4.99E+01	0.00E+00	0.00E+00	9.99E+01	0.00E+00	0.00E+00	2.00E+02	0.00E+00	0.00E+00
5.49E+01	0.00E+00	0.00E+00	1.10E+02	0.00E+00	0.00E+00	2.20E+02	0.00E+00	0.00E+00
5.99E+01	1.31E-24	2.46E-28	1.20E+02	0.00E+00	0.00E+00	2.40E+02	0.00E+00	0.00E+00
6.49E+01	6.83E-21	1.76E-24	1.30E+02	2.32E-24	6.74E-28	2.60E+02	0.00E+00	0.00E+00
6.99E+01	7.10E-18	2.06E-21	1.40E+02	1.20E-20	5.09E-24	2.80E+02	1.04E-22	6.56E-26
7.49E+01	2.23E-15	7.30E-19	1.50E+02	1.30E-17	6.40E-21	3.00E+02	2.81E-19	2.11E-22
7.99E+01	2.65E-13	9.78E-17	1.60E+02	4.24E-15	2.42E-18	3.20E+02	1.93E-16	1.68E-19
8.49E+01	1.40E-11	5.86E-15	1.70E+02	5.14E-13	3.39E-16	3.40E+02	4.26E-14	4.33E-17
8.99E+01	3.76E-10	1.79E-13	1.80E+02	2.71E-11	2.08E-14	3.60E+02	3.66E-12	4.32E-15
9.49E+01	5.71E-09	3.10E-12	1.90E+02	7.13E-10	6.33E-13	3.80E+02	1.43E-10	1.95E-13
9.99E+01	5.33E-08	3.32E-11	2.00E+02	1.04E-08	1.07E-11	4.00E+02	2.84E-09	4.50E-12
1.05E+02	3.28E-07	2.36E-10	2.10E+02	9.09E-08	1.09E-10	4.20E+02	3.20E-08	5.85E-11
1.10E+02	1.42E-06	1.19E-09	2.20E+02	5.17E-07	7.25E-10	4.40E+02	2.21E-07	4.67E-10
1.15E+02	4.51E-06	4.42E-09	2.30E+02	2.03E-06	3.34E-09	4.59E+02	1.00E-06	2.45E-09
1.20E+02	1.11E-05	1.28E-08	2.40E+02	5.81E-06	1.13E-08	4.79E+02	3.20E-06	9.02E-09
1.25E+02	2.18E-05	2.97E-08	2.50E+02	1.27E-05	2.91E-08	4.99E+02	7.55E-06	2.45E-08
1.30E+02	3.56E-05	5.77E-08	2.60E+02	2.23E-05	6.01E-08	5.19E+02	1.39E-05	5.16E-08
1.35E+02	5.03E-05	9.64E-08	2.70E+02	3.27E-05	1.03E-07	5.39E+02	2.09E-05	8.81E-08
1.40E+02	6.31E-05	1.43E-07	2.80E+02	4.18E-05	1.53E-07	5.59E+02	2.71E-05	1.27E-07
1.45E+02	7.27E-05	1.92E-07	2.90E+02	4.83E-05	2.02E-07	5.79E+02	3.13E-05	1.62E-07
1.50E+02	7.88E-05	2.39E-07	3.00E+02	5.22E-05	2.44E-07	5.99E+02	3.38E-05	1.87E-07
1.55E+02	8.22E-05	1.19E-03	3.10E+02	5.42E-05	2.76E-07	6.19E+02	3.50E-05	2.03E-07
1.60E+02	8.40E-05	3.17E-07	3.20E+02	5.51E-05	2.99E-07	6.39E+02	3.55E-05	2.12E-07
1.65E+02	8.48E-05	3.47E-07	3.30E+02	5.55E-05	3.15E-07	6.59E+02	3.57E-05	2.17E-07
1.70E+02	8.51E-05	3.71E-07	3.40E+02	5.56E-05	3.25E-07	6.79E+02	3.58E-05	2.19E-07
1.75E+02	8.53E-05	3.90E-07	3.50E+02	5.57E-05	3.32E-07	6.99E+02	3.58E-05	2.20E-07
1.80E+02	8.54E-05	4.05E-07	3.60E+02	5.57E-05	3.36E-07	7.19E+02	3.58E-05	2.20E-07
1.85E+02	8.54E-05	4.17E-07	3.70E+02	5.58E-05	3.39E-07	7.39E+02	3.58E-05	2.20E-07
1.90E+02	8.54E-05	4.27E-07	3.80E+02	5.58E-05	3.41E-07	7.59E+02	3.58E-05	2.21E-07
1.95E+02	8.55E-05	4.34E-07	3.90E+02	5.58E-05	3.42E-07	7.79E+02	3.58E-05	2.21E-07
2.00E+02	8.55E-05	4.40E-07	4.00E+02	5.58E-05	3.42E-07	7.99E+02	3.58E-05	2.21E-07

B.2 Neptunium Profile in Volcanic and Alluvial Aquifers

Table B.3. Neptunium transport in volcanic aquifer at different flow velocities.

200 cells	92m/yr	400 cells	46m/yr	800 cells	23m/yr
Years (300)	TOT Np	Years (600)	TOT Np	Years (800)	TOT Np
9.99E+01	0.00E+00	2.00E+02	0.00E+00	4.00E+02	0.00E+00
1.10E+02	0.00E+00	2.20E+02	0.00E+00	4.40E+02	0.00E+00
1.20E+02	0.00E+00	2.40E+02	0.00E+00	4.79E+02	0.00E+00
1.30E+02	0.00E+00	2.60E+02	0.00E+00	5.19E+02	0.00E+00
1.40E+02	0.00E+00	2.80E+02	0.00E+00	5.59E+02	0.00E+00
1.50E+02	0.00E+00	3.00E+02	0.00E+00	5.99E+02	0.00E+00
1.60E+02	0.00E+00	3.20E+02	0.00E+00	6.39E+02	0.00E+00
1.70E+02	2.16E-25	3.40E+02	0.00E+00	6.79E+02	0.00E+00
1.80E+02	1.56E-15	3.60E+02	4.18E-17	7.19E+02	7.18E-18
1.90E+02	4.31E-09	3.80E+02	2.55E-09	7.59E+02	2.03E-09
2.00E+02	3.70E-06	4.00E+02	3.47E-06	7.99E+02	3.36E-06
2.10E+02	6.45E-06	4.20E+02	6.45E-06	8.39E+02	6.45E-06
2.20E+02	6.45E-06	4.40E+02	6.45E-06	8.79E+02	6.45E-06
2.30E+02	6.45E-06	4.59E+02	6.45E-06	9.19E+02	6.45E-06
2.40E+02	6.45E-06	4.79E+02	6.45E-06	9.59E+02	6.45E-06
2.50E+02	6.45E-06	4.99E+02	6.45E-06	9.99E+02	6.45E-06
2.60E+02	6.45E-06	5.19E+02	6.45E-06	1.04E+03	6.45E-06
2.70E+02	6.45E-06	5.39E+02	6.45E-06	1.08E+03	6.45E-06
2.80E+02	6.45E-06	5.59E+02	6.45E-06	1.12E+03	6.45E-06
2.90E+02	6.45E-06	5.79E+02	6.45E-06	1.16E+03	6.45E-06
3.00E+02	6.45E-06	5.99E+02	6.45E-06	1.20E+03	6.45E-06

Table B.4. Neptunium transport in alluvial aquifer at different flow velocities.

100 cells			200 cells			400 cells		
20m/yr			10m/yr			5m/yr		
Years (200)	TOT Np	Sorption	Years (400)	TOT Np	Sorption	Years (800)	TOT Np	Sorption
4.99E+01	0.00E+00	0.00E+00	9.99E+01	0.00E+00	0.00E+00	2.00E+02	0.00E+00	0.00E+00
5.49E+01	0.00E+00	0.00E+00	1.10E+02	0.00E+00	0.00E+00	2.20E+02	0.00E+00	0.00E+00
5.99E+01	0.00E+00	0.00E+00	1.20E+02	0.00E+00	0.00E+00	2.40E+02	0.00E+00	0.00E+00
6.49E+01	3.58E-22	9.25E-26	1.30E+02	0.00E+00	0.00E+00	2.60E+02	0.00E+00	0.00E+00
6.99E+01	3.72E-19	1.08E-22	1.40E+02	6.32E-22	1.51E-25	2.80E+02	5.31E-24	2.93E-27
7.49E+01	1.17E-16	3.85E-20	1.50E+02	6.88E-19	1.91E-22	3.00E+02	1.51E-20	1.15E-23
7.99E+01	1.39E-14	5.17E-18	1.60E+02	2.25E-16	7.24E-20	3.20E+02	1.04E-17	9.25E-21
8.49E+01	7.35E-13	3.10E-16	1.70E+02	2.72E-14	1.02E-17	3.40E+02	2.29E-15	2.39E-18
8.99E+01	1.98E-11	9.51E-15	1.80E+02	1.44E-12	6.25E-16	3.60E+02	1.97E-13	2.40E-16
9.49E+01	3.00E-10	1.65E-13	1.90E+02	3.79E-11	1.91E-14	3.80E+02	7.69E-12	1.09E-14
9.99E+01	2.80E-09	1.78E-12	2.00E+02	5.50E-10	3.25E-13	4.00E+02	1.53E-10	2.53E-13
1.05E+02	1.73E-08	1.27E-11	2.10E+02	4.83E-09	3.34E-12	4.20E+02	1.72E-09	3.31E-12
1.10E+02	7.45E-08	6.38E-11	2.20E+02	2.74E-08	2.23E-11	4.40E+02	1.19E-08	2.66E-11
1.15E+02	2.37E-07	2.38E-10	2.30E+02	1.08E-07	1.04E-10	4.59E+02	5.39E-08	1.41E-10
1.20E+02	5.82E-07	6.91E-10	2.40E+02	3.08E-07	3.61E-10	4.79E+02	1.71E-07	5.21E-10
1.25E+02	1.14E-06	1.62E-09	2.50E+02	6.74E-07	9.76E-10	4.99E+02	4.04E-07	1.43E-09
1.30E+02	1.87E-06	3.16E-09	2.60E+02	1.18E-06	2.14E-09	5.19E+02	7.40E-07	3.03E-09
1.35E+02	2.64E-06	5.32E-09	2.70E+02	1.73E-06	3.86E-09	5.39E+02	1.11E-06	5.23E-09
1.40E+02	3.31E-06	7.92E-09	2.80E+02	2.20E-06	5.98E-09	5.59E+02	1.43E-06	7.63E-09
1.45E+02	3.81E-06	1.07E-08	2.90E+02	2.54E-06	8.21E-09	5.79E+02	1.65E-06	9.77E-09
1.50E+02	4.13E-06	1.35E-08	3.00E+02	2.73E-06	1.02E-08	5.99E+02	1.77E-06	1.14E-08
1.55E+02	4.30E-06	1.60E-08	3.10E+02	2.83E-06	1.19E-08	6.19E+02	1.83E-06	1.25E-08
1.60E+02	4.39E-06	1.82E-08	3.20E+02	2.88E-06	1.32E-08	6.39E+02	1.85E-06	1.31E-08
1.65E+02	4.43E-06	2.01E-08	3.30E+02	2.89E-06	1.41E-08	6.59E+02	1.86E-06	1.34E-08
1.70E+02	4.44E-06	2.17E-08	3.40E+02	2.90E-06	1.47E-08	6.79E+02	1.86E-06	1.36E-08
1.75E+02	4.45E-06	2.30E-08	3.50E+02	2.90E-06	1.51E-08	6.99E+02	1.86E-06	1.37E-08
1.80E+02	4.45E-06	2.40E-08	3.60E+02	2.90E-06	1.54E-08	7.19E+02	1.86E-06	1.37E-08
1.85E+02	4.45E-06	2.49E-08	3.70E+02	2.90E-06	1.56E-08	7.39E+02	1.86E-06	1.38E-08
1.90E+02	4.45E-06	2.56E-08	3.80E+02	2.90E-06	1.57E-08	7.59E+02	1.86E-06	1.38E-08
1.95E+02	4.45E-06	2.62E-08	3.90E+02	2.90E-06	1.58E-08	7.79E+02	1.86E-06	1.38E-08
2.00E+02	4.45E-06	2.67E-08	4.00E+02	2.90E-06	1.59E-08	7.99E+02	1.86E-06	1.38E-08

B.3 Plutonium Profile in Volcanic and Alluvial Aquifers

Table B.5. Plutonium transport in volcanic aquifer at different flow velocities.

200 cells	92m/yr	400 cells	46m/yr	800 cells	23m/yr
Years (300)	TOT Pu	Years (600)	TOT Pu	Years (1200)	TOT Pu
9.99E+01	0.00E+00	2.00E+02	0.00E+00	4.00E+02	0.00E+00
1.10E+02	0.00E+00	2.20E+02	0.00E+00	4.40E+02	0.00E+00
1.20E+02	0.00E+00	2.40E+02	0.00E+00	4.79E+02	0.00E+00
1.30E+02	0.00E+00	2.60E+02	0.00E+00	5.19E+02	0.00E+00
1.40E+02	0.00E+00	2.80E+02	0.00E+00	5.59E+02	0.00E+00
1.50E+02	0.00E+00	3.00E+02	0.00E+00	5.99E+02	0.00E+00
1.60E+02	0.00E+00	3.20E+02	0.00E+00	6.39E+02	0.00E+00
1.70E+02	0.00E+00	3.40E+02	0.00E+00	6.79E+02	0.00E+00
1.80E+02	7.27E-20	3.60E+02	1.94E-21	7.19E+02	3.28E-22
1.90E+02	2.01E-13	3.80E+02	1.19E-13	7.59E+02	9.45E-14
2.00E+02	1.72E-10	4.00E+02	1.62E-10	7.99E+02	1.57E-10
2.10E+02	3.00E-10	4.20E+02	3.00E-10	8.39E+02	3.00E-10
2.20E+02	3.00E-10	4.40E+02	3.00E-10	8.79E+02	3.00E-10
2.30E+02	3.00E-10	4.59E+02	3.00E-10	9.19E+02	3.00E-10
2.40E+02	3.00E-10	4.79E+02	3.00E-10	9.59E+02	3.00E-10
2.50E+02	3.00E-10	4.99E+02	3.00E-10	9.99E+02	3.00E-10
2.60E+02	3.00E-10	5.19E+02	3.00E-10	1.04E+03	3.00E-10
2.70E+02	3.00E-10	5.39E+02	3.00E-10	1.08E+03	3.00E-10
2.80E+02	3.00E-10	5.59E+02	3.00E-10	1.12E+03	3.00E-10
2.90E+02	3.00E-10	5.79E+02	3.00E-10	1.16E+03	3.00E-10
3.00E+02	3.00E-10	5.99E+02	3.00E-10	1.20E+03	3.00E-10

Table B.6. Plutonium transport in alluvial aquifer at different flow velocities.

20 cells			40 cells			80 cells		
20m/yr			10m/yr			5m/yr		
Years (200)	TOT Pu	Sorption	Years (400)	TOT Pu	Sorption	Years (800)	TOT Pu	Sorption
4.01E+01	0.00E+00	0.00E+00	8.02E+01	0.00E+00	0.00E+00	1.60E+02	0.00E+00	0.00E+00
4.51E+01	5.09E-25	2.55E-29	9.02E+01	0.00E+00	0.00E+00	1.80E+02	0.00E+00	0.00E+00
5.01E+01	1.85E-22	1.85E-26	1.00E+02	0.00E+00	0.00E+00	2.00E+02	0.00E+00	0.00E+00
5.51E+01	1.92E-20	2.83E-24	1.10E+02	1.16E-24	1.49E-28	2.20E+02	0.00E+00	0.00E+00
6.01E+01	1.06E-18	5.91E-23	1.20E+02	9.12E-22	1.51E-25	2.40E+02	0.00E+00	0.00E+00
6.51E+01	3.50E-17	1.99E-21	1.30E+02	1.92E-19	3.47E-23	2.61E+02	2.12E-22	4.73E-26
7.01E+01	7.40E-16	5.20E-20	1.40E+02	1.76E-17	3.46E-21	2.81E+02	9.46E-20	2.41E-23
7.52E+01	1.05E-14	6.87E-19	1.50E+02	7.80E-16	1.68E-19	3.01E+02	1.36E-17	3.97E-21
8.02E+01	1.04E-13	1.04E-17	1.60E+02	1.80E-14	4.33E-18	3.21E+02	7.62E-16	2.58E-19
8.52E+01	7.19E-13	1.41E-16	1.70E+02	2.33E-13	6.33E-17	3.41E+02	1.94E-14	7.70E-18
9.02E+01	3.56E-12	8.28E-16	1.80E+02	1.78E-12	5.61E-16	3.61E+02	2.53E-13	1.20E-16
9.52E+01	1.27E-11	3.36E-15	1.90E+02	8.58E-12	3.21E-15	3.81E+02	1.89E-12	1.08E-15
1.00E+02	3.36E-11	1.02E-14	2.00E+02	2.78E-11	1.26E-14	4.01E+02	8.77E-12	6.16E-15
1.05E+02	6.80E-11	2.46E-14	2.10E+02	6.48E-11	3.66E-14	4.21E+02	2.75E-11	2.41E-14
1.10E+02	1.12E-10	4.90E-14	2.20E+02	1.16E-10	8.26E-14	4.41E+02	6.23E-11	6.94E-14
1.15E+02	1.58E-10	8.41E-14	2.30E+02	1.68E-10	1.54E-13	4.61E+02	1.09E-10	1.56E-13
1.20E+02	1.98E-10	1.29E-13	2.40E+02	2.10E-10	2.47E-13	4.81E+02	1.54E-10	2.87E-13
1.25E+02	2.30E-10	1.82E-13	2.51E+02	2.38E-10	3.55E-13	5.01E+02	1.90E-10	4.57E-13
1.30E+02	2.52E-10	2.40E-13	2.61E+02	2.54E-10	4.72E-13	5.21E+02	2.11E-10	6.53E-13
1.35E+02	2.65E-10	3.02E-13	2.71E+02	2.61E-10	5.94E-13	5.41E+02	2.22E-10	8.61E-13
1.40E+02	2.74E-10	3.65E-13	2.81E+02	2.64E-10	7.17E-13	5.61E+02	2.27E-10	1.07E-12
1.45E+02	2.78E-10	4.30E-13	2.91E+02	2.65E-10	8.40E-13	5.81E+02	2.28E-10	1.29E-12
1.50E+02	2.81E-10	4.96E-13	3.01E+02	2.65E-10	9.63E-13	6.01E+02	2.29E-10	1.50E-12
1.55E+02	2.82E-10	5.62E-13	3.11E+02	2.66E-10	1.09E-12	6.21E+02	2.29E-10	1.71E-12
1.60E+02	2.82E-10	6.27E-13	3.21E+02	2.66E-10	1.21E-12	6.41E+02	2.29E-10	1.92E-12
1.65E+02	2.83E-10	6.93E-13	3.31E+02	2.66E-10	1.33E-12	6.61E+02	2.29E-10	2.13E-12
1.70E+02	2.83E-10	7.58E-13	3.41E+02	2.66E-10	1.45E-12	6.81E+02	2.29E-10	2.33E-12
1.75E+02	2.83E-10	8.24E-13	3.51E+02	2.66E-10	1.57E-12	7.01E+02	2.29E-10	2.54E-12
1.80E+02	2.83E-10	8.89E-13	3.61E+02	2.66E-10	1.69E-12	7.21E+02	2.29E-10	2.74E-12
1.85E+02	2.83E-10	9.54E-13	3.71E+02	2.66E-10	1.81E-12	7.42E+02	2.29E-10	2.94E-12
1.90E+02	2.83E-10	1.02E-12	3.81E+02	2.66E-10	1.93E-12	7.62E+02	2.29E-10	3.13E-12
1.95E+02	2.83E-10	1.08E-12	3.91E+02	2.66E-10	2.04E-12	7.82E+02	2.29E-10	3.33E-12
2.00E+02	2.83E-10	1.15E-12	4.01E+02	2.66E-10	2.16E-12	8.02E+02	2.29E-10	3.52E-12

Notes: Time step = 5 year

APPENDIX C

SCALING EFFECTS

The simulation results with 200 cells and 20 cells were conducted to evaluate how the grid size would affect the simulation of flow and solute processes. A flow velocity of 10 m/yr was used for this simulation. The results for the simulation with 200 cells (cell length 10 m) and 20 cells (cell length 100 m) were provided in Table 4.11.

According to the output data in Table 4.13, noticing that the total solution concentrations of both uranium and neptunium in the simulation with 20 cells are two times higher comparing to the simulation with 200 cells one. It was suspected that this is because of the effect of stagnant zones in alluvium aquifer. To find out the reason for this phenomenon, simulations with 200 and 20 cells without any stagnant zone were conducted. The output data are listed in Table 4.14. It indicates that output concentration in the simulation with 20 cells is about two times higher than that of one with 200 cells. Also, the sorption quantity of the simulation with 20 cells with higher solution concentration is slightly higher than that of one with 200 cells. This complies with sorption principles. The assumption that it is stagnant zone associated with each transport cell making the concentration loss is discarded. In fact, the scaling effect does apply to the 1-dimensional transport modeling with PHREEQC.

Table C.1. Transport simulation of uranium and neptunium of 200 and 20 cells in alluvium aquifer.

Years	200 cells		20 cells		200 cells		20 cells	
	TOT U	Sorption	TOT U	Sorption	TOT Np	Sorption	TOT Np	Sorption
9.99E+01	0.00E+00	0.00E+00	1.15E-17	1.76E-21	0.00E+00	0.00E+00	5.97E-19	9.27E-23
1.10E+02	0.00E+00	0.00E+00	1.13E-15	1.87E-19	0.00E+00	0.00E+00	5.90E-17	9.87E-21
1.20E+02	0.00E+00	0.00E+00	5.96E-14	1.05E-17	0.00E+00	0.00E+00	3.10E-15	5.54E-19
1.30E+02	2.32E-24	6.74E-28	1.88E-12	3.52E-16	0.00E+00	0.00E+00	9.81E-14	1.85E-17
1.40E+02	1.20E-20	5.09E-24	3.86E-11	7.62E-15	6.32E-22	1.51E-25	2.01E-12	4.01E-16
1.50E+02	1.30E-17	6.40E-21	5.38E-10	1.12E-13	6.88E-19	1.91E-22	2.80E-11	5.91E-15
1.60E+02	4.24E-15	2.42E-18	5.29E-09	1.16E-12	2.25E-16	7.24E-20	2.76E-10	6.15E-14
1.70E+02	5.14E-13	3.39E-16	3.76E-08	8.76E-12	2.72E-14	1.02E-17	1.96E-09	4.64E-13
1.80E+02	2.71E-11	2.08E-14	1.97E-07	4.94E-11	1.44E-12	6.25E-16	1.03E-08	2.61E-12
1.90E+02	7.13E-10	6.33E-13	7.81E-07	2.12E-10	3.79E-11	1.91E-14	4.07E-08	1.12E-11
2.00E+02	1.04E-08	1.07E-11	2.40E-06	7.18E-10	5.50E-10	3.25E-13	1.25E-07	3.80E-11
2.10E+02	9.09E-08	1.09E-10	5.89E-06	1.97E-09	4.83E-09	3.34E-12	3.07E-07	1.04E-10
2.20E+02	5.17E-07	7.25E-10	1.20E-05	4.53E-09	2.74E-08	2.23E-11	6.27E-07	2.40E-10
2.30E+02	2.03E-06	3.34E-09	2.11E-05	9.01E-09	1.08E-07	1.04E-10	1.10E-06	4.79E-10
2.40E+02	5.81E-06	1.13E-08	3.27E-05	1.59E-08	3.08E-07	3.61E-10	1.71E-06	8.48E-10
2.50E+02	1.27E-05	2.91E-08	4.60E-05	2.56E-08	6.74E-07	9.76E-10	2.40E-06	1.36E-09
2.60E+02	2.23E-05	6.01E-08	5.96E-05	3.80E-08	1.18E-06	2.14E-09	3.11E-06	2.03E-09
2.70E+02	3.27E-05	1.03E-07	7.24E-05	5.28E-08	1.73E-06	3.86E-09	3.78E-06	2.82E-09
2.80E+02	4.18E-05	1.53E-07	8.37E-05	6.96E-08	2.20E-06	5.98E-09	4.36E-06	3.73E-09
2.90E+02	4.83E-05	2.02E-07	9.29E-05	8.78E-08	2.54E-06	8.21E-09	4.85E-06	4.72E-09
3.00E+02	5.22E-05	2.44E-07	1.00E-04	1.07E-07	2.73E-06	1.02E-08	5.22E-06	5.76E-09
3.10E+02	5.42E-05	2.76E-07	1.05E-04	1.26E-07	2.83E-06	1.19E-08	5.50E-06	6.82E-09
3.20E+02	5.51E-05	2.99E-07	1.09E-04	1.46E-07	2.88E-06	1.32E-08	5.69E-06	7.89E-09
3.30E+02	5.55E-05	3.15E-07	1.12E-04	1.65E-07	2.89E-06	1.41E-08	5.82E-06	8.96E-09
3.40E+02	5.56E-05	3.25E-07	1.13E-04	1.84E-07	2.90E-06	1.47E-08	5.91E-06	1.00E-08
3.50E+02	5.57E-05	3.32E-07	1.14E-04	2.02E-07	2.90E-06	1.51E-08	5.97E-06	1.10E-08
3.60E+02	5.57E-05	3.36E-07	1.15E-04	2.19E-07	2.90E-06	1.54E-08	6.00E-06	1.20E-08
3.70E+02	5.58E-05	3.39E-07	1.16E-04	2.36E-07	2.90E-06	1.56E-08	6.02E-06	1.30E-08
3.80E+02	5.58E-05	3.41E-07	1.16E-04	2.52E-07	2.90E-06	1.57E-08	6.03E-06	1.39E-08
3.90E+02	5.58E-05	3.42E-07	1.16E-04	2.68E-07	2.90E-06	1.58E-08	6.04E-06	1.48E-08
4.00E+02	5.58E-05	3.42E-07	1.16E-04	2.82E-07	2.90E-06	1.59E-08	6.04E-06	1.56E-08

Table C.2. Transport simulation of uranium and neptunium of 200 and 20 cells in alluvium aquifer without stagnant zone.

V =10m/yr	200 cells		No stagnant		20 cells		No stagnant	
Years	TOT U	Sorption	TOT U	Sorption	TOT Np	Sorption	TOT Np	Sorption
9.99E+01	0.00E+00	0.00E+00	6.97E-16	8.28E-20	0.00E+00	0.00E+00	3.63E-17	1.84E-17
1.10E+02	4.94E-22	1.41E-25	7.70E-14	9.86E-18	2.59E-23	3.99E-27	4.01E-15	2.20E-15
1.20E+02	1.39E-17	4.89E-21	4.48E-12	6.12E-16	7.34E-19	1.45E-22	2.33E-13	1.36E-13
1.30E+02	3.80E-14	1.65E-17	1.54E-10	2.24E-14	2.01E-15	4.91E-19	8.03E-12	4.98E-12
1.40E+02	1.69E-11	9.06E-15	3.37E-09	5.15E-13	8.90E-13	2.70E-16	1.75E-10	1.15E-10
1.50E+02	1.76E-09	1.18E-12	4.85E-08	7.88E-12	9.31E-11	3.54E-14	2.53E-09	1.76E-09
1.60E+02	5.77E-08	4.85E-11	4.72E-07	8.22E-11	3.05E-09	1.47E-12	2.46E-08	1.84E-08
1.70E+02	7.38E-07	7.91E-10	3.12E-06	5.92E-10	3.91E-08	2.41E-11	1.62E-07	1.32E-07
1.80E+02	4.42E-06	6.11E-09	1.39E-05	2.96E-09	2.34E-07	1.91E-10	7.22E-07	6.61E-07
1.90E+02	1.44E-05	2.60E-08	4.07E-05	1.03E-08	7.62E-07	8.52E-10	2.12E-06	2.30E-06
2.00E+02	2.95E-05	6.96E-08	7.79E-05	2.51E-08	1.56E-06	2.44E-09	4.06E-06	5.63E-06
2.10E+02	4.32E-05	1.32E-07	1.02E-04	4.58E-08	2.27E-06	4.99E-09	5.33E-06	1.03E-05
2.20E+02	5.12E-05	1.96E-07	1.13E-04	6.90E-08	2.69E-06	7.86E-09	5.88E-06	1.56E-05
2.30E+02	5.45E-05	2.47E-07	1.16E-04	9.24E-08	2.85E-06	1.04E-08	6.06E-06	2.09E-05
2.40E+02	5.54E-05	2.84E-07	1.17E-04	1.15E-07	2.90E-06	1.22E-08	6.11E-06	2.61E-05
2.50E+02	5.57E-05	3.08E-07	1.17E-04	1.37E-07	2.91E-06	1.36E-08	6.12E-06	3.11E-05
2.60E+02	5.58E-05	3.23E-07	1.17E-04	1.58E-07	2.91E-06	1.44E-08	6.12E-06	3.60E-05
2.70E+02	5.58E-05	3.33E-07	1.17E-04	1.78E-07	2.91E-06	1.50E-08	6.12E-06	4.06E-05
2.80E+02	5.59E-05	3.39E-07	1.17E-04	1.96E-07	2.91E-06	1.54E-08	6.12E-06	4.51E-05
2.90E+02	5.59E-05	3.42E-07	1.18E-04	2.15E-07	2.91E-06	1.57E-08	6.12E-06	4.94E-05
3.00E+02	5.59E-05	3.45E-07	1.18E-04	2.32E-07	2.91E-06	1.59E-08	6.12E-06	5.36E-05
3.10E+02	5.59E-05	3.46E-07	1.18E-04	2.48E-07	2.91E-06	1.60E-08	6.12E-06	5.75E-05
3.20E+02	5.59E-05	3.47E-07	1.18E-04	2.64E-07	2.91E-06	1.61E-08	6.12E-06	6.14E-05
3.30E+02	5.59E-05	3.48E-07	1.18E-04	2.79E-07	2.91E-06	1.62E-08	6.12E-06	6.50E-05
3.40E+02	5.59E-05	3.48E-07	1.18E-04	2.93E-07	2.91E-06	1.62E-08	6.12E-06	6.86E-05
3.50E+02	5.59E-05	3.48E-07	1.18E-04	3.07E-07	2.91E-06	1.62E-08	6.12E-06	7.19E-05
3.60E+02	5.59E-05	3.48E-07	1.18E-04	3.20E-07	2.91E-06	1.62E-08	6.12E-06	7.52E-05
3.70E+02	5.59E-05	3.49E-07	1.18E-04	3.32E-07	2.91E-06	1.63E-08	6.12E-06	7.83E-05
3.80E+02	5.59E-05	3.49E-07	1.18E-04	3.44E-07	2.91E-06	1.63E-08	6.12E-06	8.13E-05
3.90E+02	5.59E-05	3.49E-07	1.18E-04	3.55E-07	2.91E-06	1.63E-08	6.12E-06	8.42E-05
4.00E+02	5.59E-05	3.49E-07	1.18E-04	3.66E-07	2.91E-06	1.63E-08	6.12E-06	8.70E-05

REFERENCES

- Atkins, P. W., 1994, Physical chemistry, 5th ed: New York W.H. Freeman and Company, New York, TIC: 246986.
- Barnett, M. O., Jardine, P. M., Brooks, S. C., and Selim, H. M., 2000, Adsorption and transport of uranium (VI) in subsurface media: Soil Science Society of America Journal, v. 64, p. 908-917.
- Bauer, P., Attinger, S., and Kinzelbach, W., 2001, Transport of a decay chain in homogenous porous media: analytical solutions: Journal of Contaminant Hydrology, v. 49, p. 217-239.
- Bechtel SAIC Company, 2005, Drift-Scale THC seepage model: *Prepared for U.S. Department of Energy*, MDL-NBS-HS-000001, REV 04, 366 p.
- Bechtel SAIC Company, 2004a, Site-scale saturated zone transport, November 2004: *Prepared for U.S. Department of Energy*, MDL-NBS-HS-000010, REV 02, 366 p.
- Bechtel SAIC Company, 2004b, Unsaturated zone flow, Revision 1, May 2004: *Prepared for U.S. Department of Energy*, 500 p.
- Bechtel SAIC Company, 2004c, Technical basis document No. 1: climate and infiltration May 2004: *Prepared for U.S. Department of Energy*, REV 01, 206 p.
- Bechtel SAIC Company, 2004d, Qualification of thermodynamic data for geochemical modeling of mineral-water interactions in dilute system, November 2004: *Prepared for U.S. Department of Energy*, REV 01, 212 p.
- Bechtel SAIC Company, 2003a, Saturated zone flow and transport, Revision 2, September 2003: *Prepared for U.S. Department of Energy*, 402 p.
- Bechtel SAIC Company, 2003b, Geochemical and isotopic constraints on groundwater flow directions and magnitudes, mixing, and recharge at Yucca Mountain, July 2003: *Prepared for U.S. Department of Energy*, ANL-NBS-HS-000021 REV 01, 505 p.
- Bechtel SAIC Company, 2003c, Saturated zone flow and transport model abstraction, July 2003: *Prepared for U.S. Department of Energy*, MDL-NBS-HS-000021, REV 0, 195 p.

- Bechtel SAIC Company, 2003d, In-package chemistry abstraction: *Prepared for U.S. Department of Energy*, ANL-EBS-MD 000037, REV 02, 250 p.
- Bethke, C. M. and Brady, P. V., 2000, How the K_d approach undermines groundwater cleanup: *Ground Water*, v. 38, p. 435-443.
- Bodvarsson, G. S., Boyle, W., Patterson, R., and Williams, D., 1998, Overview of scientific investigations at Yucca Mountain: the potential repository for high level nuclear waste: *Journal of Contaminant Hydrology*, v. 38, p. 3-24.
- CRWMS M&O, 2001, Pure Phase Solubility Limits: *Prepared for U.S. Department of Energy*, ANL-EBS-MD-000017 REV 00, ICN 01, Las Vegas, Nevada, 230 p.
- CRWMS M&O 2000a, Saturated zone flow and transport process model report, August 2000: U.S. Department of Energy, Las Vegas, Nevada, TDR-NBSHS 000001 REV 00 ICN 01, 320 p.
- CRWMS M&O, 2000b, Geochemical and isotopic constraints on groundwater flow directions, mixing, and recharge at Yucca Mountain, Nevada: *Prepared for U.S. Department of Energy*, ANL-NBS-HS 000021, REV 00, 191 p.
- CRWMS M&O, 2000c, Yucca Mountain Site Description: *Prepared for U.S. Department of Energy*, TDR-CRW-GS 000001, REV 01, ICN 01, 489 p.
- Davis, J. A., and Curtis, G. P., 2003, Application of surface complexation modeling to describe Uranium (VI) adsorption and retardation at the Uranium mill tailings site at Naturita, Colorado: U.S. Geological Survey, NUREG/CR-6820, 238 p.
- Domenico, P. A., 1987, An analytical model for multidimensional transport of a decaying contaminant species: *Journal of Hydrology*, v. 91, p. 49-58.
- Domenico, P. A. and Schwartz, F. W., 1998, *Physical and chemical hydrogeology*, 2nd Ed John Wiley and Sons Inc., New York, 506 p.
- Eddebarha, A. A., Zyvoloskia, G. A., Robinson, B. A., Kwicklis, E. M., Reimus, P. W., Arnold, B. W., Corbet, T., Kuzio, S. P., Faunt, C., 2003, The saturated zone at Yucca Mountain: an overview of the characterization and assessment of the saturated zone as a barrier to potential radionuclide migration: *Journal of Contaminant Hydrology*, v. 62-63, p. 477- 493.
- Efurd, D.W., Runde, W. H., Banar, J. C., Janecky, D. R., Kaszuba, J. P., Palmer, P. D., Roensch, F. R., and Tait, C. D., 1998, Neptunium and Plutonium solubilities in a Yucca Mountain groundwater: *Environment Science and Technology*, v. 32, p. 3893-3900.

- Ewing, R. C., 1999, Nuclear waste forms for actinides: National Academy of Sciences Colloquium "Geology, Mineralogy, and Human Welfare", v. 96, p. 3432-3439.
- Fjeld, R. A., Serkiz, S. M., McGinnis, P. L., Elci, A., and Kaplan, D. I., 2003, Evaluation of a conceptual model for the subsurface transport of plutonium involving surface mediated reduction of Pu(V) to Pu(IV): *Journal of Contaminant Hydrology*, v. 67, p. 79– 94.
- Flint, A. L., Hevesi, J. A., and Flint, L. E., 1996, Conceptual and numerical model of infiltration for the Yucca Mountain area, Nevada: Milestone 3GUI623M, Denver, Colorado: U.S. Geological Survey, ACC: MOL.19970409.0087.
- Glynn, P. D., 2003, Modeling Np and Pu transport with a surface complexation model and spatially variant sorption capacities: implications for reactive transport modeling and performance assessments of nuclear waste disposal sites: *Computer and Geosciences*, v. 29, p. 331-349.
- Haschke, J. M., and Bassett, R. L., 2002, Control of plutonium dioxide solubility by amorphous tetrahydroxide: A critical review of the model: *Radiochimica Acta*, v. 90, p. 505-509.
- Langmuir, D., 1997, *Aqueous environmental geochemistry: Upper Saddle River, New Jersey*, Prentice Hall, 600 p.
- Kaplan, D. I., Serkiz, S. M., Fjeld, R. A., and Coates, J. T., 2001, Influence of pH and oxidation state on plutonium mobility through an SRS sediment: WSRC-TR 2001-00472, Rev. O, Westinghouse Savannah River Company, Aiken, S.C.
- Katz, J. J., Seaborg, G. T., and Morss, L. R., eds, 1986, *The chemistry of the actinide elements*, 2nd edition: Chapman and Hall, New York, New York, volume 2.
- Kaszuba, J. P., and Runde, W. H., 1999, The aqueous geochemistry of Neptunium: dynamic control of soluble concentrations with applications to nuclear waste disposal: *Environment Science and Technology*, v. 33, p. 4427-4433.
- Kessler, J., and Doering, T., 2000, Evaluation of the candidate high-level radionuclides waste repository at Yucca Mountain using total system performance assessment: Phase 5, Electronic Power Research Institute, Palo Alto, CA, 1000802.
- Merkel, B. J. and Planer-Friedrich, B., 2005, *Groundwater geochemistry – A practical guide to modeling of natural and contaminated aquatic systems*, Edited by Nordstrom, D. K.: Springer Berlin Heidelberg, New York, 200 p.
- Murphy, W. M., and Shock, E. L., 1999, Environmental Aqueous Geochemistry of Actinides, *in* Burns, P. C. and Finch, R., eds., *Uranium: Mineralogy*,

Geochemistry and the environment: Washington, DC, Mineralogical Society of America, v. 38, p. 221-255.

Nitsche, H., Gatti, R. C., Standifer, E. M., Lee, S. C., Müller, A., Prussin, T., Deinhammer, R. S., Maurer, H., Becraft, K., Leung, S., and Carpenter, S. A., 1993, Measured solubilities and speciations of neptunium, plutonium, and americium in a typical groundwater (J-13) from the Yucca Mountain Region: Los Alamos National Laboratory, Los Alamos, New Mexico, ACC: NNA.19930507.0136.

OCRWM, 2004, Nuclear waste policy act, March 2004: U.S. Department of Energy Office of Civilian Radioactive Waste Management, Washington, D.C., 146 p.

OCRWM, 2003a, Dissolved concentration limits of radioactive elements, June 2003: Office of Civilian Radioactive Waste Management, Las Vegas, Nevada, ANL-WIS-MD-000010, REV 02, 153 p.

OCRWM, 2003b, Saturated zone flow and transport model abstraction, August 2003: Office of Civilian Radioactive Waste Management, Las Vegas, Nevada, MDL-NBS-HS-000021, REV 00, 195 p.

OCRWM, 2001, Analysis of geochemical data for the unsaturated zone: *Prepared for* U.S. Department of Energy, ANL-NBS-HS-000017, REV 00, ICN 02, 282 p.

Paces, J. B., Ludwig, K. R., Peterman, Z. E., Neymark, L. A., 2002, $^{234}\text{U}/^{238}\text{U}$ evidence for local recharge and patterns of groundwater flow in the vicinity of Yucca Mountain, Nevada, USA: *Applied Geochemistry*, v.17, p. 751-779.

Parkhurst, L. D., and Appelo, C. A. J., 1999, User's guide to PHREEQC (Version 2): Water Resources Investigations Report 99-4259.

Pirlet, V., 2001, Overview of actinides (Np, Pu, Am) and Tc release from waste glasses: influence of solution composition: *Journal of Nuclear Material*, v. 298, p. 47-54.

Rard, J. A., 1997, Potential for radionuclide immobilization in the EBWNFE: solubility limiting phases for Neptunium, Plutonium, and Uranium: Geosciences and Environmental Technologies, Environmental Programs Directorate, Lawrence Livermore National Laboratory, University of California, p. 34.

Runde, W., Conradson, S. D., Efur, D. W., Lu, N. P. C., VanPelt, E., and Tait, C. D., 2002, Solubility and sorption of redox-sensitive radionuclides (Np, Pu) in J-13 water from the Yucca Mountain site: comparison between experiment and theory: *Applied Geochemistry*, v. 17, p. 837 - 853.

Sharp, D. W. A., 1990, *The penguin dictionary of chemistry*, 2nd edition, Penguin Books (London), 434 p.

- Viswanathan, H. S., Robinson, B. A., Valocchia, A. J., and Triay, I. R., 1998, A reactive transport model of neptunium migration from the potential repository at Yucca Mountain: *Journal of Hydrology*, v. 209, p. 251–280.
- Windt, L. D., Burnol, A., Montarnal, P., and Lee, J. van der, 2003, Intercomparison of reactive transport models applied to UO_2 oxidative dissolution and uranium migration: *Journal of Contaminant Hydrology*, v. 61, p. 303–312.
- Wronkiewicz, D. J., Bates, J. K., Gerding, T. J., Veleckis, E., and Tano, B. S., 1992, Uranium release and secondary phase formation during the unsaturated testing of UO_2 at 90 °C: *Journal of Nuclear Materials*, v. 238, p. 78-95.
- Wronkiewicz, D. J., and Buck, E. C., 1999, Uranium mineralogy and the geologic disposal of spent nuclear fuel, *in* Burns, P.C. and Finch, R., eds, *Uranium: mineralogy, geochemistry and the environment*: Mineralogical Society of America, Washington, DC, p. 475-498.

VITA

Graduate College
University of Nevada, Las Vegas

Yuyu Lin

Home Address:

3724 Kit Fox St.
Las Vegas, NV 89122

Degrees:

Bachelor of Engineering, Geological Engineering, 2003
Hohai University, China

Publications:

Lin, Y., Yu, Z., 2005, Geochemical modeling of radionuclides at Yucca Mountain, Geological Society of America, Salt Lake City Annual Meeting, Abstracts and Programs, v. 78, p. 36.

Lin, Y., 2003, Research on seepage security during the operation of dam in Shuikou Hydro-power Station, Hohai University, 37 p.

Thesis Title:

Geochemical and Transport Modeling of Selected Radionuclides at Yucca Mountain

Thesis Examination Committee:

Chair, Dr. Zhongbo Yu, Ph. D.

Committee Member, Dr. Michael Nicholl, Ph. D.

Committee Member, Dr. Gangqing Jiang, Ph. D.

Graduate Faculty Representative, Dr. Jichun Li, Ph. D.